Enzyme kinetics by isothermal titration calorimetry: applications to inhibition, activation, and allosteric interactions

Yun Wang

Department of Chemistry

McGill University

Montreal, Quebec, Canada

March, 2021

A thesis submitted to McGill University in partial fulfillment of the requirements of the degree of Doctor of Philosophy

Acknowledgement

First, I want to thank my supervisor Dr. Anthony Mittermaier for his support and guidance during my Ph.D study. I still remember my first meeting with Tony. He presented a great research proposal and it attracted my interest to the field of biophysical chemistry and protein science. Tony not only help me in science but also taught me how to become a good researcher. He showed me his very well-organized lab notebooks during his PhD study in the first term after I joined his lab. That is one of the most important merits I learned from him: attitude! Thanks Tony! Also, I really enjoy the fruitful research discussion with him. Tony is always very patient and we can always bring up good ideas. The projects Tony and I have worked on are extremely enjoyable. I have gained great research skills and knowledges in this filed under Tony's supervision. These knowledge and skills will be the solid foundation for my further career.

I would also like to thank Dr. Hanadi Sleiman, and Dr. Nicolas Moitessier for their time and help as my research committee members. Specifically, I would like to thank Dr. Karine Auclair for the fruitful collaboration and the French translation for my thesis abstract. I like to thank Ms. Chantal Marotte for all her help in the administrative matters, and to all other staff members, students, and technicians who had helped me during my PhD study.

Thank you to all the Mittermaier lab members in the past and present. Especially, I would like to thank Dr. Justin Di Trani for ITC training and great discussion. Also, I would like to thank all the undergrads and summer students who have worked with me

during my phD study. Last, I would like to thank Dr. Jinmin Guan, former member from Dr. Auclair lab, as a great collaborator.

Finally, I would like to thank my mother Junlan Li and my father Dejun Wang for all their support and guidance. My husband Jun Zhu, thank you for always beside me, shares me your great knowledge in science and being the solid support to my Ph.D study! My two big boys, Evan and Ryan, thank you for your interests to my research and concern mom’s Ph.D study!

Abstract

Enzymes play important roles in a variety of biological processes. The study of enzyme activity and regulatory mechanisms are important. Isothermal titration calorimetry (ITC) kinetic assays directly measure the heat released or absorbed by catalysis in real time, thus becoming powerful and universal techniques. This thesis is focused on the development and application of various types of ITC kinetic assays, including several new customized methods to analyze the enzyme kinetic properties and understand their mechanistic details. Four novel customized ITC-based methods: 1) transient assay, 2) activation assay, 3) single turn-over assay, and 4) 2-dimensional assay, were developed. These assays overcome some limitations of previous developed ITC methods and can be used to extend the application of ITC methods.

In chapter 2, a transient ITC assay is developed to study the inhibition and activation behavior of the product ADP with aminoglycoside phosphotransferase [APH(3')-IIIa], pantothenate kinases from *Escherichia coli* (*Ec*PanK), and *Pseudomonas aeruginosa* (*Pa*PanK). The results suggested that the enzymes respond to changes of ADP and ATP levels to regulate enzyme activity *in vivo*. In chapter 3, a single turn-over ITC assay and an activation ITC assay are developed to characterize ATP hydrolysis by APH(3')-IIIa. The results suggested the existence of direct allosteric communication between the aminoglycoside- and ATP- binding pockets of APH(3')-IIIa. In chapter 4, a 2-dimensional ITC assay is demonstrated which can completely kinetically characterize bi-substrate enzyme in a single experiment. A rabbit muscle pyruvate kinase (rMPK) catalyzed phosphorylation reaction is selected as the model system. Complete kinetic profiles can be generated by the 2-dimensional ITC assay and the mechanism is determined from data analysis. These assays overcome limitations of previously developed ITC methods and other conventional enzyme assays. All these new developed ITC assays in this thesis can be generalized and applied to other interesting systems.

Abrégé

Les enzymes jouent un rôle important dans divers processus biologiques. Il est donc essentiel de poursuivre l'étude des mécanismes d'activité et de régulation des enzymes. Les tests cinétiques basés sur la titration calorimétrique isotherme (TCI) mesurent directement la chaleur libérée ou absorbée par la catalyse en temps réel, faisant d'elles des techniques puissantes et universelles. Cette thèse est axée sur le développement et l'application de nouveaux types d'essais cinétiques de TCI qui facilitent l'analyse des propriétés cinétiques des enzymes et de leur mécanisme d'action. Les quatre nouvelles méthodes développées ici incluent: 1) un essai transitoire, 2) un essai d'activation, 3) un essai en phase préstationnaire, et 4) un essai bidimensionnel. Ces essais surmontent certaines limitations des méthodes actuelle de TCI et augmentent les applications possibles de la TCI.

Dans le chapitre 2, l'essai transitoire est développé pour étudier le comportement d'inhibition et d'activation du produit ADP sur les enzymes aminoglycoside phosphotransférase [APH(3')-IIIa] et pantothénate kinases d'*Escherichia coli* (*Ec*PanK) et de *Pseudomonas aeruginosa* (*Pa*PanK). Les résultats suggèrent que les changements de concentration de l'ADP et l'ATP agissent pour réguler l'activité enzymatique *in vivo*. Ensuite, le chapitre 3 résume le développement des essais d'activation et en phase préstationnaire dans un contexte visant à caractériser l'hydrolyse de l'ATP par APH(3')-IIIa. Les résultats suggèrent l'existence d'une communication allostérique directe entre le site de liaison de l'aminoglycoside et celui de l'ATP dans cette enzyme. Finalement, l'essai bidimensionnel est discuté dans le chapitre 4, où il démontre son utilité dans la caractérisation cinétique complète d'une enzyme à bi-substrat en une seule expérience. L'enzyme modèle choisie pour cet étude est la pyruvate kinase musculaire du lapin (rMPK), qui catalyse une réaction de phosphorylation. Des profils cinétiques complets peuvent être générés avec cet essai bidimensionnel et l'analyse des données ainsi produites permet l'élucidation rapide du mécanisme réactionnel. Non seulement ces essais surmontent plusieurs limitations associées à la TCI, mais ils peuvent être généralisés et appliqués à d'autres systèmes intéressants.

Contribution of Authors

Chapter1: part 1.1 - 1.4 was reproduced with the permission from: Yun Wang, Guanyu Wang, Nicolas Moitessier and Anthony K. Mittermaier, Enzyme kinetics by isothermal titration calorimetry: allostery, inhibition, and dynamics, *Frontiers in Molecular Biosciences*, 2020, 7, 285. These parts were co-written by myself and Dr. Mittermaier.

Chapter 2 was reproduced with the permission from: Yun Wang, Jinming Guan, Justin M. Di Trani, Karine Auclair and Anthony K. Mittermaier, Inhibition and Activation of Kinases by Reaction Products: A Reporter-Free Assay, *Analytical Chemistry*, 2019, 91, 11803-11811. APH(3')-IIIa was expressed and purified by Yun Wang. *Ec*PanK and *Pa*PanK were expressed and purified by Jinming Guan. I performed all the experiments, interpreted and analyzed all the data with the help of Dr. Mittermaier and Dr. Di Trani. The manuscript was co-written by myself, Dr. Auclair and Dr. Mittermaier.

Chapter 3: 'Allosteric interactions in a kinase active site modulate background ATP hydrolysis' will be submitted to a peer-reviewed journal. I performed all the experiment, interpreted and analyzed all the data with the help of Dr. Mittermaier. The article was co-written by myself and Dr. Mittermaier.

Chapter 4: 'Rapid characterization of Bi-substrate enzymes by 2D-ITC' will be submitted to a peer-reviewed journal. I performed all the experiment, interpreted and analyzed all the data with the help of Dr. Mittermaier. The article was co-written by myself and Dr. Mittermaier.

List of Figures

List of Tables

List of Abbreviations

ADP Adenosine diphosphate

AMP-PNP Adenylyl-imidodiphosphate

Amgs Aminoglycosides

APH(3')-IIIa Aminoglycoside 3'-phosphotransferase-IIIa

ATP Adenosine triphosphate

DTT Dithiothreitol

E.C. Enzyme commission

***Ec*PanK** Pantothenate kinases from *Escherichia coli*

EDTA Ethylenediaminetetraacetic acid

ERM Empirical response model

GTP Guanosine triphosphate

GDP Guanosine diphosphate

IPTG Isopropyl β-D-thiogalactoside

ITC Isothermal titration calorimetry

IrCal Initial rate calorimetry

LB Luria broth

MM/BH Michaelis-Menten/Briggs-Haldane

NADH Reduced nicotinamide adenine dinucleotide

NPL Nucleotide positioning loop

NTPs Nucleotide triphosphates

NDPs Nucleotide diphosphates

nsAmgs Non-substrate aminoglycosides

***Pa*PanK** Pantothenate kinases from *Pseudomonas aeruginosa*

PEP Phosphoenolpyruvate

Phe phenylalanine

Pi Inorganic phosphate

PK/LDH Pyruvate kinase/lactate dehydrogenase

PMSF Phenylmethanesulfonyl fluoride

rMPK Rabbit muscle pyruvate kinase

Contents

1. Introduction

1.1 A Brief Introduction to Enzyme Kinetics

Enzymes are catalytic proteins that are ubiquitous in living systems and play central roles in virtually all cellular processes, such as metabolism, active transport, sensing, regulation, communication, and signal transduction and integration.[1-4] Consequently enzymes constitute approximately 44% of all validated drug targets, including human enzymes whose dysregulation is linked to disease, and foreign enzymes expressed by pathogens.[5] In addition, enzymes are the most efficient catalysts known and have many industrial and medical applications.[6] For example, hydrolases break polysaccharides down into their component sugars, with applications to food processing, pulp and paper, and biofuel industries.[7-9] Their high selectivity and biocompatibility have also made enzymes useful as therapeutics, for instance in the treatment of phytobezoars.[10]

1.1.1 Enzyme Kinetics

1.1.1.1 Michaelis-Menten/Briggs-Haldane (MM/BH) model

In general, enzymes show saturation kinetics, which can be rationalized according to the Michaelis-Menten/Briggs-Haldane (MM/BH) model shown in the scheme below

$$E + S \underset{k_{-1}}{\overset{k_1}{\rightleftharpoons}} ES \xrightarrow{k_{cat}} E + P \quad (1.1)$$

where an enzyme molecule (E) binds a substrate (S) with association and dissociation rate constants k_1 and k_{-1}, respectively, to form the Michaelis complex (ES). The enzyme then acts on the substrate to produce the product (P) with a rate constant k_{cat}. This kinetic scheme gives rise to the familiar MM/BH equation where the enzyme velocity, v_0, has a saturable dependence on the substrate concentration:

$$v_0 = \frac{d[P]}{dt} = -\frac{d[S]}{dt} = \frac{V_{max}[S]}{K_m + [S]}. \quad (1.1)$$

V_{max} is the maximum rate of catalysis in the theoretical presence of an infinite quantity of substrate and K_m is the concentration of substrate required to achieve half-maximal velocity, as illustrated in **Figure 1.1**. In terms of the rate constants in **Scheme 1.1**,

$$V_{max} = k_{cat}[E] \quad (1.2)$$

and

$$K_m = \frac{k_{-1} + k_{cat}}{k_1} \quad (1.3)$$

The relationship between enzyme velocity and substrate concentration can be linearized according to the double-reciprocal or Lineweaver-Burk plot, in which v_0^{-1} is plotted as a function of $[S]^{-1}$, shown below:

$$\frac{1}{v_0} = \frac{K_m}{V_{max}[S]} + \frac{1}{V_{max}} \quad (1.4)$$

The slope of the resulting straight line is K_m/V_{max}, the x-intercept is $-K_m^{-1}$ and the y-intercept is V_{max}^{-1}. The parameters K_m and k_{cat} provide simple metrics of an enzyme's behavior and quantify how activity changes in response to changing solution conditions, addition of inhibitors or activators, changes in the amino acid sequence of the enzyme, chemical modification of the substrate, or exchanging one cofactor for another, among other factors. Thus, methods for measuring K_m and k_{cat} are among the foundational techniques of molecular biosciences.

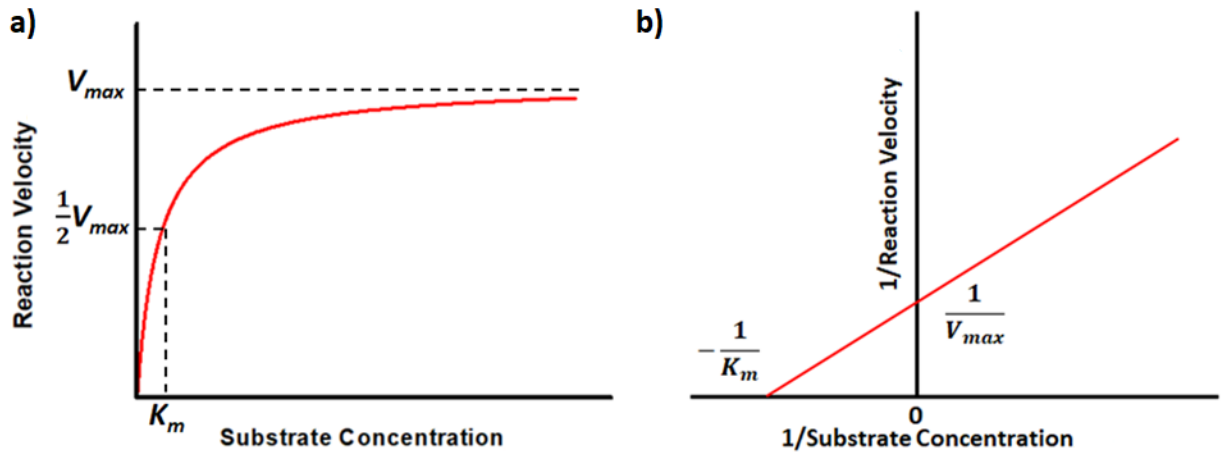

Figure 1.1 Michaelis–Menten kinetics. a) Reaction Velocity of a typical enzyme-catalyzed reaction versus substrate concentration. b) Double-Reciprocal (Lineweaver-Burk) linearized plot of the rates in a).

1.1.1.2 Kinetics of Bi-substrate Reactions

Many of enzymatic reactions are multi-substrate and/or multiproduct reactions. The Bi Bi reaction (two substrates, two products) accounts for over 60% of all enzymatic catalyzed ractions,[11] and is one of the most common types of multi-substrate systems. It differs from the unimolecular reaction, where the substrate binds to the enzyme (formation of the ES complex) and the reaction then takes place. In a bimolecular reaction, the formation of the enzyme-substrate complex and the releasing of the products may follow several distinct catalytic mechanisms. Formation of the enzyme-substrate complex falls under two major mechanistic categories: sequential or nonsequential (**Figure 1.2**). In the sequential mechanism, both substrates A and B must bind to the enzyme first to form EAB ternary complex, then catalysis takes place (EAB→EPQ). If both substrates A and B bind to the enzyme, and both products P and Q are released from the enzyme in a specific order, it is further classified as an ordered sequential mechanism (**Figure 1.2 a i**). Theorell-Chance is a special case of an ordered mechanism. There is no accumulation of the ternary complex (the concentration of EAB or EPQ remains close to zero) in the this types of reacion.[12] In contrast, if the order of substrate binding is random, the mechanism is classified as a random sequential (**Figure 1.2 a ii**). For a nonsequential (ping-pong) mechanism, catalysis takes place via a substituted enzyme intermediate. As

described in **Figure 1.2 b**, the substrate A binds to the enzyme (EA→EP), the first product dissociates, the second substrate B binds to the modified enzyme (E*) and finally the second reaction product is released (E*B→EQ).

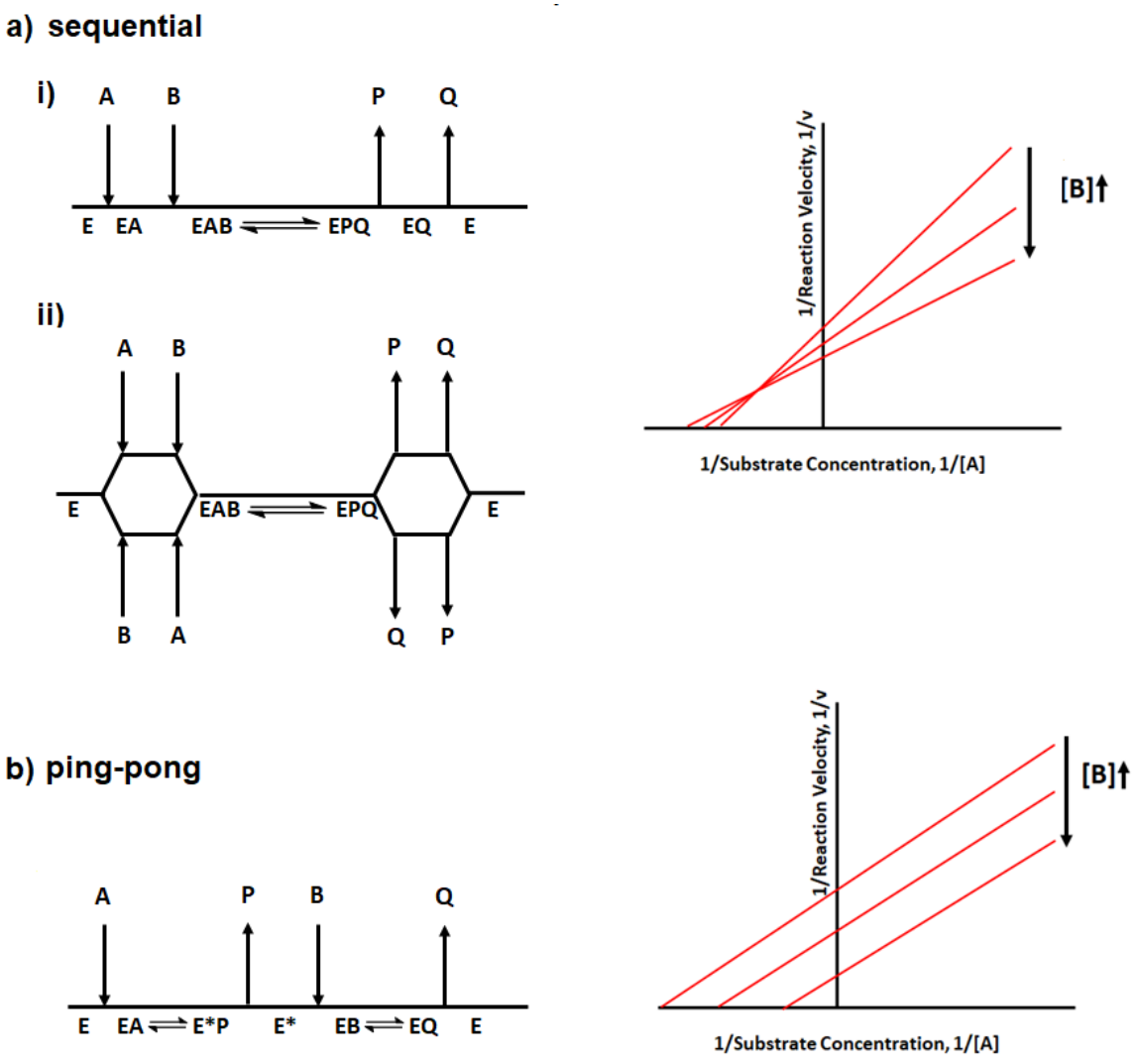

Figure 1.2. Mechanisms of bi-substrate catalysis and their corresponding Lineweaver–Burk double-reciprocal plots. a) Sequential reactions via i) ordered or ii) random mechanisms. **b)** nonsequential (ping-pong) mechanism.

The general rate equation for sequential (ordered and random) and ping-pong mechanisms are described in **Equation 1.5 and 1.6**, respectively.[13, 14]

$$v_0 = \frac{V_{max}[A][B]}{K_m^B[A]+K_m^A[B]+[A][B]+K_i^A K_m^B} \quad (1.5)$$

$$v_0 = \frac{V_{max}[A][B]}{K_m^B[A]+K_m^A[B]+[A][B]} \quad (1.6)$$

where V_{max} is the maximum rate when both A and B are saturating, $K_m{}^A$ is the Michaelis constant for A when B is saturating, $K_m{}^B$ is the Michaelis constant for B when A is saturating and $K_i{}^A$ is the dissociation constant for A.

The Lineweaver-Burk (double-reciprocal) forms of the sequential and ping-pong mechanisms are given by:

$$\frac{1}{v_0} = \frac{1}{V_{max}} + \frac{K_m^A}{V_{max}[A]} + \frac{K_m^B}{V_{max}[B]} + \frac{K_i^A K_m^B}{V_{max}[A][B]} \quad (1.7)$$

$$\frac{1}{v_0} = \frac{1}{V_{max}} + \frac{K_m^A}{V_{max}[A]} + \frac{K_m^B}{V_{max}[B]} \quad (1.8)$$

The mechanism for the sequential and ping-pong can be readily distinguished using a double-reciprocal plot by plotting $1/v$ against 1/[A] at varies concentrations of B, as illustrated in **Figure 1.2**. The sequential mechanism yields a series of intersecting straight lines; and the ping-pong mechanism yields a series of parallel lines. When the

concentration of substrate B in a large saturating excess, the terms that contain $\frac{K_m^B}{[B]}$ in **Equation 1.7 and 1.8** go to zero. Thus, the rate equation for a bimolecular reaction can be simplified into pseudo-unimolecular respective to substrate A.

1.1.1.3 Enzyme inhibition

Enzyme can be inhibited by the presence of any organic chemical, inorganic metal, or biosynthetic compound due to their covalent or non-covalent interactions with enzyme active site. The enzyme inhibitors are small molecules that can reduce or completely inhibit the enzyme activity sites by reversible or irreversible interaction. The irreversible inhibitors tightly bind to the enzyme active site and are popular used to identify functional groups of the enzyme active sites at which location they bind.[15] Reversible inhibitors make reversible association with the enzyme. A quantitative analysis of the reversible enzyme inhibition typically involves determination of the mode (competitive, uncompetitive, or mixed) and the inhibitor dissociation constant K_i. For mixed-mode inhibitors, there are separate K_i values for binding to E and to ES. Apparent K_m^{app} and k_{cat}^{app} values are measured at different concentrations of inhibitor [I] and analyzed collectively to extract the inhibition parameters. For a competitive inhibitor

$$k_{\mathrm{cat}}^{\mathrm{app}} = k_{\mathrm{cat}}; \qquad \mathrm{K_m^{app}} = \mathrm{K_m}\left(1 + \frac{[\mathrm{I}]}{\mathrm{K_i}}\right) \tag{1.9}$$

and a double-reciprocal plot of $1/v_0$ vs 1/[S] obtained at different [I] gives a series of lines that intersect at the y-axis. For an uncompetitive inhibitor

$$k_{\mathrm{cat}}^{\mathrm{app}} = \frac{k_{\mathrm{cat}}}{1+\frac{[\mathrm{I}]}{\mathrm{K_i'}}}; \qquad \mathrm{K_m^{app}} = \frac{\mathrm{K_m}}{1+\frac{[\mathrm{I}]}{\mathrm{K_i'}}} \tag{1.10}$$

where K_i' is the dissociation constant for the inhibitor and ES complex and a double-reciprocal plot gives a series of parallel lines. For mixed inhibitors

$$k_{\mathrm{cat}}^{\mathrm{app}} = \frac{k_{\mathrm{cat}}}{1+\frac{[\mathrm{I}]}{\mathrm{K_i'}}}; \qquad \mathrm{K_m^{app}} = \mathrm{K_m}\frac{\left(1+\frac{[\mathrm{I}]}{\mathrm{K_i}}\right)}{\left(1+\frac{[\mathrm{I}]}{\mathrm{K_i'}}\right)} \tag{1.11}$$

and a double-reciprocal plot gives a series of lines that intersect elsewhere than the y-axis. In the case that $K_i = K_i'$, the inhibitor is said to be non-competitive and the lines intersect at the x-axis.

The products of enzymatic reactions are reversible inhibitors of the enzymes. A decrease in the rate of the enzymatic reaction due to the accumulation of products plays an important role in the balance of and most economic usage of metabolic pathways. The competitive product inhibition is the most common type, where the reaction product binds to the free enzyme and blocks the substrate. In a multiple substrate reaction, the product from one substrate may block the binding site of this substrate and slow down the reaction,

but the co-substrate may not be displaced. In this case, the product acts as a non-competitive inhibitor towards to the co-substrate. The inhibition mechanisms for a multi-substrate reaction are more complex. Our special research interest is studying the product inhibition kinetics of the Bi Bi enzymatic reactions.

1.1.1.4 Allostery and Cooperativity

Allostery is a key feature of biological systems in which covalent modification or ligand binding at one site influences the activity at distant sites in a macromolecule or macromolecular assembly. Allosteric regulation plays a central role in metabolism and cell signaling [16] and has been identified as a source of new drug targets [17-22]; thus, detailed descriptions of allostery have far-reaching implications. [23] For example, the downstream products of a biosynthetic pathway can down-regulate the activity of the enzyme catalyzing the first committed step, maintaining balance between different branches of core metabolism through the process of feedback inhibition.[24, 25] Alternatively, enzymes may require allosteric activators in order to function, providing an extra layer of control.[26, 27] In the special case that the substrate itself acts as an allosteric effector, enzyme kinetics necessarily deviate from the classical MM/BH model. This can often be accounted for

mathematically with a Hill coefficient of cooperativity, *n*, such that the enzyme velocity is given by the expression

$$v_0 = \frac{V_{max}[S]^n}{K_m{}^n + [S]^n} \quad (1.12)$$

Values of $n>1$ indicate positive cooperativity, such that substrate binding makes an enzyme more active towards additional substrates, and give characteristically sigmoidal v_0 vs [S] plots. In a simple interpretation, an enzyme with a given Hill coefficient, *n*, either binds exactly *n* molecules of substrate or none at all. When binding a molecule of substrate at an allosteric site reduces enzyme activity towards additional substrates (substrate inhibition), enzyme velocity can often be described by the expression

$$\frac{d[P]}{dt} = \frac{V_{max}[S] + V'_{max}\left(\frac{[S]^2}{K_i'}\right)}{K_m + [S]\left(1 + \frac{K_m}{K_i}\right) + \left(\frac{[S]^2}{K_i'}\right)} \quad (1.13)$$

where V_{max} is the maximum velocity of the reaction when the allosteric site is empty, V'_{max} is the maximum velocity when the allosteric site is filled, and K_i and K'_i are the equilibrium dissociation constants for substrate binding at the allosteric site when the active site is empty and filled, respectively. [28]

1.1.2 Enzyme Activity Assay

1.1.2.1 Techniques for Measurement Enzyme Activity

Most enzyme assays measure the concentrations of substrate and/or product as a function of time. The rates of disappearance and/or appearance give the enzyme velocity, which can be fitted according to **Equations 1.1** or **1.4**. Note that care must be taken in the choice of enzyme and substrate concentrations in order to ensure that both K_m and k_{cat} can be robustly extracted from the data.[29] These experiments can be classified in two types: continuous (or real-time) and discontinuous assays.[30] In a continuous assay, the concentrations of substrates or products are measured in the reaction mixture at the same time as catalysis proceeds. For the most part, they employ spectroscopies, such as fluorimetry, UV/vis absorption, or nuclear magnetic resonance, and rely on substrates and products having different spectroscopic signatures.[31-34] While this is sometimes true in the native reaction, in many cases continuous assays require experimental modifications. Substrates can be chemically altered so that they change color or fluoresce when converted to products.[34] While convenient, this approach has the drawback that a customized substrate must be produced for each enzyme of interest, and non-native chromogenic or fluorogenic substrates do not necessarily have the same reaction kinetics

as the natural substrate. Alternatively, in coupled enzyme assays, the reaction mixture includes secondary enzymes that accept the product of the first enzymatic reaction as a substrate and produce downstream spectroscopic changes, such as the interconversion of NAD^+ and NADH that have very different extinction coefficients for light at 340 nm.[32, 35] This approach allows native substrates to be used, but the assay places limitations on the composition of the reaction mixtures, for example product inhibition or activation studies are impossible,[35] and accurate results depend on choosing appropriate concentrations of the coupled enzymes and secondary substrates. When it is not possible to monitor substrate or product concentrations in real time, discontinuous enzyme assays must be used. In these experiments, the reaction is quenched at various time points after initiation and the substrates and products are separated by an ancillary technique, such as liquid chromatography, gel electrophoresis, centrifugation, or mass spectrometry, [36-38] and quantified, for instance spectroscopically, radiometrically, or by an immunosorbent assay.[39-41] These additional steps add time, expense, and uncertainty to the characterization process.

Isothermal titration calorimetry (ITC) is well known as a powerful tool for studying host/guest binding interactions, but has recently gained in popularity as a general and

versatile kinetic assay [42-44]. ITC has the advantage of directly measuring the heat flow produced by catalysis in real time [44, 45]. Since most chemical reactions are either exothermic or endothermic, ITC can be applied to study virtually any enzymatic reaction, without the need for customized reporter molecules, additional coupled enzymes, or post-reaction separation. Furthermore, kinetic ITC experiments can be performed with conventional dilute enzymatic reaction mixtures, even with opaque samples, and require far less enzyme than ITC binding studies.[46]

1.1.2.2 Experimental Approaches for Measuring Enzyme Activity

There are three types of experimental approach that are commonly applied in activity assays:[47] 1) Initial rate experiments measure the initial rate of the product formation during a short period following initiation of the reaction. Typically, the reaction mixture contains a large excess amount of substrate over the enzyme in order to achieve a quasi-steady state condition ($[S]_t \approx [S]_0$). [48] The kinetic parameters can be obtained through a set of experiments under varying concentration of substrate, as illustrated in **Figure 1.3 a)**. 2) Progress curve experiments,[49] measure the progress of product formation ($[P]_t=0 \rightarrow [P]_t=[S]_0$) or the substrate depletion ($[S]_t=[S]_0 \rightarrow [S]_t=0$) during the entire

reaction time. If the initial concentration of substrate is higher than K_m (usually, $\geq 2.5K_m$) [49], the full kinetic curve can be observed, and the V_{max} and K_m obtained, as shown in **Figure 1.3 b)**. Conversely, if the substrate concentration lower than K_m, only the linear region of the kinetic curve is observed, and the ratio of V_{max}/ K_m is defined. 3) Transient kinetics experiments, measure the burst rate during the initial phase before the reaction reaches steady state. In order to observe the rapid burst phase, typically, a substantially high enzyme concentration is needed. This experiment approach requires a rapid mixing/observation technique (e.g. quench flow method).

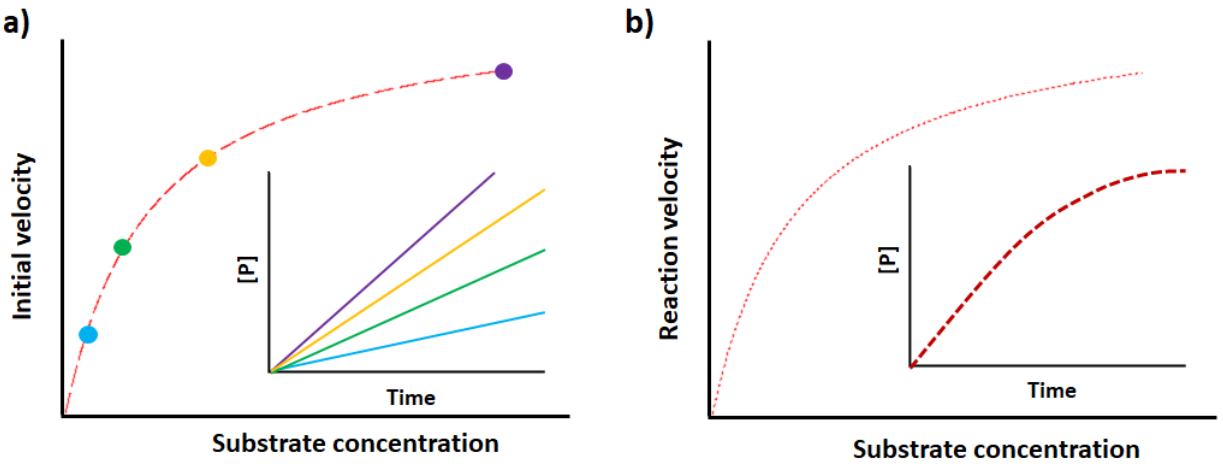

Figure 1.3 Experimental approaches used to study enzymatic reaction kinetics. a) initial rate experiments **b)** progress curve experiments.

1.2 Enzyme kinetics by Isothermal Titration Calorimetry (ITC)

1.2.1 Instrumentation

1.2.1.1 ITC Instrument

ITC instruments measure in real time the thermal power that results when one solution (in a syringe) is titrated into another (in a sample cell), as illustrated in **Figure 1.4**. A pair of cells, typically coin-shaped or cylindrical with volumes on the order of 200 to 1400 μL, are termed the sample and reference cells and contain the analyte solution and reference buffer (or pure water) respectively.[50, 51] The cells are housed inside a thermostated adiabatic jacket, that is maintained at a temperature slightly below the user-specified value for the cells. Electric resistive heaters, termed the feedback and reference heaters are located on the outer surfaces of the sample and reference cells, respectively, and must supply a constant flow of heat to maintain the cell temperatures at their set point. A Seebeck device sandwiched between the two cells detects any differences in temperature (ΔT) and modulates the power supplied to the feedback heater in order to keep the temperatures of the two cells identical. An automated injection syringe protrudes into the sample cell, which is stirred either by rotation of the paddle-shaped syringe, or

by the action of a separate propeller, depending on the make and model of the instrument. A series of injections (typically between 1 and 20 μL) is made into the sample cell. If the reaction between the injectant and analyte is exothermic, there will be a concomitant drop in the power supplied by the feedback heater to maintain a constant temperature. Conversely, if the reaction is endothermic, there will be an increase in feedback power. Once the reaction is complete or the rate becomes negligible, and no further heat is produced or absorbed in the sample cell, the feedback power returns to baseline.

The raw output of an ITC instrument is the feedback power measured as a function of time (typically at 1 second intervals). When characterizing binding or reaction thermodynamics, the deflection of the ITC signal from baseline is integrated over the entire injection, and is used to extract enthalpy differences between the unreacted and reacted states (i.e. free vs bound or substrates vs products). When characterizing kinetics, the instantaneous output power is interpreted in terms of the reaction velocity, since the rate of heat production or absorption in sample cell is directly proportional to the rate of the reaction. This is slightly complicated by the fact that the ITC signal lags behind heat events in the cell, however there are several approaches to overcoming this issue, as discussed in later sections. Furthermore, it should be noted that obtaining accurate

reaction rates requires accurate heat rates, so it is important to calibrate the calorimetric response. [52]

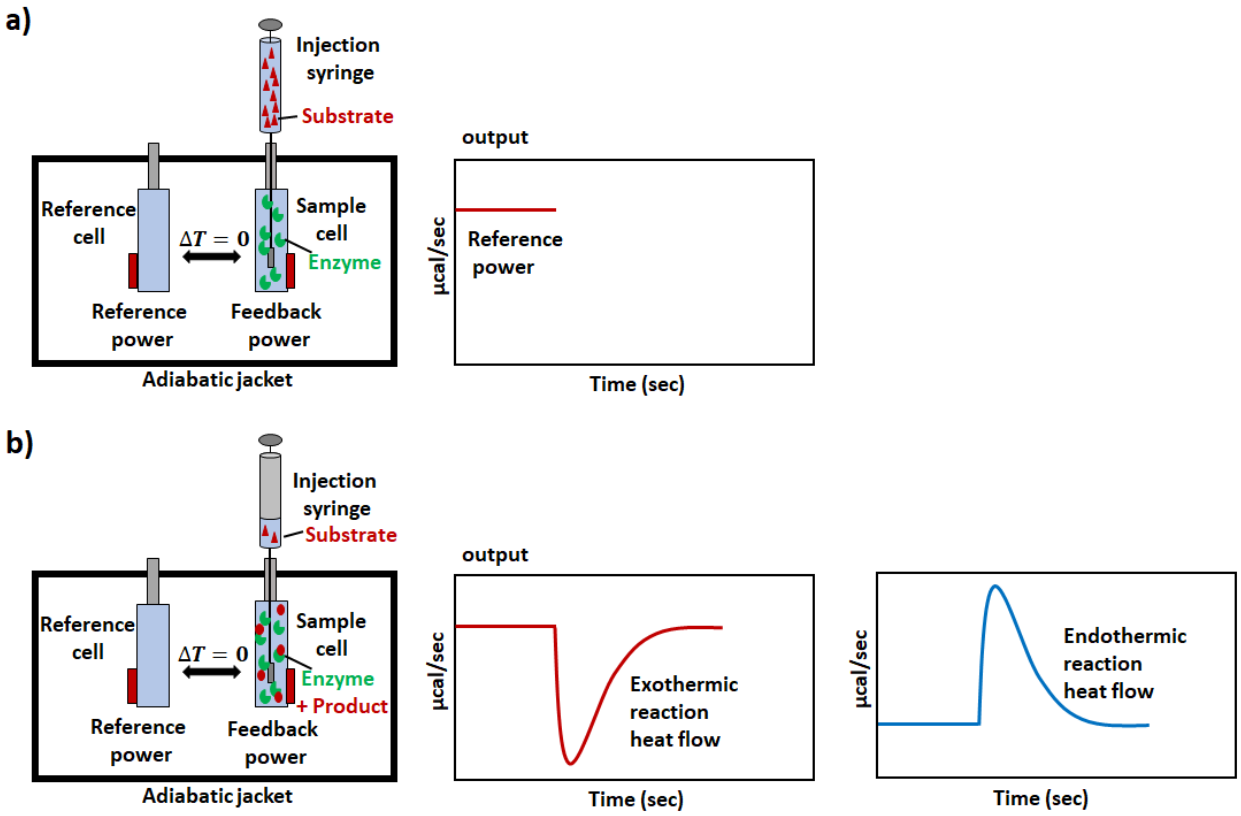

Figure 1.4. A typical ITC enzyme kinetics experiment. a) Before injection of the substrate into the sample cell, the flat baseline shown that the feedback power on the sample is equal to the constant power on the reference cell. **b)** The reaction is initiated when substrate in the syringe is injected into the sample cell containing enzyme. If the reaction is exothermic (endothermic), less (more) feedback power must be supplied to the sample cell to keep it at the same temperature as the reference cell. The instantaneous value of the feedback power is the ITC output.

1.2.1.2 Current ITC Instruments

There are a variety of models of ITC instruments currently available on the market, most of them from Malvern instruments and TA instruments. In particular, there are four models made by Malvern instruments: VP-ITC, ITC-200, PEAQ-ITC and PEAQ-ITC automated; and two model made by TA instruments: Affinity ITC and Nano ITC. All the ITC models operate under the same principle as describe above, with cell temperatures from 2°C to 80°C. [50, 51] However, the cells and syringe volume, stirring speed, noise level and response time are different in each model, and summarized in **Table 1.1**.

Table 1.1 Isothermal Titration Calorimetry parameter specifications.[50, 51]

Model	Cell volume (µL)	Syringe volume (µL)	Stir speed (rpm)	Noise level ($nCals^{-1}$)	Response time (s)
VP-ITC	1400	280	0 to 1088	0.5	20
ITC-200	200	40	0 to 1500	0.2	10
PEAQ-ITC	200	40	0 to 400	0.15	8
PEAQ-ITC Automated	200	40	0 to 400	0.15	8
Nano ITC (standard volume)	1000	100 or 250	0 to 400	0.6	18
Nano ITC (low volume)	190	50	0 to 400	0.3	11
Affinity ITC (standard volume)	1000	up to 250	0 to 200	0.6	18
Affinity ITC (low volume)	190	up to 250	0 to 200	0.3	11

1.2.2 Methods

1.2.2.1 Background

The instantaneous rate of heat production in the ITC sample cell, dQ/dt, is directly proportional to the reaction velocity (v_0=d[P]/dt) and the enthalpy change of the reaction catalyzed ($\Delta_r H = H_{product} - H_{substrate}$), according to

$$\frac{dQ}{dt} = V_{cell}\Delta_r H \frac{d[P]}{dt} \quad (1.14)$$

where V_{cell} is the volume of the sample cell. Thus with ITC-derived dQ/dt values obtained as a function of time, it is straightforward to precisely calculate enzyme velocity at any point in the experiment, provided $\Delta_r H$ and V_{cell} are known. This is obtained from the integrated area of an ITC peak obtained by injecting a known amount of substrate into a sample cell containing sufficient enzyme to rapidly convert it entirely to product,

$$\Delta_r H = \frac{\int_{t=0}^{\infty} \frac{dQ}{dt} dt}{n_S} \quad (1.15)$$

where n_S is the number of moles of substrate injected. In their seminal 2001 paper, Todd and Gomez describe two main approaches for designing ITC experiments that rapidly measure v_0 as a function of substrate concentration, allowing the enzyme kinetic parameters to be extracted by fits to **Equations 1.1** or **1.4**. They referred to these as

"Pseudo-first Order" and "Continuous" assays, although these terms have been largely replaced with "multiple injection" and "single injection" and we will use the latter terms here. A broad variety of ITC enzyme kinetics experiments have been developed in subsequent years, however most build on one or the other approach, so it is worthwhile to describe them in some detail, as foundational to the field. In both types of experiment, the reaction is initiated one or more times by mixing enzyme and substrate solutions via injection(s) from the syringe into the sample cell. However, the two methods differ in the concentrations of enzyme and substrate used, the appearance and information content of the data, and the analysis.

1.2.2.2 Multiple Injection Assays

In a multiple injection ITC enzyme kinetic assay, enzyme concentration in the cell is chosen to be sufficiently low but high enough to provide a good signal and substrate concentration in the syringe sufficiently high so that substrate depletion during the experiment is negligible.[44] As a result, the instantaneous heat (dQ/dt) and ITC signal are ideally constant (horizontal) between substrate injections and resemble a series of steps, one per injection (**Figure 1.5 a,b**). The displacement of each step relative to the initial

baseline is directly proportional to v_0, according to **Equation 1.14**. Exothermic and endothermic reactions give descending and ascending steps, respectively, if the raw feedback power is plotted as a function of time. The injections are designed such that early steps have $[S] << K_m$ and the final injections have nearly saturated the enzyme with $[S] >> K_m$. The concentration of substrate present in the sample cell after each injection is known from the concentration of substrate in syringe and volumes of all injections, while the reaction velocity can be read directly from the vertical position of each step, tracing out a complete Michaelis Menten curve (**Figure 1.5 c**). In practice, we find that the condition of negligible substrate consumption is met when $[E] \leq (10^{-4}\ s) \times K_m/k_{cat}$. Enzyme concentrations that are too high will give steps that slope towards the initial baseline, and will lead to overestimates in the amount of substrate present at each step. Enzyme concentrations that are too low will lead to disappearingly small steps that are obscured by instrument noise.

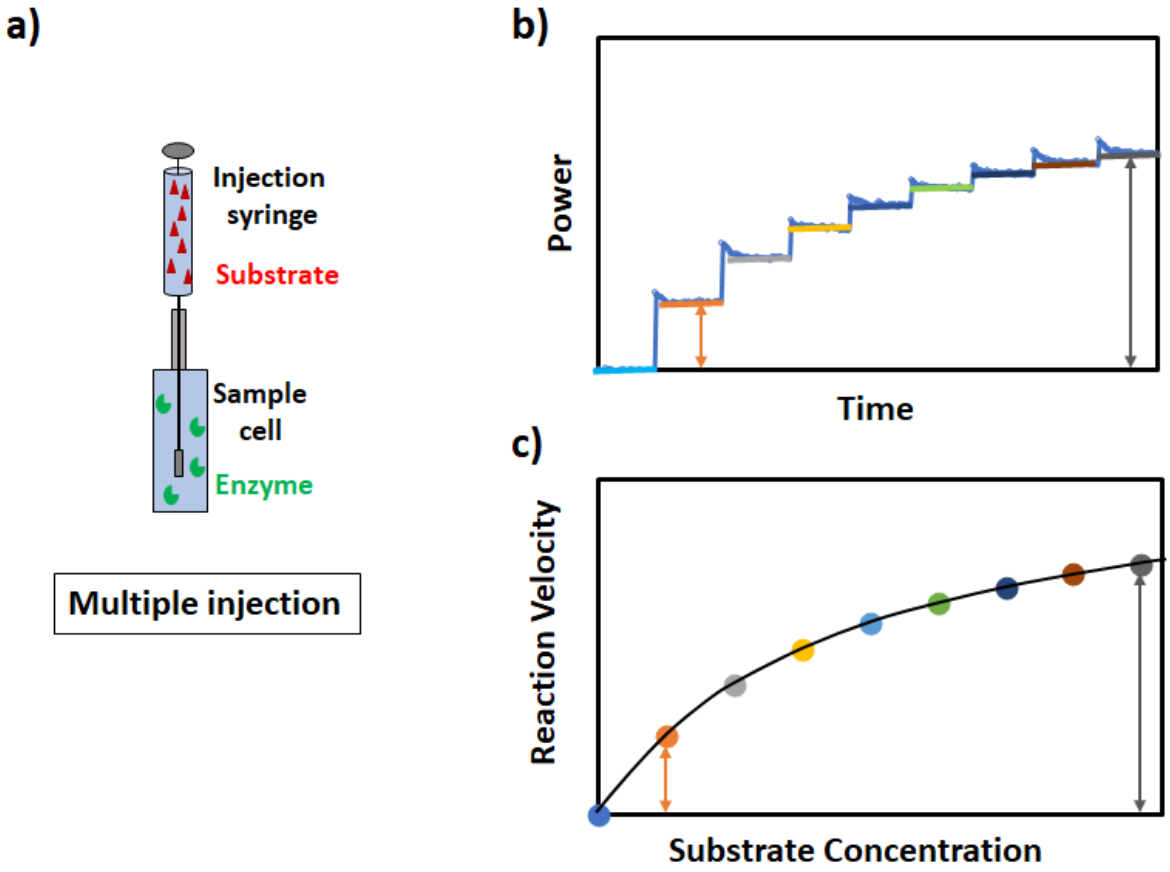

Figure 1.5. Multiple injection assays. a) The reaction is initiated when substrate in the syringe is injected into the sample cell containing enzyme. **b)** ITC thermogram generated by a multiple injection assay. **c)** Reaction velocity versus substrate concentration calculated from b).

There are several potential advantages to multiple injection assays compared to single injection ones. Firstly, they can accommodate substantially lower enzyme concentrations. It should be noted that $\Delta_r H$ must be determined in a separate measurement for multiple injection assays, while it is obtained directly from single injection data, thus comparable

amounts of enzymes can be consumed when all the necessary experiments are factored in. Secondly, the readout portions of the experiment, i.e. the approximately horizontal signals, are easy to distinguish from injection artifacts, which themselves tend to be smaller since less substrate is added in each injection. Finally, product accumulation is also less than for single injection assays. In a single injection assay, the amount of product present near the end of an ITC peak is necessarily several-fold greater than the K_m, since the enzyme is initially saturated with substrate. In contrast, much less substrate is converted to product during a multiple-injection experiment, ideally less than 5%.[53] Thus much less product is produced during a multiple injection assay compared to a single injection one. This is advantageous when strong product inhibition is present [54], although conversely, if product inhibition is of interest yet relatively weak, single injection assays would be the more sensitive option. Furthermore, since the data are drawn from post-injection periods where the enzyme velocities have stabilized to constant values, the timescale of the instrument response to changing heat flow can be ignored, simplifying the analysis. The main disadvantages are that the determination of a single pair of k_{cat} and K_m values requires a complete series of injections, making this technique relatively slow, and that the total amount of heat generated is much less, making it more susceptible to instrument noise.

1.2.2.3 Single Injection Assays

In a single injection ITC kinetic assay, the amount of enzyme is typically chosen to be large enough so that the injected substrate can be fully converted to product on the timescale of minutes or tens of minutes. The concentration of substrate is chosen so that the injection appreciably saturates the enzyme, i.e. the concentration of substrate in the sample cell immediately after the injection is several-fold higher than the K_m.[42, 55] Single injection assays can be initiated either by injecting substrate (syringe) into enzyme (cell) or enzyme (syringe) into substrate (cell) (**Figure 1.6 a**). Either case, the ITC feedback power exhibits a large deflection immediately after the injection, decreasing for exothermic reactions and increasing for endothermic ones due to the heat released or absorbed by catalysis. Large heat flows continue as long as the enzyme remains saturated with substrate. The signal gradually returns to the pre-injection baseline as the substrate is consumed as shown in **Figure 1.6 b**. It should be noted that single injection assays are usually performed with substantially more dilute enzyme, leading to peaks that are much broader, on the order of 20 to 60 minutes. Single-injection ITC data can be fitted directly by numerically integrating **Equation 1.1** to give [S](t) and v_0(t), and calculating dQ/dt as a function of time according to **Equation 1.14**, or using non-linear least squares optimization to find the values of K_m and k_{cat} that best reproduce the experimental values.

This approach has the advantage that the baseline and instrument response time can be fitted along with the MM/BH parameters. [55, 56] Alternatively, the concentration of substrate present at any time, *t*, during the heat spike can be calculated by recognizing that the fraction of total substrate remaining at *t* is equal to the ratio of the heat generated after time *t* relative to the total amount of heat generated during the heat spike:

$$[S](t) = \frac{\int_t^\infty \frac{dQ}{dt} dt}{\int_0^\infty \frac{dQ}{dt} dt} [S](t = 0) \quad (1.16)$$

Together the v_0 and [S] values trace out a complete Michaelis-Menten curve (**Figure 1.6 c**). We find that substrate is consumed sufficiently rapidly for this technique to be applied when $[E] \geq (10^{-2}\ s) \times K_m/k_{cat}$. When the concentration of enzyme is too low, the heat spike persists for such a long time (several hours or more) that the return to baseline is difficult to distinguish. However the enzyme must be at a low enough concentration so that the return to baseline takes at least seconds to tens of seconds.

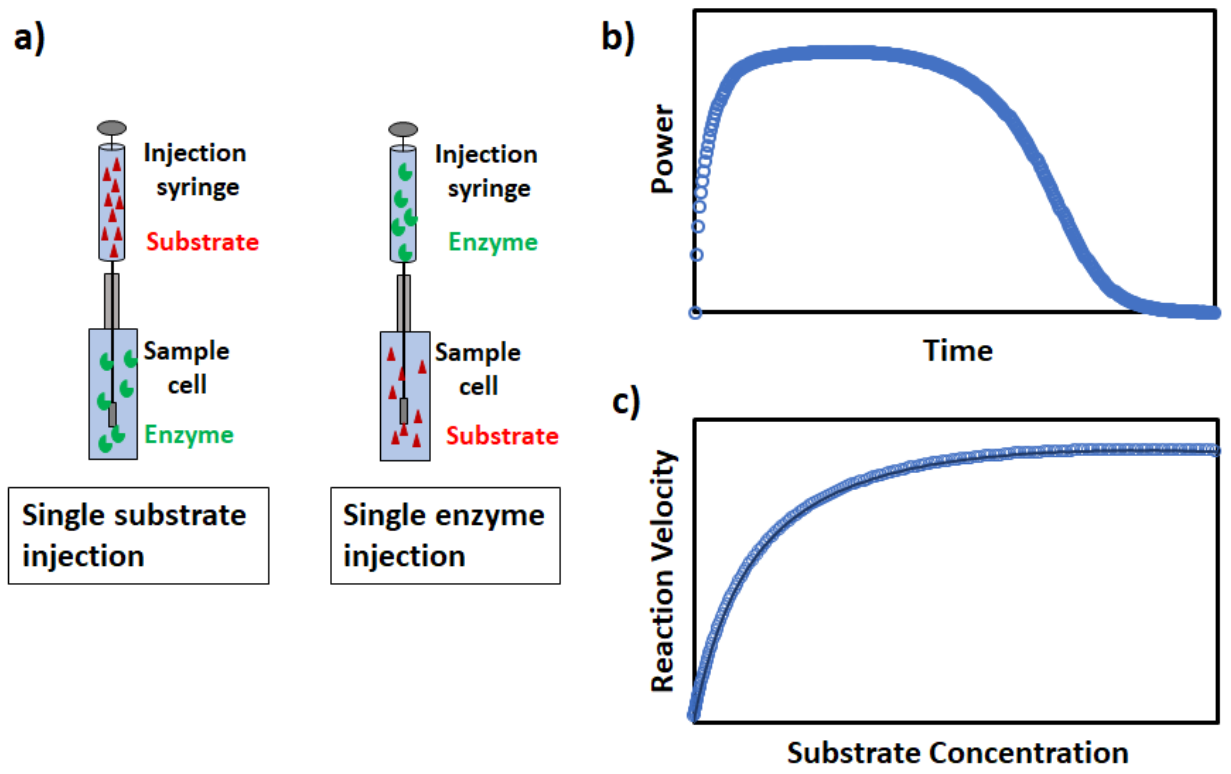

Figure 1.6. Single injection assays. a) The reaction is initiated when substrate in the syringe is injected into the sample cell containing enzyme (single substrate injection method), or enzyme in the syringe is injected into the sample cell containing substrate (single enzyme injection method). **b)** ITC thermogram generated by a single injection assay. **c)** Reaction velocity versus substrate concentration calculated from b).

The defining feature of this approach is that a full enzyme kinetic characterization is achieved in a single injection. Thus, with substrate in the syringe, it is straightforward to perform many single injection measurements within the same ITC experiment, simply by programming several injections (as many as 10 or 20) spaced at appropriate intervals. [42, 54, 57-64] For the sake of clarity, we will refer to these as recurrent single injection

experiments, to distinguish them from the very different approach termed multiple injection experiments (**Section 1.2.2.2**, above). At the simplest level, recurrent single injection experiments provide repeat measurements of enzyme kinetic parameters and improve the effective signal to noise ratio, although they do not replace true replicate experiments for estimating parameter uncertainties. Catalytic activity is repeatedly characterized over a period of time, giving information on the stability of the enzyme. [59] These experiments also provide a sensitive measure of product inhibition (or activation), since the product accumulates in the sample cell with each injection. [54, 64] The recurrent single injection approach can be adapted to rapidly characterize other types of inhibition as well, as described in **Section 1.3.3**. [42]

Alternatively, single-injection assays can be performed with enzyme in the syringe. This variation is preferable for substrates that are poorly soluble, or those that form suspensions rather than solutions, since they can remain at working (diluted) concentration in the sample cell with constant stirring throughout the experiment [62, 65-70]. Similarly, if very high substrate concentrations (100s of mM) are needed (eg. for enzymes with very large K_m values), it can be unfeasible to inject sufficient amounts of substrate without generating large injection heat artefacts, related to the large dilutions. Instead,

the concentrated substrate can be equilibrated in the sample cell and small injections of dilute enzyme can be used to initiate the reaction.[71, 72] Lastly, the barrel of the injection syringe lies exterior to ITC insulated jacket. If experiments are being performed at temperatures approaching the enzyme melting point, placing the enzyme in the syringe (which is at ambient temperature) allows it to spend as little time as possible at high and destabilizing temperatures.[68, 70, 73] It is worth noting that with enzyme in the syringe, recurrent single injection assays, as described above, are not possible, since the maximum concentration of substrate is necessarily present at the beginning of the measurement and cannot be replenished once conversion to product is complete. Another consideration is that small amounts of material can leak from the tip of the injection syringe during the long initial equilibration step, as well as between injections (although these delays are shorter). While this is true for both substrate- and enzyme-injection setups, the leakage is potentially far more serious with enzyme in the syringe, as this can act on the substrate in sample cell throughout the equilibration period, consuming much or all of it before the experiment has begun. In contrast, leakage of a few μL of substrate from the tip of the syringe does not dramatically imperil the procedure. Consequently, it is recommended to employ a buffer "plug" when injecting enzyme, a few μL of buffer that is drawn up into the needle after loading the syringe with an enzyme solution.[74, 75]

1.2.2.4 Rapid Enzyme Kinetics Measured by ITC

In many cases, the ITC signal can be considered nearly equal (and technically opposite) to the instantaneous rate of heat generation in the sample cell (i.e. ≈–dQ/dT). This approximation holds when the relevant portions of the heat signal vary slowly with time, such as in multiple injection assays and in cases where the peaks for single injection assays are broad (tens of minutes). For short reactions with rapidly varying heat signals, the situation becomes substantially more complicated. There are several physical processes that must occur before the heat generated by enzymatic catalysis is detected in the ITC output, [44, 76]These include a heat transfer delay, which is the length of time necessary for the solid phase thermocouple to detect the small change in sample cell temperature[77-80] and the electronic response that alters the power supplied to the feedback heater, driving the temperature gradient between the cells back to zero.[78] These steps are typically described collectively as an instrument response function, $f(t)$ which can be thought of as the instrument signal that would result from an instantaneous burst of heat being released in the sample cell. If the release of heat in the sample cell is described by the time-dependent function $h(t)$, then the instrument output is given by

$$g(t) = f(t) \otimes h(t) = \int_0^t f(\tau)g(t-\tau)d\tau \qquad (1.17)$$

where $\otimes$ indicates the convolution. The finite instrument response has the effect of spreading out the observed signal compared to the actual heat profile, such that peaks begin more gradually and die away more slowly. The instrument response function is often assumed to have a simple exponential shape, [76, 79, 81-83] $f(t) \propto exp\left\{-\frac{t}{\tau}\right\}$, where τ is referred to as the response time and is typically on the order of 5 to 15 seconds. [76]Accounting for the instrument response can be done in one of two ways. In the first, non-linear least squares fitting can be used to find the enzyme kinetic parameters that generate an instantaneous heat function, $h(t)$, which when convoluted with the assumed instrument response function, $f(t)$, best reproduces the ITC peak shape, $g(t)$. In the second, one can use the Tian equation and the assumed value of τ to mathematically remove the spreading effect of the instrument response.[84]

Our lab has recently shown that the assumption of a simple exponential response function is incompatible with experimental ITC peak shapes, and that $f(t)$ is a more complicated function of time.[56] Di Trani *et al*. termed this approach an empirical response model (ERM), and it reproduces ITC peaks quantitatively, producing sub-second time resolution.[56] This approach is only really necessary when measuring reactions that take place on the same timescale as the instrument response (i.e. roughly less than 20-30

seconds). For slow reactions that take tens of minutes or more to complete, the instrument response can be largely ignored, while for intermediate timescale reactions, the approximation of a single instrument response time, τ, is adequate.

An alternative approach, termed initial rate calorimetry (IrCal), avoids the issue of modeling the instrument response function altogether.[85] Honarmand *et al.* found empirically that the initial slope of the ITC signal is proportional to the peak velocity of the enzyme after the injection. The constant of proportionality can be determined by calibration experiments. A series of substrate injections of different sizes is made, and the initial slopes of the injections reveal how the ν_0 varies with [S]. One drawback of this approach is that each injection gives only a single ν_0 value, in contrast to a typical ITC single injection assay, which yields tens to hundreds of ν_0 values at different [S].

1.3 ITC Enzyme Kinetics Applications

1.3.1 Overview

A comprehensive search of the scientific literature and identified 73 publications between 2001 and 2019 reporting ITC-derived kinetic data on 59 different enzymes including hydrolases, transferases, oxidoreductases, lyases, ligases, and a protein folding

chaperonin are listed in **Table 1.2**. The authors explained their choice of ITC with a variety of reasons, including that ITC can represent the only continuous assay available, that it can exploit the native substrate where alternative continuous assays require chemically-modified chromogenic or fluorogenic substrates, that ITC avoids potential artifacts associated with coupled enzyme assays, and that ITC allows continuous assays to be performed on heterogeneous and spectroscopically opaque mixtures. Multiple injection-type ITC experiments were used for 35 enzymes, single injection-type ITC experiments were used for 27 enzymes, and enzyme-injection assays were used for 8 enzymes. Several of these publications focused on the development of new ITC kinetics approaches, such as IrCal and ERM above, and others are described below. Many of these studies focused on characterizing homogeneous enzymes exhibiting classical MM/BH kinetics. However many others described more complex systems, such as enzymes with cooperative kinetics, .[56, 61, 63, 71, 72, 86] those interacting with allosteric effectors or inhibitors,[27, 42, 71, 72, 87-89] and those in heterogeneous media, such as insoluble substrate [69, 90-93] or even living cells. [94-97]

Table 1.2. ITC Enzyme Kinetics Publications

Enzyme Class	Reaction	Enzyme	Organism	Reference	Advantage of ITC	Method
Hydrolase						
Esterase	hydrolysis of ester bond	Phosphotriesterase (OpdA)	*Agrobacterium radiobacter*	[98]	Traditional uses chromogenic Modified substrate.	Multiple injection; Single substrate injection; Single enzyme injection
		Glycerophospodiest-erase (GpdQ)	*Enterobacter aerogenes*	[98]	Same as above	Multiple injection; Single substrate injection
		Cyclic nucleotide-diesterase (Rv0805)	*Mycobacterium tuberculosis*	[98]	Same above	Multiple injection; Single substrate injection
		Phosphodiesterase (PDE1)	*Bos taurus*	[99, 100]		Multiple injection
		alkaline phosphatase	*Bos taurus*	[85]		others
		RNases (ribonucleases)	*Bos taurus*	[25, 64]		Single substrate injection; Modified single substrate injection
		Acetylcholinesterase (AChE)	*Electrophorus electricus*	[101, 102]	Neither the product nor substrate of AChE are suitable for direct	Multiple injection; Single substrate injection

					spectrophotometric evaluation.	
		sulfatases	*Patella vulgate*	[85]		others
Glycosylase	hydrolysis of glycosyl compounds	Pullulanase	*Klebsiella pneumoniae*	[68, 70, 73]	Entangled alginate medium and immobilized, insoluble support matrix.	Single enzyme injection
		exo-polygalacturonases (PGs)	*Rhizopus oryzae*	[103]	The using of reducing sugars (e.g. dinitrosalicylic acid, Somogyi–Nelson) may overestimate or underestimate reducing sugars.	Multiple injection; Single substrate injection
		nucleoside hydrolase (MtIAGU-NH)	*Mycobacterium tuberculosis*	[104]		Single enzyme injection
		α-Amylase	*Drosophila melanogaster; Homo sapiens; Sus scrofa*	[65-67]	Conventional α-Amylase activity uses a modified substrate (e.g. chromophore-containing (CNP) maltoheptaose), which may influence the binding and catalysis mechanisms.	Single enzyme injection
		sialidase	*Arthrobacter ureafaciens*	[105]		Multiple injection

		Invertase	*Saccharomyces cerevisiae*	[59]	Membrane immobilized enzyme.	Modified single substrate injection
		Chitinases	*Arthrobacter sp. TAD20; Serratia marcescens; Serratia marcescens*	[69, 106]	Insoluble substrate.	Single enzyme injection
		β-glucosidase (BG)	*Pyrococcus furiosus; Thermobifida fusca; Prunis dulcus*	[28, 107, 108]	Immobilized enzyme.	Multiple injection; Single substrate injection
		xylanase	*Aspergillus aculeatus*	[109]	Chemical-reducing-end sugars are not always reliable.	Multiple injection
		endo-Glucanases (EGs)	*Trichoderma reesei*	[93]	The conventional uses a Modified substrate.	Single substrate injection
		Cellulases	*Hypocrea jecorina; Trichoderma reesei; Aspergillus niger;*	[90, 92]	No alternative simple and quantitative to characterize a saccharification of cellulosic biomass.	Single substrate injection
		cellobiohydrolase (Cel6A)	*Hypocrea jecorina*	[91]	The use of chromogenic substrates or modified oligosaccharides do not reflect the enzymatic activity of complex substrates. ITC uses a	Multiple injection; Single substrate injection

					native substrate (e.g. soluble, insoluble, and complex substrate).	
Epoxide hydrolase	hydrolysis of trans-substituted epoxides	epoxide hydrolase (hsEH)	*Homo sapiens*	[58]	Conventional uses LC-MS/MS	Single substrate injection; Modified single substrate injection
Acid anhydride hydrolases	hydrolysis of acid anhydride	Nucleoside triphosphate diphosphohydrolases (NTPDases)	*Rattus norvegicus*	[110]		Multiple injection
		Lupin Diadenosine 5',5-P1, P4-Tetraphosphate Hydrolase (Ap4A)	*Lupinus angustifolius*	[111]		Multiple injection; Single substrate injection
Proteases / Peptidases	Hydrolysis of peptide bonds	Trypsin	*Bos Taurus*	[42, 55-57, 60, 112]	Conventional real-time uses modified chromogenic substrates.	Multiple injection; Single substrate injection; Modified single substrate injection Others (ERM)
		Nattokinase (NK)	*Bacillus subtilis*	[113]		Modified single substrate injection
		Prolyl carboxypeptidase (PRCP)	*Homo sapiens*	[114]		Multiple injection

		prolyl oligopeptidase (POP)	*Homo sapiens*	56, 88		Modified Multiple injection; Single substrate injection; Others (ERM)
		Pepsin	*Sus scrofa*	115		Multiple injection; Single substrate injection
		d, d-dipeptidase enzyme VanX	*Enterococcus faecalis; vancomycin-resistant Enterococci*	94	Conventional uses capillary electrophoresis. *In vivo* application of ITC.	Single substrate injection
Amido-hydrolase	hydrolysis of amide or amine bonds	β-lactamase	*Halophile Chromohalobacter sp. 560; Pseudomonas aeruginosa; Escherichia coli; Staphylococcus aureus; Acinetobacter baumannii*	95-97, 116, 117	*In vivo* ITC application.	Multiple injection; Single substrate injection
		Urease	*Sporosarcina pasteurii*	118, 119		Multiple injection
		Maleamate Amidohydrolase (NicF)	*Bordetella bronchiseptica*	120		Multiple injection

deaminase	Removal of an amino group	dCMP deaminase	*Schistosoma mansoni*	[87]		Multiple injection
Transfer-ases						
Phospho-transferase	transfer of phosphate groups	Gluconokinase	*Homo sapiens*	[121]	Conventional uses coupled enzymes.	Multiple injection
		Hexokinase (HK)	*Saccharomyces cerevisiae*	[44, 122, 123]	The use of labeled substrates caused a large variation of K_m for glucose and fructose[124].	Multiple injection; Single substrate injection
		Arginine kinase	*Litopenaeus vannamei*	[125]		Multiple injection
		aminoglycoside 3′-phosphotransferase-IIIa (APH (3′)-IIIa)	*Enterococcus faecalis*	[54]	ITC allows real-time measurement of ADP interactions (unlike coupled)	Modified single substrate injection
		pantothenate kinases (*Ec*PanK, *Pa*PanK)	*Pseudomonas aeruginosa, Escherichia coli*	[54]	Same as above	Modified single substrate injection
		protein kinase C	*Rattus norvegicus*	[126]		Modified single substrate injection
		pyruvate kinase	*Oryctolagus Cuniculus*	[71, 72]	Conventional uses coupled enzymes.	Single enzyme injection
		Taurocyamine kinase (PsTK)	*Phytophthora sojae*	[127]		Multiple injection

Glycosyl-transferase	formation of glycosidic linkages	glycogen phosphorylase (GP)	*Oryctolagus Cuniculus*	[128]	Custom-ITC based method directly monitored reaction kinetics in both glycogen synthesis and phosphorolysis directions.	Single enzyme injection
		Levansucrase (SacB)	*Bacillus subtilis*	[129]		Single substrate injection
Oxidoreductases						
	redox reaction	versatile peroxidase (VP)	*Bjerkandera adjusta*	[61, 63]	Complex humic substances substrates.	Single substrate injection
		Putrescine oxidase (PUO)	*Micrococcus rubens*	[130]	Immobilized enzyme	Single substrate injection
		dihydrofolate reductase (DHFR)	*Schistosoma mansoni*	[131]		Multiple injection
		recombinant human flavincontaining monooxygenase 3 (hFMO3)	*Homo sapiens*	[89]		Multiple injection; Single substrate injection
		diaphorase	*Clostridium kluyveri*	[85]		others
		laccase	*Trametes versicolor*	[85]		others

		phenylalanine hydroxylase (PHA)	*Homo sapiens*	[86]		Multiple injection; Single enzyme injection
		dihydroorotate dehydrogenase (TcDHODH)	*Trypanosoma cruzi*	[132]	ITC employs native substrate.	Multiple injection
Lyase						
	elimination reaction	Adenylosuccinate lyase (SmADSL)	*Schistosoma mansoni*	[133]		Multiple injection
		Acetolactate synthase	*unknown*	[44]		Multiple injection
		Heparin lyase	*Flavobacterium heparinum*	[44]		Multiple injection
		Rubisco	*Rhodospirillum rubrum*	[44]		Multiple injection
Ligases						
	Covalently links two substrates	CTP synthase	*Lactococcus lactis*	[27]		Multiple injection
		pyruvate carboxylase	*Bos taurus*	[44]		Multiple injection
Isomerases						
		Chaperonin GroEL	*Escherichia coli*	[44]		Multiple injection

1.3.2 Allostery and Cooperativity

ITC represents a powerful tool for characterizing complex enzyme allosteric interactions. For instance, ITC was used to measure the kinetics of pyruvate kinase (PK) [71, 72] which catalyzes the transfer of a phosphate from phosphoenolpyruvate to ADP as part of the last step of glycolysis. Allosteric binding of the amino acid phenylalanine (Phe) shifts PK to an inactive form, and is believed to be related to cellular damage in the genetic disease phenylketonuria.[134, 135] Winzor and co-workers were interested in how the presence of osmolytes affected the active/inactive transition. PK has traditionally been studied using a coupled enzyme assay, which is suboptimal for studying the effects of high concentrations of osmolytes, since it is challenging to distinguish effects on PK from effects on the secondary enzymes of the coupled assay. ITC avoids these issues, since enzyme activity is detected directly. They performed enzyme injection assays (**Figure 1.7 a**), where the displacement in the baseline after enzyme is injected is proportional to the velocity of the reaction. While this approach avoids large injection artefacts, it is somewhat time consuming as separate experiment must be performed for each data point in **Figure 1.7 b**. They obtained standard MM/BH curves in the absence of Phe. In the presence of 6 mM Phe, the curve shifts to right, indicating a lower substrate affinity, and develops sigmoidal character, a hallmark of positive cooperativity. Interestingly, addition

of the osmolyte proline shifted the curve back to the original location, corresponding to a return of the inactive state to the active state.

In another example, Di Trani *et al*. recently used ITC to characterize prolyl-oligopeptidase (POP) a validated drug target for multiple myeloma,[43] allowing study of the native peptide substrate, rather than the chemically-modified colorogenic substrate analog that is typically used. The authors performed ITC single injection assays and found that at lower enzyme concentrations, data were well fit by the standard MM/BH equation, while at higher concentrations, cooperativity became more apparent, with $n>2$ at an enzyme concentration of 2 μM (**Figure1.7 4c,d**). At the high enzyme concentrations where this behavior becomes apparent, the reactions go to completion in 10 seconds or less, underlining the potential of ITC to characterize rapid reaction kinetics.[45]

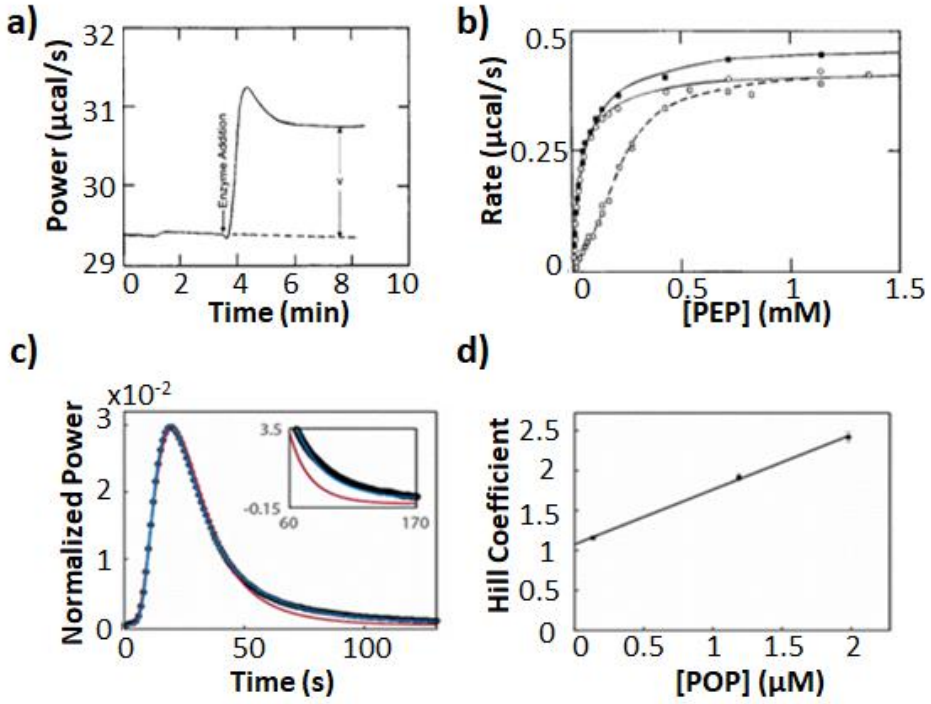

Figure 1.7. Non-MM/BH enzyme kinetics observed by ITC. a) Single enzyme injection experiments with pyruvate kinase in the syringe and phosphoenolpyruvate and ADP in the sample cell. The displacement of the horizontal baseline is proportional to the velocity of the enzyme **b)** Baseline displacements (ΔP) obtained at different [PEP] (O), in the presence of phenylalanine as an allosteric effector (□), and in the presence of phenylalanine and proline as a molecular crowding agent (■). **c)** Single injection assay with substrate (thyrotropin releasing hormone) in the syringe and prolyloligopeptidase (POP) in the sample cell. Points are experimental data, red and blue curves are the best fits with classical MM/BH model, and cooperative model (Equation 1.12) with n=2.4, respectively. **d)** Dependence of the extracted Hill coefficient on POP concentration (0.125, 1.2, and 2 µM). Figure 1.7 a) and b) reproduced from Lonhienne *et al.* [72] with permission. Figure 1.7 c) and d) reproduced from Di Trani *et al.*[45] with permission.

1.3.3 Enzyme Inhibition

Characterization of enzyme inhibition can largely be accomplished with the experiments described in **Section 1.2.2**. For example, ITC was used to characterize inhibitors of pancreatic α-amylase, which hydrolyses starches into monosaccharides in the gut.[67] It has been proposed that a variety of polyphenol plant metabolites inhibit α-amylase, slowing glucose absorption by the intestine, and reducing spikes in insulin levels with implications for the management of diabetes.[136] The authors tested a panel of naturally occurring polyphenols, together with the known potent α-amylase inhibitor acarbose. They used a single injection assay where α-amylase was injected into 1 mM trisaccharide substrate, with or without 100 μM of each phenolic inhibitor. The resulting ITC isotherms are shown in **Figure 1.8 a** and MM/BH plots calculated from these data are shown in **Figure 1.8 b**. Interestingly, all of the polyphenols affected both the k_{cat} of the enzyme (indicated by the height of the asymptote in **Figure 1.8 b** and the K_m, indicating mixed modes of inhibition, although the curves were not fitted quantitatively in this study. Mixed inhibition was also observed using experiments with a colorimetric assay detected by UV/vis spectroscopy. Note that while these assays were performed injecting enzyme into substrate pre-incubated with inhibitor, similar assays can also be performed by injecting substrate into enzyme pre-incubated with inhibitors. [89]

When ITC inhibition experiments are performed with the inhibitor loaded in the sample cell prior to data collection, then the procedure must be repeated several times in order to accurately measure inhibition parameters. This demands a considerable investment of time, since the cleaning, loading, equilibration, and data collection must be performed separately for each inhibitor concentration. Our lab has developed a procedure for considerably shortening this timeline, allowing much higher throughput of samples.[42] This approach is a variation of a standard recurrent single injection assay, with the modification that the syringe contains both substrate and inhibitor. A series of injections is made with each ITC peak giving a k_{cat} and K_m pair (**Figure 1.8 c,d**). The inhibitor accumulates with each injection, such that the activity of the enzyme decreases in each successive peak, and provides a thorough sampling of different inhibitor concentrations. Typical data are shown in **Figure 1.8 c**, with each peak clearly broader than the preceding one, reflecting slower catalysis by the enzyme (trypsin inhibited with benzamidine in this case). Each peak is complete within 5-10 minutes and a total data set can be collected in under an hour. The peaks were analyzed by fitting directly to the raw ITC data. The extracted k_{cat}^{app} was very similar for each peak, while the K_m^{app} increased linearly with increasing peak number and inhibitor concentration (**figure 1.8 d**), as expected for a competitive inhibitor (**Equation 1.9**). The y-intercept of the line is K_m and

the slope is K_m/K_i. Alternatively, the peaks can be deconvoluted using the empirical response function and converted to double-reciprocal plots in a model-free manner. The data give a series of straight lines that intersect at the y-axis, consistent with the competitive inhibition mechanism of benzamidine. This approach gives full kinetic characterization for as many as ten different inhibitor concentrations in a single experiment, providing assessment of inhibition mode and strength.

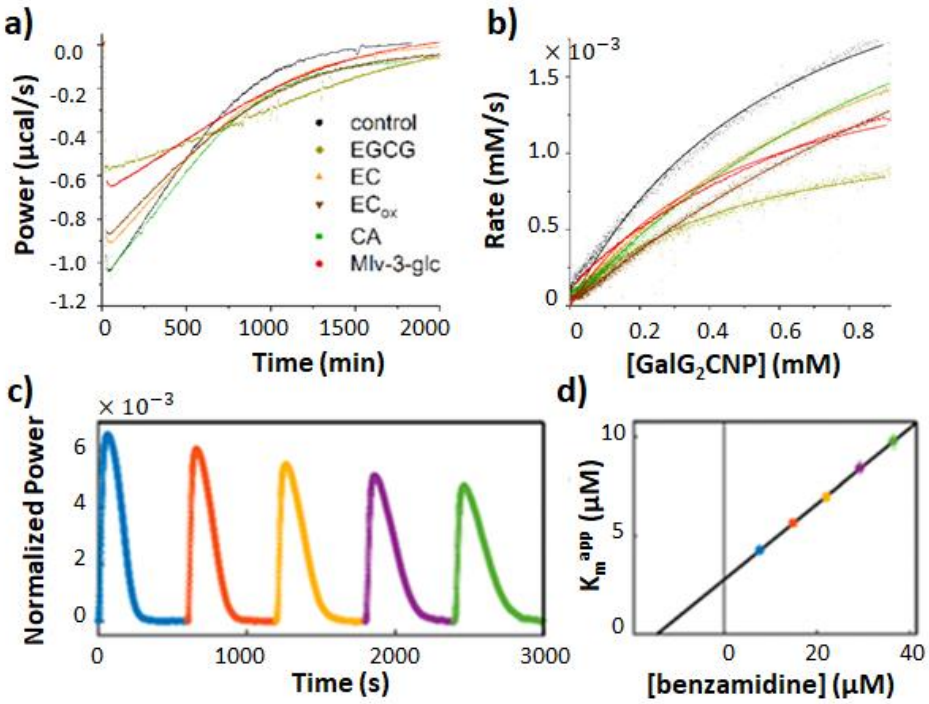

Figure 1.8. Enzyme inhibition characterized by ITC. a) Single enzyme injection assay with α-amylase in the syringe and the substrate2-chloro-4-nitrophenyl-maltoside (GalG2CNP) in the syringe together with a variety of inhibitors: ACA (acarbose), CA (chlorogenic acid), EC (epicatechin), ECox(oxidized epicatechin), EGCG

(epigallocatechin gallate), Mlv-3-glc (malvidin-3-glucoside). **b)** MM/BH curves calculated from the curves in (A). **c)** Single injection assay with substrate (benzoyl-L-arginine ethyl ester) and inhibitor (benzamidine) in the syringe and trypsin in the sample cell. **d)** K_m^{app} values extracted from direct fits to each of the injections (different colours) in (c). Figure 1. 8 a) and b) reproduced from Kaeswurm *et al.*[67] with permission. Figure 1. 8 c) and d) reproduced from Di Trani *et al.*[42] with permission.

1.3.4 Heterogeneous Mixtures

A unique aspect of ITC enzyme kinetic assays is their general ability to provide real-time measurements on opaque systems that are unsuitable for typical bulk spectroscopic techniques. One example of this is ITC enzyme kinetics experiments performed on suspensions of living cells. [94-97] Comparing the behavior of enzymes *in vitro* and *in situ* is critical for understanding how they work in living systems and can reveal how enzyme kinetics are tied to additional layers of biological dynamics. Furthermore, studying enzymes in the intact organism avoids the question of whether activity has been compromised by extraction and circumvents the need for purification steps at all. For instance, Zhang *et al.* used ITC to study the metallo-β-lactamase NDM-1 in living cultures of *E coli.* [96] NDM-1 cleaves carbapenems, providing bacterial resistance to these "last resort" β-lactam antibiotics. This study paves the way for using ITC both as a rapid

screen for inhibitors of antibiotic resistance genes, and also as a tool for probing the resistance profiles of clinical isolates.

Other examples of opaque reaction mixtures are those involving insoluble substrates [69, 90-93] or enzymes immobilized on insoluble matrices, [108, 130, 137, 138] where the components are combined as a suspension or slurry. These mixtures are of great industrial importance, in part because the insoluble carbohydrate polymers cellulose and chitin are the two most abundant organic compounds on earth, present in large quantities in vascular plants and arthropod exoskeletons, respectively. [139] Cellulose and chitin modifying enzymes have many potential applications in biofuel production, chemical upcycling, agriculture, and textile production.[140] Gerday and co-workers used ITC to characterize the activity of psychrophilic bacterial chitinases, which hydrolyse glycosidic bonds in chitin.[69] This study vividly illustrates how ITC data can give information not only on enzyme kinetics, but also on the dynamic processes to which the enzyme activity is linked.

1.4 Advantage of ITC for the Study of Enzyme Kinetics

The methods and examples discussed above illustrate the power and potential of ITC as a universal enzyme assay. ITC offers real-time monitoring of enzymatic reactions in

cases where other types of continuous assays are unavailable. This is exemplified by human soluble epoxide hydrolase,[58] where previous work had relied on a combination of quenching the reaction at various time points and analyzing the composition by liquid chromatography and tandem mass spectrometry.[141] The ability to employ natural substrates is another large asset for ITC. This is particularly true when the MM/BH parameters obtained for chemically modified colorigenic or fluorogenic substrate analogs do not match those obtained for the native substrate by ITC. For example, glycosidase activity can be measured spectrophotometrically with synthetic substrates, such as maltooligomer derivatives with chromogenic chloro-nitrophenyl (CNP) groups attached.[142-144] Separate studies on α-amylase and glycogen phosphorylase found the K_m values of the fluorogenic substrate analogs to be substantially lower than those of the native substrates determined by ITC, possibly due to interactions of the chromophore with the active site of the enzyme.[65,128] Thus ITC represents a simple way to accurately characterize how enzymes interact with their biologically relevant molecular partners. ITC also offers advantages for enzymes where the standard assay involves indirect readout with a coupled-enzyme system. This is particularly true when adding co-solutes or inhibitors that affect enzymatic activity since the secondary enzymes can be affected as well as the enzyme of interest, as discussed above for pyruvate kinase.[71, 72] In addition,

testing spectroscopically active inhibitors or other effector molecules can become a challenge when using spectrophotometric assays, i.e. with chromogenic or fluorogenic probes, or with coupled assays. In contrast, deeply-colored inhibitors are fully compatible with ITC inhibition assays.[110] Furthermore ITC's ability to characterize opaque samples further extends the reach of this technique beyond spectroscopically-accessible systems. The examples described above involving suspensions of live cells [94-97] and insoluble substrates[69, 90-93], illustrate how the surrounding milieu can influence enzyme activity and how ITC can be a probe of these more complex dynamics.

1.5 Thesis Objective

Isothermal titration calorimetry (ITC) is a powerful tool to study the kinetics of enzyme catalyzed reactions. It measures the heat released or absorbed in real time after the rapid mixing of enzyme and substrates. Since most chemical reactions are either exothermic or endothermic, ITC can be applied to virtually any enzyme/substrate pair, without the need to design customized reporter molecules, to couple the reaction to additional enzymes, or to perform any post-reaction separation. Furthermore, the diversity of the ITC experiments allows this technique to be widely applied to a broad

range of problems in enzymology, including the study of enzyme inhibition and activation mechanism, and/or understand the allosteric modulation and dynamic. In this thesis, four novel customized ITC-based methods: 1) transient assay, 2) activation assay, 3) single turn-over assay, and 4) 2-dimensional assay, were developed applied to study various enzyme kinetic properties. These assays overcome limitations of previous developed ITC methods and can be used to extend the application of ITC methods.

In Chapter 2, we developed a transient ITC assay to measure the effect of product ADP on kinase activities, an interaction which is challenging to be characterized by other methods. For the first time, an universal, reporter-free and continuous transient ITC assay was developed and applied for the probing of kinase inhibition or activation by ADP. Three kinases, aminoglycoside phosphotransferase (APH(3')-IIIa), pantothenate kinases from *E. coli* (*Ec*PanK), and *P. aeruginosa* (*Pa*PanK) were applied in this study. We found ADP to be an efficient inhibitor of all three kinases, with K_i values similar to or lower than the K_m values of ATP. Interestingly, ADP was an activator at low concentrations and an inhibitor at high concentrations of *Ec*PanK. This unusual effect was quantitatively modelled, and attributed to cooperative interactions between the two subunits of the dimeric enzyme. Importantly, our results suggest that at typical bacterial intracellular concentrations of ATP and ADP (approx. 1.5 mM and 180 μM respectively), all three

kinases are partially inhibited by ADP, allowing enzyme activity to rapidly respond to changes in the levels of both metabolites.

Kinases play central roles in many cellular processes, transferring the terminal phosphate groups of nucleotide triphosphates (NTPs) onto range of substrates. In the absence of substrates, kinases can also hydrolyse NTPs producing NDPs and inorganic phosphate. This may be related to the observation that NTP hydrolysis is metabolically unfavorable as it unproductively consumes the cell's energy stores. It has been suggested that substrate interactions could drive allosteric changes in NTP binding pocket, activating catalysis only when substrates are present. Structural data indeed show substrate-induced conformational rearrangements, however functional activity information is lacking. To better understanding this phenomenon, in Chapter 3, we developed an activation assay and a single turn-over assay to characterize ATP hydrolysis by the antibiotic resistance enzyme aminoglycoside-3'-phosphotransferase-IIIa (APH(3')-IIIa). We measured K_m, k_{cat}, and product inhibition constants and single-turnover kinetics in the presence and absence of non-substrate aminoglycosides (nsAmgs). We found that the presence of an nsAmg in the active site increased the chemical step of cleaving the ATP terminal phosphate by at least 10- to 20-fold under single-turnover conditions, supporting the existence of allosteric interactions that link substrate binding

to substantially enhanced catalytic rates. Our detailed kinetic data on the association and dissociation rates of nsAmgs and ADP shed light on the biophysical processes underlying the enzyme's ordered Bi-Bi reaction mechanism. Furthermore, they provide clues on how to design small-molecule effectors that could trigger efficient ATP hydrolysis and generate selective pressure against bacteria harboring the APH(3')-IIIa antibiotic resistance enzyme.

The Bi-substrates enzymatic reaction with two products form (Bi-Bi mechanism) is the commonest type in a biological process and accounts for over 60% of all known enzymatic catalysis.[145] Thus, understanding their kinetic properties is importance. In Chapter 4, a 2-dimensional ITC (2D-ITC) assay is developed which can completely kinetically characterize Bi-substrate enzyme in a single (2h) experiment. The 2D-ITC assay generates a full two dimensional map of the reaction velocity ν as a function of both substrates, enables the identification of the type of Bi-Bi mechanism (sequential or ping-pong). In addition, the discrimination of ordered versus random sequential mechanisms can be achieved based on their different behaviors with respect to product inhibition. This method correctly identified the random Bi-Bi mechanism for rMPK in a single experiment and yielded the values of quantitative kinetic parameters. We also obtained hyperbolic (MM/BH) kinetics in the absence of allosteric effector,

phenylalanine, and sigmoidal (non-MM/BH) kinetics in the presence of phenylalanine. The complete kinetic profiles both in the presence and absence of allosteric effector can be directly visualized and compared from the 2D reaction landscapes. This 2D-ITC assay can rapidly provide highly detailed and accurate information on Bi-substrate enzyme kinetics and is a potentially powerful assay for enzymologists.

1.6 References

1. Hunter, T., Protein kinases and phosphatases: The Yin and Yang of protein phosphorylation and signaling. *Cell* **1995,** *80* (2), 225-236.
2. Reyes-Turcu, F. E.; Ventii, K. H.; Wilkinson, K. D., Regulation and cellular roles of ubiquitin-specific deubiquitinating enzymes. *Annu. Rev. Biochem.* **2009,** *78*, 363-397.
3. Benhar, M.; Forrester, M. T.; Stamler, J. S., Protein denitrosylation: Enzymatic mechanisms and cellular functions. *Nat. Rev. Mol. Cell Biol.* **2009,** *10* (10), 721-732.
4. Capaldi, R. A.; Aggeler, R., Mechanism of the F1F0-type ATP synthase, a biological rotary motor. *Trends Biochem. Sci.* **2002,** *27* (3), 154-160.
5. Zheng, C. J.; Han, L. Y.; Yap, C. W.; Ji, Z. L.; Cao, Z. W.; Chen, Y. Z., Therapeutic targets: progress of their exploration and investigation of their characteristics. *Pharmacol. Rev.* **2006,** *58* (2), 259-279.
6. Choi, J.-M.; Han, S.-S.; Kim, H.-S., Industrial applications of enzyme biocatalysis: Current status and future aspects. *Biotechnology Advances* **2015,** *33* (7), 1443-1454.
7. Kuhad, R. C.; Gupta, R.; Singh, A., Microbial cellulases and their industrial applications. *Enzyme Res.* **2011**, 280696, 10 pp.
8. Sun, Y.; Cheng, J., Hydrolysis of lignocellulosic materials for ethanol production: a review. *Bioresource Technology* **2002,** *83* (1), 1-11.
9. Guzman-Maldonado, H.; Paredes-Lopez, O., Amylolytic enzymes and products derived from starch: a review. *Crit. Rev. Food Sci. Nutr.* **1995,** *35* (5), 373-403.
10. Kramer, S. J.; Pochapin, M. B., Gastric phytobezoar dissolution with ingestion of diet coke and cellulase. *Gastroenterol Hepatol (N Y)* **2012,** *8* (11), 770-772.
11. Voet, D.; Voet, J. G., *Biochemistry*. 4th edition. ed.; John Wiley & Sons: Hoboken, NJ, 2011.
12. Ulusu, N. N., Evolution of Enzyme Kinetic Mechanisms. *J Mol Evol* **2015,** *80* (5-6), 251-257.
13. Alberty, R. A., The relation between Michaelis constants, maximum velocities, and the equilibrium constant for an enzyme-catalyzed reaction. *J. Am. Chem. Soc.* **1953,** *75*, 1928-32.
14. Bisswanger, H., *Enzyme kinetics*. Wiley Online Library: 2001.
15. Robertson, J. G., Mechanistic basis of enzyme-targeted drugs. [Erratum to document cited in CA142:366594]. *Biochemistry* **2005,** *44* (24), 8918.

16. Guarnera, E.; Berezovsky, I. N., On the perturbation nature of allostery: sites, mutations, and signal modulation. *Current Opinion in Structural Biology* **2019,** *56*, 18-27.
17. Perutz, M. F., Mechanisms of cooperativity and allosteric regulation in proteins. *Quarterly Reviews of Biophysics* **1989,** *22* (2), 139-237.
18. Monod, J.; Wyman, J.; Changeux, J.-P., On the nature of allosteric transitions: a plausible model. *J Mol Biol* **1965,** *12* (1), 88-118.
19. Fenton, A. W., Allostery: an illustrated definition for the 'second secret of life'. *Trends in biochemical sciences* **2008,** *33* (9), 420-425.
20. DeDecker, B. S., Allosteric drugs: thinking outside the active-site box. *Chemistry & biology* **2000,** *7* (5), R103-R107.
21. Koshland Jr, D. E.; Nemethy, G.; Filmer, D., Comparison of experimental binding data and theoretical models in proteins containing subunits. *Biochemistry* **1966,** *5* (1), 365-385.
22. Guarnera, E.; Berezovsky, I. N., Allosteric drugs and mutations: chances, challenges, and necessity. *Current Opinion in Structural Biology* **2020,** *62*, 149-157.
23. Zhang, Y.; Doruker, P.; Kaynak, B.; Zhang, S.; Krieger, J.; Li, H.; Bahar, I., Intrinsic dynamics is evolutionarily optimized to enable allosteric behavior. *Current Opinion in Structural Biology* **2020,** *62*, 14-21.
24. Gerhart, J., From feedback inhibition to allostery: the enduring example of aspartate transcarbamoylase. *The FEBS Journal* **2014,** *281* (2), 612-620.
25. Spencer, S. D.; Raffa, R. B., Isothermal Titration Calorimetric Study of RNase-A Kinetics (cCMP → 3'-CMP) Involving End-Product Inhibition. *Pharmaceutical Research* **2004,** *21* (9), 1642-1647.
26. Lunn, F. A.; MacDonnell, J. E.; Bearne, S. L., Structural requirements for the activation of Escherichia coli CTP synthase by the allosteric effector GTP are stringent, but requirements for inhibition are lax. *Journal of Biological Chemistry* **2008,** *283* (4), 2010-2020.
27. Willemoës, M.; Sigurskjold, B. W., Steady-state kinetics of the glutaminase reaction of CTP synthase from Lactococcus lactis. *European Journal of Biochemistry* **2002,** *269* (19), 4772-4779.
28. Jeoh, T.; Baker, J. O.; Ali, M. K.; Himmel, M. E.; Adney, W. S., β-d-Glucosidase reaction kinetics from isothermal titration microcalorimetry. *Analytical Biochemistry* **2005,** *347* (2), 244-253.

29. Stroberg, W.; Schnell, S., On the estimation errors of KM and V from time-course experiments using the Michaelis–Menten equation. *Biophysical Chemistry* **2016,** *219*, 17-27.

30. Harris, T. K.; Keshwani, M. M., Chapter 7 Measurement of Enzyme Activity. In *Methods Enzymol*, Burgess, R. R.; Deutscher, M. P., Eds. Academic Press: 2009; Vol. 463, pp 57-71.

31. Shu, Q.; Frieden, C., Relation of Enzyme Activity to Local/Global Stability of Murine Adenosine Deaminase: 19F NMR Studies. *J Mol Biol* **2005,** *345* (3), 599-610.

32. Easterby, J. S., Coupled enzyme assays: a general expression for the transient. *Biochim Biophys Acta* **1973,** *293* (2), 552-8.

33. Seethala, R.; Menzel, R., A homogeneous, fluorescence polarization assay for Src-family tyrosine kinases. *Anal. Biochem.* **1997,** *253* (2), 210-218.

34. Reetz, M. T., Combinatorial and evolution-based methods in the creation of enantioselective catalysts. *Angew. Chem., Int. Ed.* **2001,** *40* (2), 284-310.

35. McKay, G. A.; Wright, G. D., Kinetic mechanism of aminoglycoside phosphotransferase type IIIa. Evidence for a Theorell-Chance mechanism. *J. Biol. Chem.* **1995,** *270* (42), 24686-92.

36. Hooff, G. P.; van Kampen, J. J. A.; Meesters, R. J. W.; van Belkum, A.; Goessens, W. H. F.; Luider, T. M., Characterization of β-Lactamase Enzyme Activity in Bacterial Lysates using MALDI-Mass Spectrometry. *Journal of Proteome Research* **2012,** *11* (1), 79-84.

37. Reetz, M. T.; Daligault, F.; Brunner, B.; Hinrichs, H.; Deege, A., Directed evolution of cyclohexanone monooxygenases: enantioselective biocatalysts for the oxidation of prochiral thioethers. *Angew Chem Int Ed Engl* **2004,** *43* (31), 4078-81.

38. Tauran, Y.; Anjard, C.; Kim, B.; Rhimi, M.; Coleman, A. W., Large negatively charged organic host molecules as inhibitors of endonuclease enzymes. *Chem. Commun. (Cambridge, U. K.)* **2014,** *50* (77), 11404-11406.

39. Butler, J. E., Enzyme-Linked immunosorbent assay. *J. Immunoassay* **2000,** *21* (2 & 3), 165-209.

40. Hastie, C. J.; McLauchlan, H. J.; Cohen, P., Assay of protein kinases using radiolabeled ATP: a protocol. *Nat. Protoc.* **2006,** *1* (2), 968-971.

41. Kerner, J.; Hoppel, C. L., Radiochemical malonyl-CoA decarboxylase assay: Activity and subcellular distribution in heart and skeletal muscle. *Anal. Biochem.* **2002,** *306* (2), 283-289.

42. Di Trani, J. M.; Moitessier, N.; Mittermaier, A. K., Complete Kinetic Characterization of Enzyme Inhibition in a Single Isothermal Titration Calorimetric Experiment. *Anal. Chem. (Washington, DC, U. S.)* **2018,** *90* (14), 8430-8435.

43. Di Trani, J. M.; De Cesco, S.; O'Leary, R.; Plescia, J.; do Nascimento, C. J.; Moitessier, N.; Mittermaier, A. K., Rapid measurement of inhibitor binding kinetics by isothermal titration calorimetry. *Nat Commun* **2018,** *9* (1), 893.

44. Todd, M. J.; Gomez, J., Enzyme kinetics determined using calorimetry: A general assay for enzyme activity? *Anal. Biochem.* **2001,** *296* (2), 179-187.

45. Di Trani, J. M.; Moitessier, N.; Mittermaier, A. K., Measuring Rapid Time-Scale Reaction Kinetics Using Isothermal Titration Calorimetry. *Anal. Chem. (Washington, DC, U. S.)* **2017,** *89* (13), 7022-7030.

46. Oezen, C.; Serpersu, E. H., Thermodynamics of Aminoglycoside Binding to Aminoglycoside-3'-phosphotransferase IIIa Studied by Isothermal Titration Calorimetry. *Biochemistry* **2004,** *43* (46), 14667-14675.

47. Schnell, S.; Chappell, M. J.; Evans, N. D.; Roussel, M. R., The mechanism distinguishability problem in biochemical kinetics: The single-enzyme, single-substrate reaction as a case study. *Comptes Rendus Biologies* **2006,** *329* (1), 51-61.

48. Waley, S. G., An easy method for the determination of initial rates. *Biochem J* **1981,** *193* (3), 1009-12.

49. Duggleby, R. G.; Clarke, R. B., Experimental designs for estimating the parameters of the Michaelis-Menten equation from progress curves of enzyme-catalyzed reactions. *Biochim. Biophys. Acta, Protein Struct. Mol. Enzymol.* **1991,** *1080* (3), 231-6.

50. TA, MICROCALORIMETRY: ITC & DSC. **2019**.

51. Malvern, MICROCAL ITC SYSTEMS:UNDERSTANDING BIOMOLECULAR INTERACTIONS. **2016**.

52. Demarse, N. A.; Quinn, C. F.; Eggett, D. L.; Russell, D. J.; Hansen, L. D., Calibration of nanowatt isothermal titration calorimeters with overflow reaction vessels. *Anal. Biochem.* **2011,** *417* (2), 247-255.

53. Hansen, L. D.; Transtrum, M. K.; Quinn, C.; Demarse, N., Enzyme-catalyzed and binding reaction kinetics determined by titration calorimetry. *Biochim. Biophys. Acta, Gen. Subj.* **2016,** *1860* (5), 957-966.

54. Wang, Y.; Guan, J.; Di Trani, J. M.; Auclair, K.; Mittermaier, A. K., Inhibition and Activation of Kinases by Reaction Products: A Reporter-Free Assay. *Analytical Chemistry* **2019,** *91* (18), 11803-11811.

55. Transtrum, M. K.; Hansen, L. D.; Quinn, C., Enzyme kinetics determined by single-injection isothermal titration calorimetry. *Methods* **2015,** *76*, 194-200.

56. Di Trani, J. M.; Moitessier, N.; Mittermaier, A. K., Measuring Rapid Time-Scale Reaction Kinetics Using Isothermal Titration Calorimetry. *Analytical Chemistry* **2017,** *89* (13), 7022-7030.
57. Maximova, K.; Wojtczak, J.; Trylska, J., Enzyme kinetics in crowded solutions from isothermal titration calorimetry. *Analytical Biochemistry* **2019,** *567*, 96-105.
58. Abis, G.; Pacheco-Gómez, R.; Bui, T. T. T.; Conte, M. R., Isothermal Titration Calorimetry Enables Rapid Characterization of Enzyme Kinetics and Inhibition for the Human Soluble Epoxide Hydrolase. *Analytical Chemistry* **2019,** *91* (23), 14865-14872.
59. Mason, M.; Scampicchio, M.; Quinn, C. F.; Transtrum, M. K.; Baker, N.; Hansen, L. D.; Kenealey, J. D., Calorimetric Methods for Measuring Stability and Reusability of Membrane Immobilized Enzymes. *Journal of Food Science* **2018,** *83* (2), 326-331.
60. Maximova, K.; Trylska, J., Kinetics of trypsin-catalyzed hydrolysis determined by isothermal titration calorimetry. *Analytical Biochemistry* **2015,** *486*, 24-34.
61. Siddiqui, K. S.; Ertan, H.; Charlton, T.; Poljak, A.; Daud Khaled, A. K.; Yang, X.; Marshall, G.; Cavicchioli, R., Versatile peroxidase degradation of humic substances: Use of isothermal titration calorimetry to assess kinetics, and applications to industrial wastes. *Journal of Biotechnology* **2014,** *178*, 1-11.
62. Pedroso, M. M.; Ely, F.; Lonhienne, T.; Gahan, L. R.; Ollis, D. L.; Guddat, L. W.; Schenk, G. J. J. J. o. B. I. C., Determination of the catalytic activity of binuclear metallohydrolases using isothermal titration calorimetry. **2014,** *19* (3), 389-398.
63. Ertan, H.; Siddiqui, K. S.; Muenchhoff, J.; Charlton, T.; Cavicchioli, R., Kinetic and thermodynamic characterization of the functional properties of a hybrid versatile peroxidase using isothermal titration calorimetry: Insight into manganese peroxidase activation and lignin peroxidase inhibition. *Biochimie* **2012,** *94* (5), 1221-1231.
64. Cai, L.; Cao, A.; Lai, L., An Isothermal Titration Calorimetric Method to Determine the Kinetic Parameters of Enzyme Catalytic Reaction by Employing the Product Inhibition as Probe. *Anal. Biochem.* **2001,** *299* (1), 19-23.
65. Lehoczki, G.; Szabó, K.; Takács, I.; Kandra, L.; Gyémánt, G., Simple ITC method for activity and inhibition studies on human salivary α-amylase. *Journal of Enzyme Inhibition and Medicinal Chemistry* **2016,** *31* (6), 1648-1653.
66. Commin, C.; Aumont-Nicaise, M.; Claisse, G.; Feller, G.; Da Lage, J.-L., Enzymatic characterization of recombinant α-amylase in the Drosophila melanogaster species subgroup: is there an effect of specialization on digestive enzyme? *Genes Genet. Syst.* **2013,** *88* (4), 251-259.

67. Kaeswurm, J. A. H.; Claasen, B.; Fischer, M.-P.; Buchweitz, M., Interaction of Structurally Diverse Phenolic Compounds with Porcine Pancreatic α-Amylase. *Journal of Agricultural and Food Chemistry* **2019,** *67* (40), 11108-11118.
68. Ali, G.; Rihouey, C.; Le Cerf, D.; Picton, L., Effect of carboxymethyl groups on degradation of modified pullulan by pullulanase from Klebsiella pneumoniae. *Carbohydrate Polymers* **2013,** *93* (1), 109-115.
69. Lonhienne, T.; Baise, E.; Feller, G.; Bouriotis, V.; Gerday, C., Enzyme activity determination on macromolecular substrates by isothermal titration calorimetry: application to mesophilic and psychrophilic chitinases. *Biochimica et Biophysica Acta (BBA) - Protein Structure and Molecular Enzymology* **2001,** *1545* (1), 349-356.
70. Ali, G.; Rihouey, C.; Larreta-Garde, V.; Le Cerf, D.; Picton, L., Molecular Size Characterization and Kinetics Studies on Hydrolysis of Pullulan by Pullulanase in an Entangled Alginate Medium. *Biomacromolecules* **2013,** *14* (7), 2234-2241.
71. Lonhienne, T. G. A.; Reilly, P. E. B.; Winzor, D. J., Further evidence for the reliance of catalysis by rabbit muscle pyruvate kinase upon isomerization of the ternary complex between enzyme and products. *Biophysical Chemistry* **2003,** *104* (1), 189-198.
72. Lonhienne, T. G. A.; Winzor, D. J., Calorimetric Demonstration of the Potential of Molecular Crowding To Emulate the Effect of an Allosteric Activator on Pyruvate Kinase Kinetics. *Biochemistry* **2002,** *41* (22), 6897-6901.
73. Ali, G.; Dulong, V.; Gasmi, S. N.; Rihouey, C.; Picton, L.; Le Cerf, D., Covalent immobilization of pullulanase on alginate and study of its hydrolysis of pullulan. *Biotechnology Progress* **2015,** *31* (4), 883-889.
74. Malvern, ITC-200 Microcalorimeter User's Manual. **2014**.
75. Malvern, VP-ITC Microcalorimeter User's Manual. **2010**.
76. Burnouf, D.; Ennifar, E.; Guedich, S.; Puffer, B.; Hoffmann, G.; Bec, G.; Disdier, F.; Baltzinger, M.; Dumas, P., kinITC: A New Method for Obtaining Joint Thermodynamic and Kinetic Data by Isothermal Titration Calorimetry. *J. Am. Chem. Soc.* **2012,** *134* (1), 559-565.
77. Ebrahimi, K.; Hagedoorn, P.-L.; Jacobs, D.; Hagen, W. R., Accurate label-free reaction kinetics determination using initial rate heat measurements. *Scientific reports* **2015,** *5*, 16380.
78. Wiseman, T.; Williston, S.; Brandts, J. F.; Lin, L.-N., Rapid measurement of binding constants and heats of binding using a new titration calorimeter. *Analytical Biochemistry* **1989,** *179* (1), 131-137.

79. García-Fuentes, L.; Barón, C.; Mayorga, O. L., Influence of dynamic power compensation in an isothermal titration microcalorimeter. *Analytical chemistry* **1998,** *70* (21), 4615-4623.

80. Freire, E.; Mayorga, O. L.; Straume, M., Isothermal titration calorimetry. *Analytical Chemistry* **1990,** *62* (18).

81. Vander Meulen, K. A.; Butcher, S. E., Characterization of the kinetic and thermodynamic landscape of RNA folding using a novel application of isothermal titration calorimetry. *Nucleic acids research* **2012,** *40* (5), 2140-2151.

82. Velázquez-Campoy, A.; López-Mayorga, O.; Cabrerizo-Vílchez, M., Determination of the rigorous transfer function of an isothermal titration microcalorimeter with peltier compensation. *Journal of thermal analysis and calorimetry* **1999,** *57* (1), 343-359.

83. López-Mayorga, O.; Mateo, P. L.; Cortijo, M., The use of different input signals for dynamic characterisation in isothermal microcalorimetry. *Journal of Physics E: Scientific Instruments* **1987,** *20* (3), 265.

84. Backman, P.; Bastos, M.; Hallen, D.; Lonnbro, P.; Wadso, I., Heat conduction calorimeters: time constants, sensitivity and fast titration experiments. *J Biochem Biophys Methods* **1994,** *28* (2), 85-100.

85. Honarmand Ebrahimi, K.; Hagedoorn, P.-L.; Jacobs, D.; Hagen, W. R., Accurate label-free reaction kinetics determination using initial rate heat measurements. *Scientific Reports* **2015,** *5* (1), 16380.

86. Pey, A. L.; Martinez, A., The activity of wild-type and mutant phenylalanine hydroxylase and its regulation by phenylalanine and tetrahydrobiopterin at physiological and pathological concentrations: An isothermal titration calorimetry study. *Molecular Genetics and Metabolism* **2005,** *86*, 43-53.

87. Scortecci, J. F.; Serrão, V. H. B.; Cheleski, J.; Torini, J. R.; Romanello, L.; DeMarco, R.; D'Muniz Pereira, H., Spectroscopic and calorimetric assays reveal dependence on dCTP and two metals (Zn2++Mg2+) for enzymatic activity of Schistosoma mansoni deoxycytidylate (dCMP) deaminase. *Biochimica et Biophysica Acta (BBA) - Proteins and Proteomics* **2017,** *1865* (11, Part A), 1326-1335.

88. Di, T. J. M.; De, C. S.; O'Leary, R.; Plescia, J.; do, N. C. J.; Moitessier, N.; Mittermaier, A. K.; do, N. C. J., Rapid measurement of inhibitor binding kinetics by isothermal titration calorimetry. *Nat Commun* **2018,** *9* (1), 893.

89. Catucci, G.; Sadeghi, S. J.; Gilardi, G., A direct time-based ITC approach for substrate turnover measurements demonstrated on human FMO3. *Chemical Communications* **2019,** *55* (44), 6217-6220.

90. Murphy, L.; Borch, K.; McFarland, K. C.; Bohlin, C.; Westh, P., A calorimetric assay for enzymatic saccharification of biomass. *Enzyme and Microbial Technology* **2010,** *46* (2), 141-146.

91. Murphy, L.; Baumann, M. J.; Borch, K.; Sweeney, M.; Westh, P., An enzymatic signal amplification system for calorimetric studies of cellobiohydrolases. *Analytical Biochemistry* **2010,** *404* (2), 140-148.

92. Murphy, L.; Bohlin, C.; Baumann, M. J.; Olsen, S. N.; Sørensen, T. H.; Anderson, L.; Borch, K.; Westh, P., Product inhibition of five Hypocrea jecorina cellulases. *Enzyme and Microbial Technology* **2013,** *52* (3), 163-169.

93. Murphy, L.; Cruys-Bagger, N.; Damgaard, H. D.; Baumann, M. J.; Olsen, S. N.; Borch, K.; Lassen, S. F.; Sweeney, M.; Tatsumi, H.; Westh, P., Origin of initial burst in activity for Trichoderma reesei endo-glucanases hydrolyzing insoluble cellulose. *J. Biol. Chem.* **2012,** *287* (2), 1252-1260.

94. Lv, M.; Zhang, Y.-J.; Zhou, F.; Ge, Y.; Zhao, M.-H.; Liu, Y.; Yang, K.-W., Real-time monitoring of D-Ala-D-Ala dipeptidase activity of VanX in living bacteria by isothermal titration calorimetry. *Analytical Biochemistry* **2019,** *578*, 29-35.

95. Wang, Q.; He, Y.; Lu, R.; Wang, W.-M.; Yang, K.-W.; Fan, Hai M.; Jin, Y.; Blackburn, G. M., Thermokinetic profile of NDM-1 and its inhibition by small carboxylic acids. *Bioscience Reports* **2018,** *38* (2).

96. Zhang, Y.-J.; Wang, W.-M.; Oelschlaeger, P.; Chen, C.; Lei, J.-E.; Lv, M.; Yang, K.-W., Real-Time Monitoring of NDM-1 Activity in Live Bacterial Cells by Isothermal Titration Calorimetry: A New Approach To Measure Inhibition of Antibiotic-Resistant Bacteria. *ACS Infectious Diseases* **2018,** *4* (12), 1671-1678.

97. Wang, W.-J.; Wang, Q.; Zhang, Y.; Lu, R.; Zhang, Y.-L.; Yang, K.-W.; Lei, J.-E.; He, Y., Characterization of β-lactamase activity using isothermal titration calorimetry. *Biochimica et Biophysica Acta (BBA) - General Subjects* **2017,** *1861* (8), 2031-2038.

98. Pedroso, M. M.; Ely, F.; Lonhienne, T.; Gahan, L. R.; Ollis, D. L.; Guddat, L. W.; Schenk, G., Determination of the catalytic activity of binuclear metallohydrolases using isothermal titration calorimetry. *JBIC Journal of Biological Inorganic Chemistry* **2014,** *19* (3), 389-398.

99. Brulfert, F.; Safi, S.; Jeanson, A.; Foerstendorf, H.; Weiss, S.; Berthomieu, C.; Sauge-Merle, S.; Simoni, É., Enzymatic activity of the CaM-PDE1 system upon addition of actinyl ions. *Journal of Inorganic Biochemistry* **2017,** *172*, 46-54.

100. Stateva, S.; Salas, V.; Benaim, G.; Menendez, M.; Solís, D.; Villalobo, A., Characterization of Phospho-(Tyrosine)-Mimetic Calmodulin Mutants. *PloS one* **2015,** *10*, e0120798.

101. de Almeida Neves, P. A.; Silva, E.; Beirão, P., Microcalorimetric Study of Acetylcholine and Acetylthiocholine Hydrolysis by Acetylcholinesterase. *Advances in Enzyme Research* **2017,** *2017*, 1-12.

102. Draczkowski, P.; Tomaszuk, A.; Halczuk, P.; Strzemski, M.; Matosiuk, D.; Jozwiak, K., Determination of affinity and efficacy of acetylcholinesterase inhibitors using isothermal titration calorimetry. *Biochimica et Biophysica Acta (BBA) - General Subjects* **2016,** *1860* (5), 967-974.

103. Mertens, J. A., Kinetic Properties of Two Rhizopus Exo-polygalacturonase Enzymes Hydrolyzing Galacturonic Acid Oligomers Using Isothermal Titration Calorimetry. *Applied Biochemistry and Biotechnology* **2013,** *170* (8), 2009-2020.

104. Wink, P. L.; Sanchez Quitian, Z. A.; Rosado, L. A.; Rodrigues, V. d. S.; Petersen, G. O.; Lorenzini, D. M.; Lipinski-Paes, T.; Saraiva Macedo Timmers, L. F.; de Souza, O. N.; Basso, L. A.; Santos, D. S., Biochemical characterization of recombinant nucleoside hydrolase from Mycobacterium tuberculosis H37Rv. *Archives of Biochemistry and Biophysics* **2013,** *538* (2), 80-94.

105. Chen, C.-S.; Lee, W.-J., Study of the Enzymatic Activity of Arthrobacter ureafaciens Neuraminidase by Isothermal Titration Calorimetry. *Journal of the Chinese Chemical Society* **2018,** *65* (2), 271-275.

106. Krokeide, I.-M.; Eijsink, V. G. H.; Sørlie, M., Enzyme assay for chitinase catalyzed hydrolysis of tetra-N-acetylchitotetraose by isothermal titration calorimetry. *Thermochimica Acta* **2007,** *454* (2), 144-146.

107. Park, S. H.; Park, K. H.; Oh, B. C.; Alli, I.; Lee, B. H., Expression and characterization of an extremely thermostable β-glycosidase (mannosidase) from the hyperthermophilic archaeon Pyrococcus furiosus DSM3638. *New Biotechnology* **2011,** *28* (6), 639-648.

108. Henzler, K.; Haupt, B.; Ballauff, M., Enzymatic activity of immobilized enzyme determined by isothermal titration calorimetry. *Analytical Biochemistry* **2008,** *378* (2), 184-189.

109. Baumann, M. J.; Murphy, L.; Lei, N.; Krogh, K. B. R. M.; Borch, K.; Westh, P., Advantages of isothermal titration calorimetry for xylanase kinetics in comparison to chemical-reducing-end assays. *Analytical Biochemistry* **2011,** *410* (1), 19-26.

110. Zebisch, M.; Krauss, M.; Schäfer, P.; Sträter, N., Crystallographic Evidence for a Domain Motion in Rat Nucleoside Triphosphate Diphosphohydrolase (NTPDase) 1. *J Mol Biol* **2012,** *415* (2), 288-306.

111. Branson, K. M.; Mertens, H. D. T.; Swarbrick, J. D.; Fletcher, J. I.; Kedzierski, L.; Gayler, K. R.; Gooley, P. R.; Smith, B. J., Discovery of Inhibitors of Lupin Diadenosine 5′,5‴-P1,P4-Tetraphosphate Hydrolase by Virtual Screening. *Biochemistry* **2009,** *48* (32), 7614-7620.

112. Aguirre, C.; Condado-Morales, I.; Olguin, L. F.; Costas, M., Isothermal titration calorimetry determination of individual rate constants of trypsin catalytic activity. *Analytical Biochemistry* **2015,** *479*, 18-27.

113. Weng, M.; Deng, X.; Bao, W.; Zhu, L.; Wu, J.; Cai, Y.; Jia, Y.; Zheng, Z.; Zou, G., Improving the activity of the subtilisin nattokinase by site-directed mutagenesis and molecular dynamics simulation. *Biochemical and Biophysical Research Communications* **2015,** *465* (3), 580-586.

114. Kehoe, K.; Van Elzen, R.; Verkerk, R.; Sim, Y.; Van der Veken, P.; Lambeir, A.-M.; De Meester, I., Prolyl carboxypeptidase purified from human placenta: its characterization and identification as an apelin-cleaving enzyme. *Biochimica et Biophysica Acta (BBA) - Proteins and Proteomics* **2016,** *1864* (11), 1481-1488.

115. Luo, Q.; Chen, D.; Boom, R. M.; Janssen, A. E. M., Revisiting the enzymatic kinetics of pepsin using isothermal titration calorimetry. *Food Chemistry* **2018,** *268*, 94-100.

116. Antunes, V. U.; Llontop, E. E.; Vasconcelos, F. N. d. C.; Lopez de los Santos, Y.; Oliveira, R. J.; Lincopan, N.; Farah, C. S.; Doucet, N.; Mittermaier, A.; Favaro, D. C., Importance of the β5-β6 Loop for the Structure, Catalytic Efficiency, and Stability of Carbapenem-Hydrolyzing Class D β-Lactamase Subfamily OXA-143. *Biochemistry* **2019,** *58* (34), 3604-3616.

117. Arai, S.; Yonezawa, Y.; Okazaki, N.; Matsumoto, F.; Shibazaki, C.; Shimizu, R.; Yamada, M.; Adachi, M.; Tamada, T.; Kawamoto, M.; Tokunaga, H.; Ishibashi, M.; Blaber, M.; Tokunaga, M.; Kuroki, R., Structure of a highly acidic β-lactamase from the moderate halophile Chromohalobacter sp. 560 and the discovery of a Cs(+)-selective binding site. *Acta Crystallogr D Biol Crystallogr* **2015,** *71* (Pt 3), 541-554.

118. Mazzei, L.; Cianci, M.; Benini, S.; Bertini, L.; Musiani, F.; Ciurli, S., Kinetic and structural studies reveal a unique binding mode of sulfite to the nickel center in urease. *Journal of Inorganic Biochemistry* **2016,** *154*, 42-49.

119. Benini, S.; Cianci, M.; Mazzei, L.; Ciurli, S., Fluoride inhibition of Sporosarcina pasteurii urease: structure and thermodynamics. *JBIC Journal of Biological Inorganic Chemistry* **2014,** *19* (8), 1243-1261.
120. Kincaid, V. A.; Sullivan, E. D.; Klein, R. D.; Noel, J. W.; Rowlett, R. S.; Snider, M. J., Structure and Catalytic Mechanism of Nicotinate (Vitamin B3) Degradative Enzyme Maleamate Amidohydrolase from Bordetella bronchiseptica RB50. *Biochemistry* **2012,** *51* (1), 545-554.
121. Rohatgi, N.; Gudmundsson, S.; Rolfsson, O., Kinetic analysis of gluconate phosphorylation by human gluconokinase using isothermal titration calorimetry. *FEBS Lett.* **2015,** *589* (23), 3548-3555.
122. Olsen, S. N., Applications of isothermal titration calorimetry to measure enzyme kinetics and activity in complex solutions. *Thermochim. Acta* **2006,** *448* (1), 12-18.
123. Bianconi, M. L., Calorimetric determination of thermodynamic parameters of reaction reveals different enthalpic compensations of the yeast hexokinase isozymes. *J. Biol. Chem.* **2003,** *278* (21), 18709-18713.
124. Bianconi, M. L., Calorimetry of enzyme-catalyzed reactions. *Biophys. Chem.* **2007,** *126* (1-3), 59-64.
125. Lopez-Zavala, A. A.; Sotelo-Mundo, R. R.; Hernandez-Flores, J. M.; Lugo-Sanchez, M. E.; Sugich-Miranda, R.; Garcia-Orozco, K. D., Arginine kinase shows nucleoside diphosphate kinase-like activity toward deoxythymidine diphosphate. *J. Bioenerg. Biomembr.* **2016,** *48* (3), 301-308.
126. Streeter, J.; Schickling, B. M.; Jiang, S.; Stanic, B.; Thiel, W. H.; Gakhar, L.; Houtman, J. C. D.; Miller, F. J., Jr., Phosphorylation of Nox1 regulates association with NoxA1 activation domain. *Circ Res* **2014,** *115* (11), 911-918.
127. Palmer, A.; Begres, B. N.; Van Houten, J. M.; Snider, M. J.; Fraga, D., Characterization of a putative oomycete taurocyamine kinase: Implications for the evolution of the phosphagen kinase family. *Comparative Biochemistry and Physiology Part B: Biochemistry and Molecular Biology* **2013,** *166* (3), 173-181.
128. Szabó, K.; Kandra, L.; Gyémánt, G., Studies on the reversible enzyme reaction of rabbit muscle glycogen phosphorylase b using isothermal titration calorimetry. *Carbohydrate Research* **2019,** *477*, 58-65.
129. Méndez-Lorenzo, L.; Porras-Domínguez, J. R.; Raga-Carbajal, E.; Olvera, C.; Rodríguez-Alegría, M. E.; Carrillo-Nava, E.; Costas, M.; López Munguía, A., Intrinsic Levanase Activity of Bacillus subtilis 168 Levansucrase (SacB). *PloS one* **2015,** *10* (11), e0143394-e0143394.

130. Henao-Escobar, W.; Domínguez-Renedo, O.; Alonso-Lomillo, M. A.; Cascalheira, J.; Dias-Cabral, A.; Arcos-Martínez, M., Characterization of a Disposable Electrochemical Biosensor Based on Putrescine Oxidase from Micrococcus rubens for the Determination of Putrescine. *Electroanalysis* **2014,** *27*.

131. Serrão, V. H. B.; Romanello, L.; Cassago, A.; de Souza, J. R. T.; Cheleski, J.; DeMarco, R.; Brandão-Neto, J.; Pereira, H. D. M., Structure and kinetics assays of recombinant Schistosoma mansoni dihydrofolate reductase. *Acta Tropica* **2017,** *170*, 190-196.

132. Cheleski, J.; Wiggers, H. J.; Citadini, A. P.; da Costa Filho, A. J.; Nonato, M. C.; Montanari, C. A., Kinetic mechanism and catalysis of Trypanosoma cruzi dihydroorotate dehydrogenase enzyme evaluated by isothermal titration calorimetry. *Analytical Biochemistry* **2010,** *399* (1), 13-22.

133. Romanello, L.; Serrão, V. H. B.; Torini, J. R.; Bird, L. E.; Nettleship, J. E.; Rada, H.; Reddivari, Y.; Owens, R. J.; DeMarco, R.; Brandão-Neto, J.; Pereira, H. D. M., Structural and kinetic analysis of Schistosoma mansoni Adenylosuccinate Lyase (SmADSL). *Molecular and Biochemical Parasitology* **2017,** *214*, 27-35.

134. van Spronsen, F. J.; Hoeksma, M.; Reijngoud, D.-J., Brain dysfunction in phenylketonuria: Is phenylalanine toxicity the only possible cause? *Journal of Inherited Metabolic Disease* **2009,** *32* (1), 46.

135. Hörster, F.; Schwab, M. A.; Sauer, S. W.; Pietz, J.; Hoffmann, G. F.; Okun, J. G.; Kölker, S.; Kins, S., Phenylalanine Reduces Synaptic Density in Mixed Cortical Cultures from Mice. *Pediatric Research* **2006,** *59* (4), 544-548.

136. Hanhineva, K.; Torronen, R.; Bondia-Pons, I.; Pekkinen, J.; Kolehmainen, M.; Mykkanen, H.; Poutanen, K., Impact of dietary polyphenols on carbohydrate metabolism. *Int. J. Mol. Sci.* **2010,** *11*, 1365-1402.

137. Mason, M.; Scampicchio, M.; Quinn, C. F.; Transtrum, M. K.; Baker, N.; Hansen, L. D.; Kenealey, J. D., Calorimetric Methods for Measuring Stability and Reusability of Membrane Immobilized Enzymes. **2018,** *83* (2), 326-331.

138. Ali, G.; Dulong, V.; Gasmi, S. N.; Rihouey, C.; Picton, L.; Le Cerf, D., Covalent immobilization of pullulanase on alginate and study of its hydrolysis of pullulan. **2015,** *31* (4), 883-889.

139. Berlemont, R.; Martiny, A. C.; Martiny, A. C., Glycoside Hydrolases across Environmental Microbial Communities. *PLoS Comput Biol* **2016,** *12* (12), e1005300.

140. Turner, P.; Mamo, G.; Karlsson, E. N., Potential and utilization of thermophiles and thermostable enzymes in biorefining. *Microbial Cell Factories* **2007,** *6* (1), 9.

141. Morisseau, C.; Inceoglu, B.; Schmelzer, K.; Tsai, H.-J.; Jinks, S. L.; Hegedus, C. M.; Hammock, B. D., Naturally occurring monoepoxides of eicosapentaenoic acid and docosahexaenoic acid are bioactive antihyperalgesic lipids. *J. Lipid Res.* **2010,** *51* (12), 3481-3490.

142. Klaus, L.; Barbara, G.; Florian, R., Evaluation of a Direct α-Amylase Assay Using 2-Chloro-4-nitrophenyl-α-D-maltotrioside. *Clinical Chemistry and Laboratory Medicine (CCLM)* **1999,** *37* (11-12), 1053-1062.

143. Ramasubbu, N.; Ragunath, C.; Sundar, K.; Mishra, P. J.; Gyemant, G.; Kandra, L., Structure-function relationships in human salivary α-amylase: role of aromatic residues. *Biologia (Bratislava, Slovakia)* **2005,** *60* (Suppl. 16), 47-56.

144. Morishita, Y.; Iinuma, Y.; Nakashima, N.; Majima, K.; Mizuguchi, K.; Kawamura, Y., Total and pancreatic amylase measured with 2-chloro-4-nitrophenyl-4-O-β-D-galactopyranosylmaltoside. *Clin. Chem. (Washington, D. C.)* **2000,** *46* (7), 928-933.

145. Cornish-Bowden, A., Chapter 6 - Two-substrate reactions. In *Fundamentals of Enzyme Kinetics*, Cornish-Bowden, A., Ed. Butterworth-Heinemann: 1979; pp 99-129.

2. Inhibition and activation of kinases by reaction products: a quick, reporter-free assay

2.1 Introduction

Kinases are a large family of enzymes that catalyze the transfer of a phosphoryl group from ATP to a range of acceptors, including proteins, lipids, and other small molecules, generating phosphorylated products and ADP. They play important roles in a wide variety of cellular processes [1], and are implicated in cancer [2], neurodegeneration [3], diabetes [4], and antibiotic resistance [5], among other health challenges. Mechanisms of kinase activity and regulation have been intensively studied for decades [1]. Nevertheless, some key aspects remain poorly understood, such as the role played by the reaction products in modulating kinase function. A few kinase studies have reported inhibition by ADP [6-9], but the scope and functional implications of this phenomenon have not been explored.

The relative scarcity of information on kinase/ADP interactions stems, at least in part, from a lack of suitable biochemical assays. Kinase activity has historically been evaluated using a radiometric assay, which employs γ-^{32}P (or ^{33}P) -ATP as a substrate and monitors the radiolabelled product [10, 11]. In addition to the safety and regulatory drawbacks of handling radiation, this method also requires the post-reaction separation of unreacted ATP from the phosphorylated product, which adds time, expense, and uncertainty to the measurements. Whereas non-radioactive, continuous variants of this assay have been

developed, in which phosphorylation alters the spectroscopic properties of substrate analogs [12, 13], they are of limited generality since a different reporter, often diverging considerably from the native substrate, must be designed for each enzyme of interest. Alternatively, several kinase assays that monitor ADP production are available. They involve antibody- or aptamer-based ADP sensors [14-16], or coupled enzyme systems in which ATP is regenerated from ADP and phosphoenol pyruvate by pyruvate kinase, and pyruvate is reduced by lactate dehydrogenase, with the concomitant formation of NAD^+ detected spectrophotometrically [17]. These methods are safe, simple, continuous, commercially available, and generally applicable, and they have become widely used. They cannot however be applied to measure the effects of ADP on kinase activity, since ADP is either bound to sensors or converted to ATP as quickly as it is produced. There is currently no general, continuous enzyme assay available to examine the effect of ADP on kinase activity.

Isothermal titration calorimetry (ITC) was originally designed to investigate host/guest binding interactions, but has recently gained in popularity as a general kinetic assay [18-20]. ITC has the advantage of directly measuring the heat released or absorbed by catalysis in real time [20, 21]. Since most chemical reactions are either exothermic or

endothermic, ITC can be applied to study virtually any enzymatic reaction, without the need for customized reporter molecules, additional coupled enzymes, or post-reaction separation. Furthermore, kinetic ITC experiments can be performed with conventional dilute enzymatic reaction mixtures, even with opaque samples, and require far less enzyme than ITC binding studies [22]. Notably, ITC is also well suited to characterizing product inhibition [18, 23], although only a few studies have explored this area, and to our knowledge, none have addressed ADP/kinase interactions. There are a handful of examples of ITC kinetic studies with kinases [20, 24-26], but none of these have addressed inhibition by ADP. Finally, it must be noted that traditional ITC binding experiments have been widely used to study ligand interactions with kinases (a PubMed search for kinase and ITC yields more than 500 articles). However, ITC kinetics experiments contain far more information on enzymatic activity than do binding experiments, which is crucial for understanding potential regulatory roles of ADP.

We applied ITC to investigate the modulation of kinases by ADP, focusing on three bacterial enzymes that represent potential antimicrobial drug targets: the enterococcal aminoglycoside 3'-phosphotransferase-IIIa (APH(3′)-IIIa), and pantothenate kinases from *Pseudomonas aeruginosa* (*Pa*PanK), and *Escherichia coli* (*Ec*PanK). APH(3′)-IIIa

phosphorylates aminoglycosides at the 3'-hydroxyl group, thereby conferring bacterial resistance to these antibiotics. APH(3′)-IIIa inhibitors could potentially be administered together with aminoglycosides in order to re-sensitize drug-resistant bacteria[27-29]. PanK enzymes catalyse the first committed step of coenzyme A biosynthesis, *i.e.* pantothenate phosphorylation [30]. The prokaryotic type I and type III enzymes, typified by *Ec*PanK and *Pa*PanK, respectively, have been identified as promising targets for the development of new antimicrobials [31-33]. Application of our method demonstrates for the first time that these kinases are activated and/or inhibited by the reaction product ADP, revealing a novel feedback mechanism with important implications in bacterial biology.

2.2 Methods

2.2.1 ITC Experiments Conditions

All ITC experiments were performed in triplicate using an ITC_{200} isothermal titration calorimeter (MicroCal, Northampton, USA) with a stirring speed of 750 RPM and injection rate 0.5 µL/s. We obtained identical results with stirring speeds ranging from 550 to 950 rpm, injection rates of 0.5 µL/s to 1 µL/s and using either the ITC200 (V_{cell}=200 µL) or the VP-ITC (MicroCal, Northampton, USA) (V_{cell}=1.43 mL), (Figure

S2.6). APH(3')-IIIa experiments were carried out at 37℃ in 50 mM Tris buffer pH 7.5, 40 mM KCl, and 10 mM $MgCl_2$. For *Ec*PanK, experiments were carried out at 25℃ in 50mM Tris pH 7.5, 250 mM NaCl, 2 mM $MgCl_2$. For *Pa*PanK, experiments were carried out at 37℃ in 50 mM Tris pH 7.5, 10mM $MgCl_2$, 60mM NH_4Cl. Dilution of the cell contents with each injection was calculated using the Origin Software supplied with the instrument (MicroCal, Northampton, USA).

2.2.2 ITC Transient Assays

ATP→APH(3')-IIIa Cell: (2 μM APH(3')-IIIa + 120μM kanamycin A), Syringe: (240 μM ATP + 240 μM kanamycin A + 0, 240, 360, or 480 μM ADP), 1×0.2 μL injection (data discarded) followed by 7×5 μL injections every 300 seconds.

kanamycin A→APH(3')-IIIa Cell: (2 μM APH(3')-IIIa + 375 μM ATP), Syringe: (240 μM ATP + 240 μM kanamycin A), 1×0.2 μL (data discarded) followed by 7×5 μL injections every 100 seconds.

ATP→*Pa*PanK Cell: (11 μM *Pa*PanK + 1.8 mM pantothenate), Syringe: (2.5 mM ATP + 2.5 mM pantothenate), 1×0.2 μL injection (data discarded) followed by 9×4 μL injections every 1300 seconds.

ATP→*Ec*PanK Cell: (3.2 μM *Ec*PanK + 2 mM pantothenate), Syringe (1.2 mM ATP + 1.2 mM pantothenate), 1×0.2 μL injection (data discarded) followed by 7×5 μL injections

every 800 seconds or Syringe (0.6 mM ATP + 0.6 mM pantothenate), 1×0.2 µL injection (data discarded) followed by 7×4 µL injections every 800 seconds.

2.2.3 ITC Saturation Assay

APH(3')-IIIa Cell: (30 nM APH(3')-IIIa + 120 µM kanamycin A), Syringe: (2.5 mM ATP + 2.5 mM kanamycin A), 3×10 µL injections every 200 seconds.

***Ec*PanK** Cell: (100 nM *Ec*PanK + 3 mM pantothenate), Syringe (4mM ATP + 4 mM pantothenate), 3×12 µL injections every 250 seconds.

2.3 Results

2.3.1 Background

Our method consists of a pair of complementary ITC experiments, In the first, referred to as the "transient assay", the calorimeter sample cell contains a mixture of enzyme and an excess of one substrate (either aminoglycoside or pantothenate), while the syringe holds a solution of the other substrate, ATP. It measures the relative inhibition or activation of the enzyme as ADP accumulates in the cell with successive injections of ATP. (Note that we also ran a variation of this experiment as a control in which the sample cell held a mixture of kinase and ATP and the syringe contained the other substrate.) The second type of experiment, termed the "saturation assay", measures the maximum

velocity of the enzyme at high concentrations of ATP and the second substrate under conditions where ADP does not accumulate significantly.

2.3.2 ITC Transient Assay: APH(3')-IIIa Exhibits Product Inhibition.

ITC transient assay data for kanamycin A phosphorylation by APH(3′)-IIIa are shown in **Figure 1a**. The y-axis indicates the rate of heat generation in the sample cell, where negative values correspond to exothermic reactions, with time plotted on the x-axis. Dilute ATP (mixed with an equimolar quantity of kanamycin A) was injected into the sample cell which contained APH(3′)-IIIa and a saturating excess of kanamycin A (120 μM, $K_m^{kanA} \approx 12$ μM[27]). The widths of the resultant peaks correspond to the length of time needed to fully consume the injected ATP. Each peak is broader than the preceding one, indicating that the enzyme velocity is reduced with successive injections. This is not due to substrate depletion, since each injection contains equal amounts of kanamycin A and ATP so the total amount of kanamycin A in the cell is largely invariant throughout the experiment. Instead, this behaviour is characteristic of product inhibition [20, 23], since the products (ADP and phospho-kanamycin A) accumulate in the cell with each injection. Notably, the inverse experiment in which dilute kanamycin A (mixed with an equimolar

quantity of ATP) is injected into APH(3′)-IIIa saturated with ATP produced a series of identical peaks (**Figure 2.1c**). This strongly suggests that ADP, and not phospho-kanamycin A, acts as an inhibitor of APH(3′)-IIIa. APH(3′)-IIIa follows an ordered bi-bi reaction mechanism with ATP binding first and ADP dissociating last [34]. Following this mechanism[35], ADP should act as a competitive inhibitor (versus ATP) when the ATP concentration is varied and kanamycin A is saturating (**Figure 2.1a**), and should not inhibit the enzyme when the kanamycin A concentration is varied and ATP is saturating (**Figure 2.1c**), as was seen experimentally. In contrast, if phospho-kanamycin A acted as an inhibitor, no peak broadening would be observed in **Figure 2.1a**, and progressively broader peaks would be expected in **Figure 2.1c**.

The peak broadening quantifies the extent of inhibition. Indeed, the return of each peak to baseline follows mono-exponential kinetics with a first-order rate constant that decreases as the degree of inhibition increases. This can be derived from the ordered bi-bi rate equation for APH(3′)-IIIa, which reduces to the simple Michaelis-Menten form when the enzyme is saturated with kanamycin A according to [36]

$$v_0 = \frac{k_{\mathrm{cat}}[\mathrm{APH}]_0[\mathrm{ATP}]}{[\mathrm{ATP}]+\mathrm{K_m}'} \qquad (2.1)$$

where

$$K_m' = K_m^{ATP}\left(1 + \frac{[ADP]}{K_i^{ADP}}\right), \quad (2.2)$$

K_m^{ATP} is the Michaelis Menten constant for ATP in the absence of ADP and K_i^{ADP} is the inhibition constant for ADP. We used dilute injections of ATP to avoid excessive inhibition, such that [ATP]<<K_m'. In this regime, the enzyme velocity scales linearly with ATP concentration, $v_0 \approx [APH]_0 \frac{k_{cat}}{K_m'}[ATP]$. If one assumes that the effective rate constant,

$$k_{eff} = [APH]_0 \frac{k_{cat}}{K_m'} \quad (2.3)$$

does not vary substantially during the acquisition of a single ITC peak, then the concentration of ATP decreases exponentially, $[ATP] = [ATP]_0 \exp\{-k_{eff} t\}$, following each injection. The ITC signal is proportional to the velocity of the reaction, v_0, and hence to [ATP], therefore each raw ITC peak returns to baseline exponentially. A semi-log plot of the baseline-subtracted ITC signal should thus be linear with a slope equal to k_{eff}, as observed experimentally (**Figure 2.1b**). The slopes decrease with successive injections as ADP accumulates and K_m' increases. As expected, a similar treatment of the inverse experiment (saturating ATP with kanamycin A injections) yields identical slopes for all injections (**Figure 2.1d**). We note that the concentration of ADP does, in fact, increases as a result of catalysis during the acquisition of each peak, which should in principle lead

to curved (concave) plots in **Figure 2.1b**. The fact that we observe highly linear plots suggests that the variation in [ADP] and K_m' within the portion of each peak analyzed is negligible. Therefore, to a close approximation k_{eff} may be treated as a constant for each individual peak and inhibition of APH(3′)-IIIa by ADP can be analyzed purely in terms of variations in k_{eff} values obtained for different peaks.

The dependence of k_{eff} values on ADP concentration yields both the inhibition constant for ADP, K_i^{ADP}, and the specificity coefficient of the enzyme, k_{cat}/K_m^{ATP}. Combining **Equations 2.2** and **2.3** gives:

$$\frac{[APH]_0}{k_{eff}} = \frac{K_m^{ATP}}{k_{cat}}\left(1 + \frac{[ADP]}{K_i^{ADP}}\right) \tag{2.4}$$

Consequently, when the total enzyme concentration, $[APH]_0$, divided by k_{eff} is plotted as a function of ADP concentration, a straight line is expected with a slope of $K_m^{ATP}/(k_{cat}K_i^{ADP})$, a y-intercept of K_m^{ATP}/k_{cat}, and the y-intercept divided by the slope yielding K_i^{ADP}.

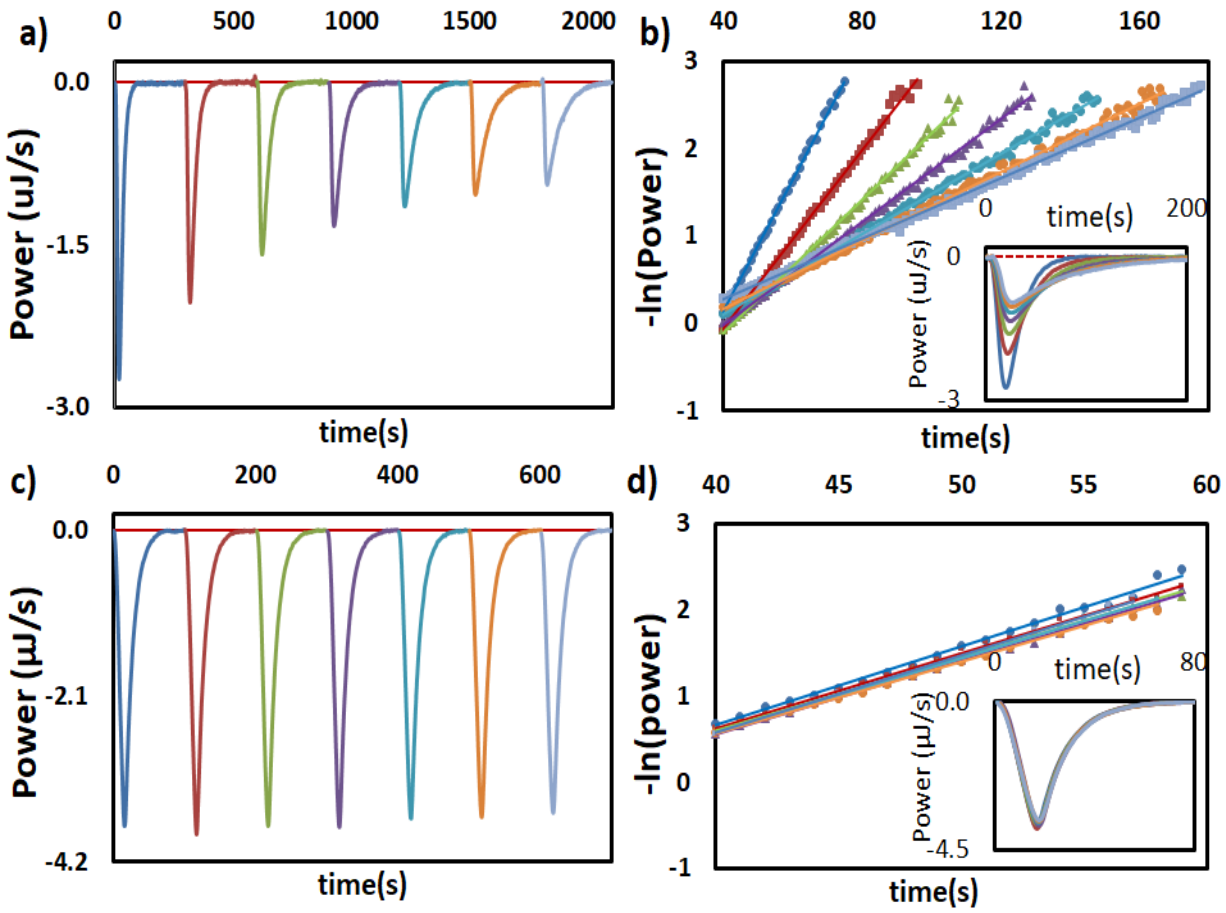

Figure 2.1. ITC transient assay measurement for APH(3')-IIIa. a) ITC transient assay data for APH(3')-IIIa pre-saturated with kanamycin A before injections of ATP. (7×5µL 240µM ATP + 240µM kanamycin A → 200 µL 2µM APH(3')-IIIa + 120µM kanamycin A) **b)** Semi-logarithmic plot of the ITC signal (dQ/dt (µJ/s) versus time) for the exponentially decaying regions in panel a. Linear regression results (solid lines) are overlaid with the experimental data (solid circles), where different colors represent different injections; the inset shows an overlay of the ITC peaks. **c)** ITC transient assay data for APH(3')-IIIa pre-saturated with ATP and injections of kanamycin A. (7×5µL 240µM ATP + 240µM kanamycin A → 200 µL 2µM APH(3')-IIIa + 375µM ATP) **d)** Semi-logarithmic plot of the ITC signal (dQ/dt (µJ/s) versus time) for the exponentially decaying regions in panel c. Linear regression results (solid lines) are overlaid with the experimental data (solid circles), where different colors represent different injections; the inset shows an overlay of the ITC peaks.

2.3.3 Validation of ITC Transient Assay Confirms APH(3')-IIIa Inhibition by ADP.

In order to validate the transient assay methodology, we employed the method of standard additions, which consists of premixing ATP with varying amounts of ADP in the injection syringe, leading to varying accumulation of ADP after each injection (**Figure S2.5**). Experiments with four different concentrations of ADP were performed. Slopes (k_{eff}) were extracted as in **Figure 2.1b**, d, used to calculate $[APH]_0/k_{eff}$, and plotted in **Figure 2.2a**. For each experiment, $[APH]_0/k_{eff}$ was found to increase monotonically as a function of injection number, reflecting decreasing reaction rates. Steeper slopes and more marked rate reductions are obtained for experiments with higher ADP syringe concentrations, confirming that APH(3′)-IIIa is inhibited by ADP. Furthermore, when $[APH]_0/k_{eff}$ values are plotted as a function of total [ADP] present in the sample cell (calculated at the mid-point of each peak), all data points collapse to the same line (**Figure 2.2b**), as predicted by **Equation 2.4**. The y-intercept divided by the slope gives $K_i^{ADP} = 7.3 \pm 0.2$ μM which is, to our knowledge, the first determination of an ADP inhibition constant for APH(3′)-IIIa.

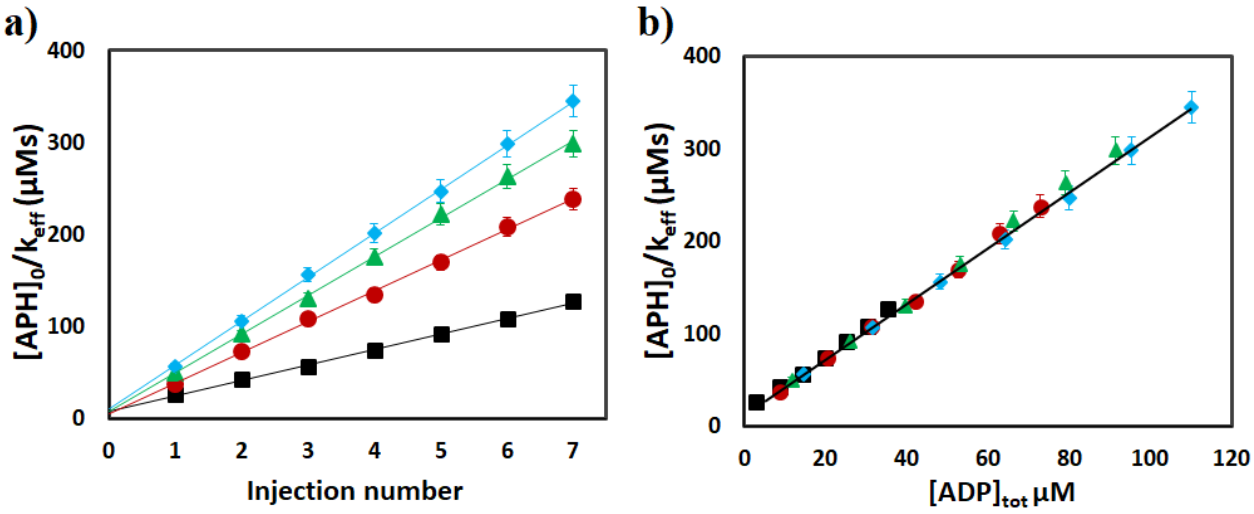

Figure 2.2. ITC transient assay measurement for APH(3')-IIIa with four differenct concentrations of ADP. **a)** Plot of enzyme concentration divided by rate of catalysis ($[APH]_0/k_{eff}$) versus injection number for four ITC transient assays performed on 2 μM of APH(3')-IIIa presaturated with 120 μM kanamycin A. Injections contained ATP (240 μM) + kanamycin A (240 μM) + ADP at 0 μM (■), 240 μM (●), 360 μM (▲) and 480 μM (◆) **b)** Plot of $[APH]_0/k_{eff}$ versus $[ADP]_{tot}$ from a. $[ADP]_{tot}$ values were calculated for the midpoint of each peak (where half the injected ATP has been converted to ADP) according to the total number of moles of ATP and ADP added from all previous injections plus the ADP of the current injection plus one half of the ATP of the current injection, divided by the volume of the sample cell. Linear regression results are overlaid with the experimental data.

2.3.4 ITC Saturation Assay: Measurement of APH(3')-IIIa Maximal Velocity and Determination of Kinetic Parameters.

Finally, we used the ITC saturation assay to measure the value of k_{cat} for APH(3')-IIIa. In this technique, concentrated ATP was added to the cell, which contained kanamycin A-saturated enzyme. The concentration of APH(3')-IIIa was roughly 40-fold lower than that used for the transient assay, such that little ATP was consumed or ADP produced during the course of the experiment. Consequently, the velocity of the enzyme was essentially constant between injections and the value of the ITC signal did not change with time, producing approximately horizontal lines in the power vs time plots (**Figure 2.3**). Each injection was accompanied by small exothermic peak similar to those of a blank (enzyme-free) experiment, which we attribute to the enthalpy of dilution (**Figure S2.7**). The first injection resulted in a downward shift of the ITC signal, reflecting an increase in enzyme velocity. Essentially no further shifts were obtained for the second or third injections suggesting that a saturating concentration of ATP was reached with [ATP]>>K_m'. The total shift in the ITC signal (ΔP) is proportional to the maximum enzyme velocity according to [20]

$$\Delta P = \Delta H_{react} \cdot k_{cat} \cdot [APH]_0 \cdot V_{cell} \quad (2.5)$$

where V_{cell} is the volume of the ITC cell (200 µL) and ΔH_{react} is the enthalpy change for the phosphorylation reaction, which can be obtained by integrating the peaks obtained in the transient assay (giving total heat released) and dividing by the total number of moles of ATP injected. The combination of transient and saturation ITC assays therefore gives k_{cat}, K_m^{ATP}, ΔH_{react}, and K_i^{ADP}, listed in **Table 2.1**. The values of k_{cat} and K_m (1.4 ± 0.06 s^{-1} and 26 ± 0.9 µM) are within experimental error of values previously reported for APH(3')-IIIa using the pyruvate kinase/lactate dehydrogenase coupled assay, providing validation for the ITC method used here. Interestingly, the K_i^{ADP} value (7.3 ± 0.2 µM) is quite a bit lower than K_m^{ATP}, suggesting that ADP can compete effectively with ATP in the active site of the enzyme.

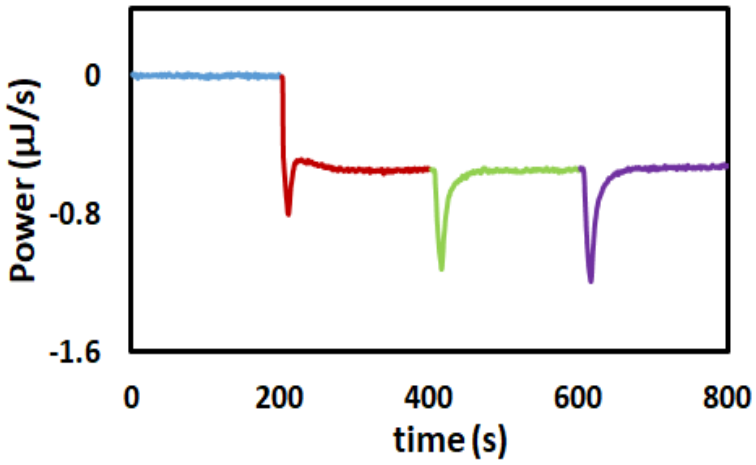

Figure 2.3. ITC saturation assay measurement for APH(3')-IIIa at 37°C. Red, green, and purple traces identify the first, second, and third injections, respectively. (3× 10µL 2.5 mM ATP + 2.5 mM kanamycin A → 200 µL 30 nM APH(3')-IIIa + 120 µM kanamycin A)

2.3.5 *Pa*PanK is Inhibited by ADP, while *Ec*PanK can be Inhibited or Activated by ADP.

We then repeated these experiments with *Pa*PanK and *Ec*PanK. Enzyme activity was substantially lower for *Pa*PanK than for APH(3')-IIIa, leading to roughly 10-fold larger $[\mathrm{PanK}]_0/k_{\mathrm{eff}}$ values in the ITC transient assay (**Figure 2.4a**). The K_m^{ATP} for this enzyme is reported to be on the order of 3 mM [37], and it was therefore not possible to fully saturate the enzyme with ATP, as required to measure k_{cat} using the ITC saturation assay. Nevertheless, the reciprocal of the y-intercept (**Figure 2.4a**) gives the specificity constant, k_{cat}/K_m = 510 ± 10 M^{-1} s^{-1}, which is within a factor of 4 of the published value, 140 M^{-1} s^{-1}, obtained using the pyruvate kinase/lactate dehydrogenase coupled assay [37]. The extracted value of K_i^{ADP} = 2.1 ± 0.4 mM is similar to, yet slightly lower than, the published K_m^{ATP} (3 mM)[37].

Surprisingly, *Ec*PanK was found to exhibit a behaviour in the ITC transient assay that differs dramatically from those of either APH(3')-IIIa or *Pa*PanK. Values of $[EcPanK]_0/k_{\mathrm{eff}}$ showed a curvilinear dependence on ADP concentration, initially decreasing for [ADP] less than ca. 25 μM, before increasing linearly with increasing ADP for concentrations greater than ca. 50 μM. This corresponds to enzyme activity increasing

with ADP at low concentrations, *i.e.* ADP activation, and activity decreasing with ADP at higher concentrations, *i.e.* ADP inhibition.

Table 2.1. Kinetic parameters, molar enthalpy and ADP inhibition constant for the activity of APH(3')-IIIa, *Pa*PanK, and *Ec*PanK.

Enzyme	**APH(3')-IIIa**	***Pa*PanK**	***Ec*PanK**
Substrate	Kanamycin A	Pantothenate	Pantothenate
ITC assay			
K_m^{ATP}(μM)	26.3 ± 0.9	n.d	80 ± 20 [a]
k_{cat}^{ATP} (s^{-1})	1.42 ± 0.06	n.d	1.06 ± 0.05
k_{cat}/K_m($M^{-1}s^{-1}$)	(5.4±0.2)×10^4	510±10	(1.8±0.1)×10^4
K_i^{ADP}(μM)	7.3 ± 0.2	2100±400	28.1 ± 2.7 [b]
ΔH_{react} (kJ/mol)	-62.4 ± 0.4	-53.2± 0.9	-56.9 ± 0.8
PK/LDH			
K_m^{ATP}(μM)	27.7 ± 3.7 [27]	3160 [37]	57 ± 5
k_{cat}^{ATP} (s^{-1})	1.76±0.08 [27]	0.42 [37]	1.46 ± 0.03
k_{cat}/K_m($M^{-1}s^{-1}$)	6.37 ×10^4	140	2.56 ×10^4

[a] $K_m=1/K_{s2}$, calculation based on **Equation 2.9**.

[b] K_i^{ADP} was the average value of the $1/K_{p1}$ and $1/K_{p2}$, based on **Equation 2.9**.

2.3.6 A Cooperative Model for Activation and Inhibition of *Ec*PanK by ADP.

The unexpected pattern of ADP activation/inhibition for *Ec*PanK yields intriguing clues into its catalytic mechanism. It is likely that this behaviour is related to energetic communication between the active sites of this dimeric enzyme. *Ec*PanK has previously been reported to exhibit cooperative kinetics, such that binding a molecule of ATP in the first active site increases ATP binding at the second active site [38]. We therefore tested whether a simple cooperative model could account for activation of the enzyme at low [ADP] and inhibition at high [ADP]. Note that the enzyme forms a stable dimer as detected by both size exclusion chromatography and analytical ultracentrifugation[38], therefore we did not consider dimer dissociation in our analysis. We applied one of the kinetic schemes developed for cooperative dimeric enzymes by Ishikawa and co-workers [39], in which it is assumed that an active site is catalytically competent if and only if the other active site is bound to either ATP substrate (S) or ADP product (P). In other words, an active site is inactive if the other site is empty:

(2.6)

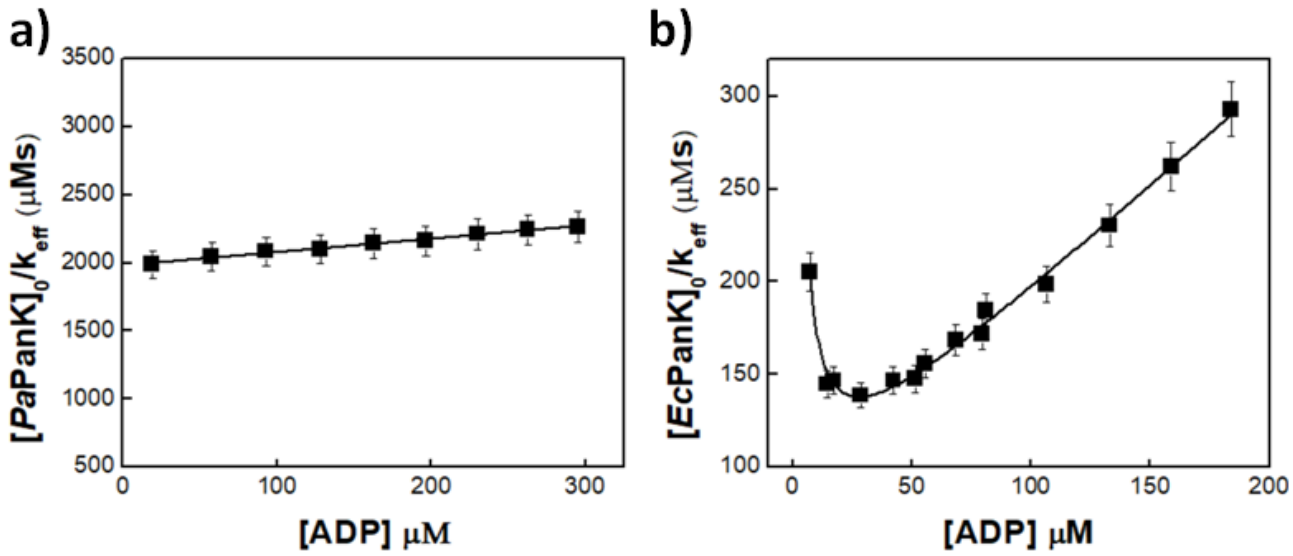

Figure 2.4. ITC transient assay measurement for PanK. a) Plot of enzyme concentration divided by rate of catalysis ($[Pa\text{PanK}]_0/k_{\text{eff}}$) versus [ADP] for *Pa*PanK pre-saturated with pantothenate. Linear regression results (solid line) are overlaid with the experimental data (squares). **b)** Plot of enzyme concentration divided by rate of catalysis ($[Ec\text{PanK}]_0/k_{\text{eff}}$) versus [ADP] for *Ec*PanK. The fit to **Equation 2.9** (solid curve) is overlaid with the experimental data (squares).

Note that there is no direct conversion of ES to EP since the singly-bound enzyme is not active. Only ESS and ESP undergo catalysis to yield ESP and EPP, respectively. This model explains the concentration-dependent switch from activation to inhibition, since at low concentrations of S and P, increasing the amount of P helps to drive the conversion of the inactive ES form into the active ESP form. At high concentrations of P, the product out-competes the substrate and the enzyme becomes increasingly trapped in the inactive EPP form. The rate equation corresponding to this scheme (in the rapid equilibration limit and assuming an irreversible chemical step) is given by: [39]:

$$v_0 = [Ec\text{PanK}]_0 \frac{k_{\text{cat}}(2\text{K}_{\text{S1}}\text{K}_{\text{S2}}[\text{S}]^2+2\text{K}_{\text{S2}}\text{K}_{\text{P1}}[\text{S}][\text{P}])}{1+2\text{K}_{\text{S1}}[\text{S}]+\text{K}_{\text{S1}}\text{K}_{\text{S2}}[\text{S}]^2+2\text{K}_{\text{P1}}[\text{P}]+\text{K}_{\text{P1}}\text{K}_{\text{P2}}[\text{P}]^2+2\text{K}_{\text{S2}}\text{K}_{\text{P1}}[\text{S}][\text{P}]} \quad (2.7)$$

where $\text{K}_{\text{S1,2}}$ and $\text{K}_{\text{P1,2}}$ are the affinity constants for binding the first and second molecules of substrate (ATP) and product (ADP), respectively (note that association constants are used here to simplify the expressions, in contrast to K_i which is a dissociation constant). In the low ATP limit, where $\text{K}_{\text{S1,2}}[\text{S}] << 1$, **Equation 2.7** reduces to

$$v_0 \approx \frac{[Ec\text{PanK}]_0 k_{\text{cat}} 2\text{K}_{\text{S2}}\text{K}_{\text{P1}}[\text{P}]}{1+2\text{K}_{\text{P1}}[\text{P}]+\text{K}_{\text{P1}}\text{K}_{\text{P2}}[\text{P}]^2}[\text{S}] \equiv k_{\text{eff}}[\text{S}] \quad (2.8)$$

Therefore experimentally-determined values of $[Ec\text{PanK}]_0/k_{\text{eff}}$ should obey the following curvilinear relationship with product (ADP) concentration:

$$\frac{[Ec\text{PanK}]_0}{k_{\text{eff}}} = \frac{1+2\text{K}_{\text{P1}}[\text{P}]+\text{K}_{\text{P1}}\text{K}_{\text{P2}}[\text{P}]^2}{k_{\text{cat}}2\text{K}_{\text{S2}}\text{K}_{\text{P1}}[\text{P}]} \quad (2.9)$$

This equation was fit to the experimental data and gives quantitative agreement as shown in **Figure 2.4b**, supporting the idea that ADP binding to one subunit activates the catalytic activity of the adjacent subunit. Furthermore, the extracted parameters provide insight into the interaction of *Ec*PanK with ATP and ADP. The fit yielded similar affinity constants for binding the first and second molecules of the ADP product, K_{P1} = $(4.1\pm0.4)\times10^4\text{M}^{-1}$ and K_{P2} = $(3.1\pm0.3)\times10^4\text{M}^{-1}$, as well as $k_{\text{cat}}\text{K}_{\text{S2}}$ = $(1.35\pm0.07)\times10^4$ $\text{M}^{-1}\text{s}^{-1}$. This value, together with the results of the saturation assay (**Figure S2.2**) k_{cat} = 1.06 ± 0.05 s^{-1}, give the equilibrium constant for binding ATP to an enzyme with an

already-occupied subunit $K_{S2}=(1.3\pm0.3)\times10^4$ M^{-1}, *i.e.* substrate binding affinity for the activated enzyme. This corresponds to a dissociation constant of 80±20 μM, which is remarkably close to the previously reported Michaelis-Menten constant for this enzyme, K_m = 136 μM.[38] The small discrepancy may be due to the fact that our measurements were performed at 25°C while the previous work was carried out at 37°C. In addition, when we used the pyruvate kinase/lactate dehydrogenase coupled assay (**Figure S2.1**) to characterize *Ec*PanK under the same conditions as the ITC experiments, and fit the data to a simple Michaelis-Menten kinetic model, the resulting K_m (57 ± 5 μM) matches $1/K_{S2}$=80±20 μM to within experimental error. Thus the ITC enzyme kinetic data are quantitatively consistent with a simple allosteric model in which ligand binding at one active site is required for catalytic activity at the other active site. A deeper understanding of the mechanism allosteric communication could be provided by structural biology techniques such as NMR titration analyses [40, 41].

2.4 Discussion

2.4.1 Implications of ADP Inhibition at Physiological Concentrations.

In all three bacterial kinases studied here, the product ADP competed efficiently with the substrate ATP to inhibit the enzyme. In APH(3')-IIIa, the measured K_i^{ADP} was roughly 3-fold lower than the K_m^{ATP}. In *Pa*PanK, the measured K_i^{ADP} was also slightly lower than the previously reported K_m^{ATP} value. Finally, despite the fact that *Ec*PanK exhibited a more complex kinetic behavior with activation occurring at low product concentrations, the apparent enzyme affinity for ADP ($K_{P1,2}$) was still roughly three-fold tighter than for ATP (K_{S2}), and resulted in efficient inhibition at concentrations greater than ca. 50 μM. There are several factors that could explain why, for all three kinases, the K_i^{ADP} values are lower than the K_m^{ATP} values. Firstly, the enzymes could actually bind ADP more tightly than ATP, although this is not necessarily the case as detailed below. For APH(3')-IIIa, higher affinity for ADP seems reasonable, based on the overall acidic nature of the protein. The nominal isoelectric point of APH(3')-IIIa is 4.4 and the net charge of the protein is predicted to be –19 at neutral pH, therefore reduced electrostatic

repulsion with ADP compared to ATP could result in higher affinity for the product. In contrast, the PanK enzymes have much less net charge (-4.3 and -0.9 at pH 7 for *Pa*PanK and *Ec*PanK) and it is less clear why ADP would bind more tightly to this enzyme than ATP. Alternatively, the fact that K_i^{ADP} is an equilibrium binding constant whereas K_m^{ATP} is a steady-state kinetic parameter can lead to differences in these values even when the affinities are similar. In Briggs-Haldane kinetics, $K_m = (k_{off} + k_{cat})/k_{on}$, where k_{on} and k_{off} are the association and dissociation rate constants of the substrate. If k_{cat} is comparable or larger than k_{off}, then K_m is substantially higher than the true equilibrium dissociation constant for substrate, $K_d = k_{off}/k_{on}$. Therefore, the fact that K_i^{ADP} values are lower than K_m^{ATP} values in these systems could be largely a reflection of the fact that ATP is a substrate and ADP is not. We note that for *Ec*PanK, the fitted model assumed rapid equilibria of the enzyme with substrates and products, in order to simplify the mathematics, but a more complete kinetic treatment could include Briggs-Haldane type considerations as well.

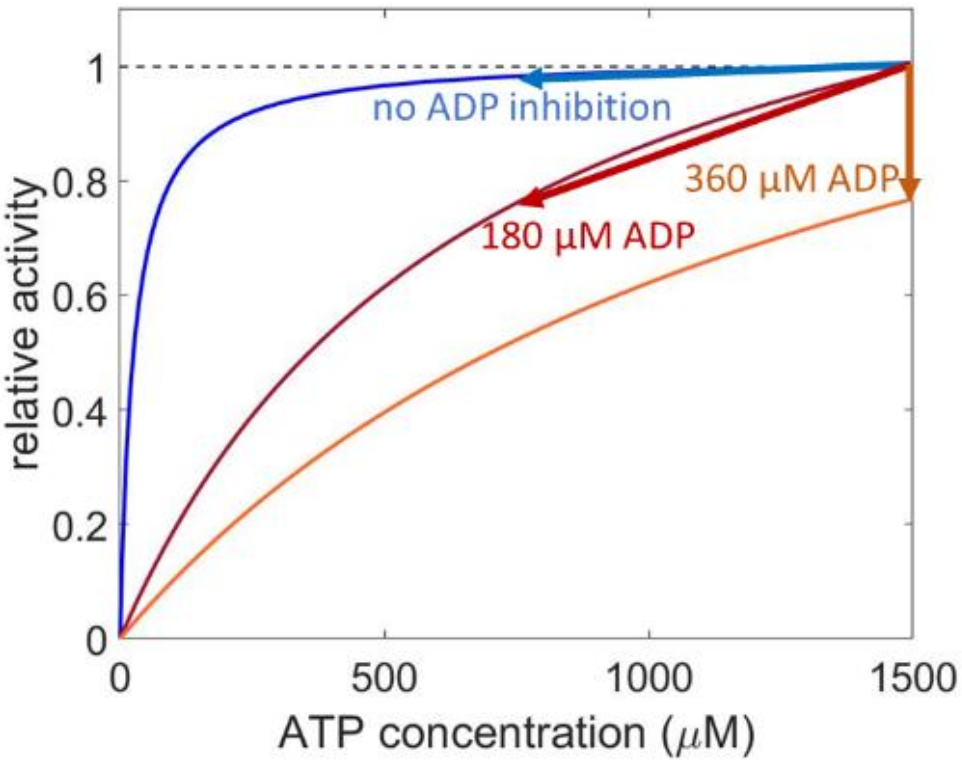

Figure 2.5. APH(3')-IIIa activity with (orange, red) and without (blue) ADP inhibition at physiological ATP and ADP concentrations. Activity values are normalized to 1 for [ATP]=1.5 mM, [ADP]=180 μM. For red and orange curves, K_i=7μM while for the blue curve, K_i=∞ (i.e. no inhibition).

Regardless of the underlying physical mechanisms, the fact that ADP is a relatively potent inhibitor of these bacterial kinases has interesting implications for how they respond to variations in cellular ATP and ADP concentrations. ATP concentrations in *E. coli* show significant cell-to-cell variability, ranging from 0.5-5 mM, with an average of

1.5 mM [42], while the ratio of ATP:ADP was found to vary from about 6:1 to 10:1, depending on the growth conditions [43]. At 1.5 mM, the ATP concentration is more than 50-fold greater than the K_m^{ATP} values of APH(3')-IIIa and *Ec*PanK. Therefore in the absence of ADP inhibition, these enzymes would be completely saturated and quite insensitive to even large changes in ATP concentration, as illustrated in **Figure 2.5**. For example, a 50% reduction in ATP concentration (1.5 to 0.75 mM) would only reduce the rate of kinase activity by about 2%. However, at roughly 180 μM, the concentration of ADP is roughly 25-fold higher than K_i^{ADP}. According to Equation 2.2, this results in the effective K_m' for ATP increasing by about 26-fold to about 700 μM, much closer to the intracellular ATP concentration. In this regime, a 50% decrease in ATP concentration would result in a much larger 25% reduction in enzyme activity. Under these conditions, the kinase activity also becomes quite sensitive to the concentration of ADP. For example, a 2-fold increase in ADP concentration would result in a roughly 24% decrease in kinase activity. In other words, the inhibition of APH(3')-IIIa and *Ec*PanK by ADP is entirely responsible for their ability to respond to changes in both ATP and ADP concentrations, such that both exhaustion of ATP and accumulation of ADP reduce enzyme activity. We hypothesize that this slow-down of kinase activity in times of energy depletion reduces non-essential ATP consumption and may contribute to the fitness of the organism.

2.4.2 Generality of the Method

The ITC-based approach presented here enjoys several advantages over alternative methods for characterizing kinase interactions with ADP. Existing kinase ADP inhibition data are derived from ATP radiolabeling assays[6, 8, 9], which require special safety training and regulatory oversight. They are also discontinuous assays, meaning that the phosphorylated product must be separated from the unreacted ATP after the reaction is completed, introducing additional complexity and uncertainty into the measurements. Continuous assays with modified fluorescent substrates could in principle detect kinase/ADP interactions, although to our knowledge they have typically been performed in a semi-quantitative high-throughput screening manner and no ADP inhibition has been reported[12, 13]. We note that this approach cannot be used with the natural (non-fluorescent) substrates and that the fluorophore tags are roughly the same size as the aminoglycoside and pantothenate substrates used here. Thus fluorescence-based approaches are considerably less general than the ITC method presented herein. As described above, the commonly-used PK/LDH coupled enzyme assay cannot measure ADP inhibition at all, since the steady-state concentration of ADP is held near zero[17]. Finally, it should be mentioned that ITC binding assays can measure kinase/ADP interactions directly[44, 45]. These are distinct from the work presented here; binding assays

detect the heat released or absorbed by formation of a kinase/ADP complex, while our kinetic assays detect the heat released by the phosphotransfer reaction itself and monitor how catalysis is affected by the presence of ADP. ITC kinetic assays offer several advantages compared to binding experiments. Firstly, the kinetic assays establish a direct link between ADP and enzyme activity, while binding experiments do not. For example, unlike our kinetic assay, a traditional binding experiment would be unable to detect the activation of *Ec*PanK at low [ADP] followed by its inhibition at high [ADP], thus critical details of the consequences of ADP binding would be lost. Secondly, kinetic assays generally require much lower enzyme concentrations than binding experiments, since each enzyme molecule undergoes multiple turnovers, generating heat with every cycle. For example, our APH(3')-IIIa assays employed enzyme concentrations up to 2 μM, whereas a binding experiment would have required about 10-fold the K_i [22], i.e. about 70 μM or 35-fold more. This detail is important for kinases that are difficult to produce or weakly soluble.

Despite its advantages, there are some caveats to our method. Firstly, the sensitivity of the experiment depends on the rate at which heat is produced by the enzyme. This, in turn, depends on the turnover number, k_{cat}, and the enthalpy of the reaction, ΔH. Very

slow enzymes or phosphotransfer reactions with very low enthalpy could, in principle, produce such weak ITC signals that the accuracy of the method could be compromised. We note that the signal-to-noise ratio obtained here was excellent, as evinced by the low degree of scatter in linear plots of **Figures 2.1** and **S2.3-2.5** and the experiment could probably tolerate substantially smaller ITC signals. Furthermore, the values of k_{cat} and ΔH_{react} obtained here are typical of those for kinases reported in the literature[24, 25], so we anticipate that our data are fairly representative. Nevertheless, a pathologically slow enzyme with a small ΔH_{react} could be better suited to a substrate-detected method such as ATP radiolabeling. Secondly, our method relies on the buildup of ADP in the sample cell. If inhibition were to be extremely weak, it could be difficult to inject enough ADP and/or ATP to achieve distinct changes in enzyme kinetics from one injection to the next. We successfully applied the method to *Pa*PanK, where the K_i^{ADP} is upwards of 2 mM, but as seen in the shallow slope of **Figure 2.4a**, this is approaching the experimental limit. We estimate that much weaker binding ($K_i^{ADP} \approx 5$mM or greater) would be challenging to measure accurately.

Our ITC kinetic data demonstrate that kinase/ADP interactions can take a variety of forms. They can serve as probes to examine allosteric communication between active

sites in multi-subunit enzymes, and they can profoundly affect how kinases respond to changes in the cellular environment. There exists an enormous diversity of kinase and ATP-hydrolyzing systems where additional information on ADP inhibition would be of value. For instance, many multi-subunit molecular machines are driven by ATP hydrolysis, including chaperonins[46], proteasomes[47], active transporters[48], DNA isomerases[49], and molecular motors such as kinesin[50]. Knowledge of how these proteins interact with ADP can shed light on their mechanisms of action and regulation. For example, it was shown that ADP is a non-competitive inhibitor of the bacterial chaperonin GroEL, implying a "two-stroke" cycle of catalysis involving the two heptameric rings[51, 52]. However, these measurements were made using GroEL particles covalently tagged with the fluorescent probe pyrene, which fortuitously undergoes large changes in fluorescence upon nucleotide binding[53]. The activity of molecular machines for which such a fluorescence assay does not exist can be monitored by the PK/LDH coupled enzyme assay[54], but this method cannot be used to study ADP interactions. In principle, our ITC-based method can be used to measure how the catalytic rates of unmodified molecular machines acting on their native substrates are affected by ADP, providing a new window into their functional mechanisms.

In addition, it is widely recognized that the dysregulation of kinase-mediated cell signaling is central to many forms of cancer. Typically, kinase involvement in oncogenesis includes changes in epigenetic and post-translation modifications, chromosomal translocations, and mutations[55]. The results of the current study point to an additional factor that would bear further exploration. APH(3')-IIIa is structurally homologous to many eukaryotic (and human) protein kinases[56], suggesting that their activity may also be governed by ADP inhibition, leading to reduced activity when ATP levels drop and/or ADP levels rise. Interestingly, a substantially reduced ATP/ADP ratio has been suggested as a hallmark of cancer cells and essential for the Warburg effect, the predominance of aerobic glycolysis in cancerous tissues.[57] The drop in the ATP/ADP ratio could reduce kinase activity considerably in a heterogenous manner that depends on the values K_m^{ATP} and K_i^{ADP} for each enzyme. The ITC experiments presented here are rapid to perform, do not require large amounts of material, and can be universally applied to essentially all kinases. They can thus be of great utility in better understanding this fundamental aspect of kinase activity.

2.5 Conclusion

Kinases are ubiquitous in nature and are implicated in many human diseases. Although kinase inhibition by ADP is a potential regulatory mechanism, it is largely unexplored due to a lack of suitable continuous assays. Here we show that isothermal titration calorimetry (ITC) is uniquely suited to characterizing ADP kinase interactions. We applied it to three bacterial kinases, detecting unexpected ADP activation and discovering that ADP inhibition allows some kinases to respond to changes in the cellular concentrations of both ATP and ADP. These results highlight the power of ITC to shed light on this potentially widespread phenomenon.

2.6 Supporting Information

2.6.1 Protein Expression and Purification

APH(3')-IIIa expression and purification

Cell culture and protein purification were performed according to the method from McKay and Wright.[27] Transformed E. coli BL21 (DE3) cells were grown at 37°C in 4L of Luria broth (LB) supplemented with 100 μg/mL ampicillin for about 4 hours until the

OD600 reached 0.5 to 0.6. Protein expression was induced with the addition of 1mM Isopropyl-β-D-thiogalactopyranoside (IPTG, CHEM-IMPEX, 00194). After incubation for another 2.5 hours, cells were harvested by centrifugation at 4°C at 3000×g for 10min. APH(3')- IIIa was purified by resuspending cells in 25 mL of cell lysis buffer (50 mM Tris, pH 7.5, 5mM ethylenediaminetetraacetic acid (EDTA, CHEM-IMPEX,000139) , 200mM NaCl, 1mM phenylmethanesulfonyl fluoride (PMSF SIGMA-ALDRICH,P7626) , 0.1 mM DTT); then lysed by sonication for 3 cycles (sonicating 3 minutes, waiting for 1 minute) at 50% cycle duty, power 5 with a Branson Sonifier 450. The lysate was centrifuged at 4°C, 47810×g for 30min, and the supernatant was loaded onto an pre-equilibrated (buffer A, 50mM Tris pH 8.0, 1mM EDTA) anion-exchange Macro-prep® High Q Media (BIO-RAD, 1560040) column(9mmX100mm), washed with four column volume of Buffer A. A linear gradient 0-50% buffer B (50mM Tris pH 8.0; 1mM EDTA; 1000mM NaCl) was applied over six column volumes. The pyruvate kinase/lactate dehydrogenase (PK/LDH) coupled-assay was used to monitor the elution of APH(3')-IIIa. The fractions containing enzyme were concentrated to 10mL then injected onto HiLoad™ 16/600 Superdex™ 75 pg (GE healthcare) column using an Äkta Avant chromatography system from GE healthcare (Piscataway, NJ 08855-1327, USA) running FPLC buffer [50mM Tris pH 7.5; 1mM EDTA; 150mM NaCl]. The fractions containing

APH(3')-IIIa were concentrated by Amicon® Ultra centrifuge filters with 10 kDa molecular weight cutoffs (SIGMA-ALDRICH, #Z706345). Samples were dialyzed in 4 L of dialysis buffer [50mM Tris pH 7.5; 40mM KCl; 10mM MgCl2; 5% glycerol] for 10h, and stored at -80°C before use. The final concentration of APH(3')-IIIa was determined by the Beer-Lambert law from absorbance measured at 280nm using a extinction coefficient of 48735M-1cm-1[58].

_Ec_PanK and _Pa_PanK expression and purification

The expression and purification of *Ec*PanK was achieved followed the published method[59, 60]. For *Pa*PanK, the pET28a(+)/PanK plasmid was generously provided by Dr. Suzanne Jackowski and was transformed into E. coli RosettaTM (DE3) cells. The cells were allowed to grow at 37°C in 50 mL LB medium supplemented with 50 µg/mL kanamycin for 15 hours. 10 mL of this culture was transferred into 1 L LB medium supplemented with 50 µg/mL kanamycin. The cells were allowed to grow at 37°C to an OD600 of 0.5 to 0.6, before induction with 1 mM IPTG and shaking at 37°C for another 3 hours. The cell culture was S-4 centrifuged at 4°C, 5000 × g for 15 min. The cell pellet was washed with 50 mL PBS buffer and re-pelleted at 4°C, 5000 × g for 15 min. The cell

pellet was resuspended in 30 mL lysis buffer (20 mM Tris pH 7.9, 500 mM NaCl, 1 mM PMSF, 1 mg/mL lysozyme, 5 mM β-mercaptoethanol, and 5 mM imidazole). The mixture was incubated on ice for 30 min, then sonicated on ice for 8 cycles (sonicating 15 s, waiting for 105 s) at 85% cycle duty, power 8 with a Branson Sonifier 450. The cell debris was removed by centrifugation at 4°C, 10,000 × g for 1 h. The supernatant was applied to a pre-equilibrated (20 mM Tris pH7.9, containing 0.5 M NaCl, 5 mM β-mercaptoethanol, 5 mM imidazole) Ni-NTA (QIAGEN, Cat No./ID: 30310) column (6 mL slurry) at a flow rate of 0.5–0.8 mL/min. The column was then washed with 100 mL Tris-HCl buffer (20 mM, pH 7.9, containing 0.5 M NaCl, 5 mM β-mercaptoethanol) before slowly increasing the imidazole concentration to 250 mM over 10 column volumes. The flow rate was kept between 0.5–2 mL/min. The purest fractions were pooled and dialyzed three times against 4 L of 50 mM Tris-HCl buffer, pH = 7.5, containing 1 mM DTT and 1 mM EDTA. The final enzyme concentration was determined by using the Bradford Assay with bovine serum albumin as standard [61].

2.6.2 Coupled Enzyme Assay

*Ec*PanK activity was measured using the pyruvate kinase/lactate dehydrogenase coupled assay. The decrease in NADH concentration was detected by monitoring the spectral absorbance at 340 nm and assuming an extinction coefficient of 6220 M−1·cm−1. The reaction mixtures (200 µL), contained *Ec*PanK (0.15 µM), pantothenate (1.56 mM), NADH (0.3 mM), phospho(enol)pyruvate (2 mM), MgCl2 (10 mM), KCl (20 mM), PK/LDH enzymes from rabbit muscle (10 µL, 6-10 units of pyruvate kinase, 9-14 units lactate dehydrogenase SIGMA ALDRICH P0294), and Tris-HCl pH 7.6 (50 mM), in each well of a 96-well microtiter plate. The reaction was initiated with the addition of ATP at the desired concentration (0-1.5 mM) at 25°C. All experiments were performed in triplicate.

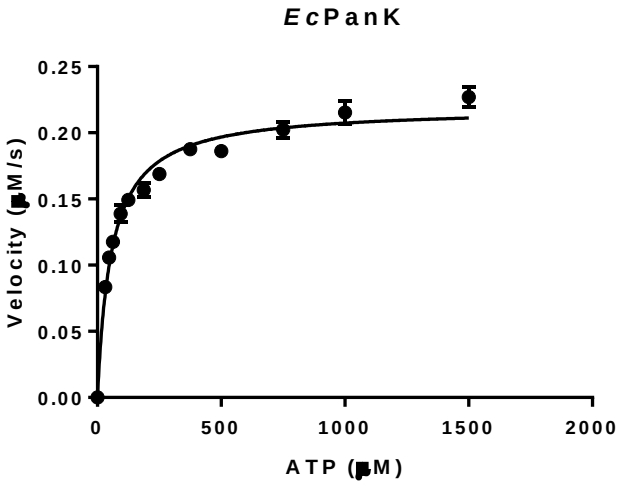

Figure S2.1. *Ec*PanK activity assay. Enzyme velocities determined from the initial slopes of NADH absorbance measurements determined with a fixed pantothenate concentration of 1.56 mM and the ATP concentration varying between 0 and 1.5 mM.

2.6.3 PanK ITC Enzyme Assays

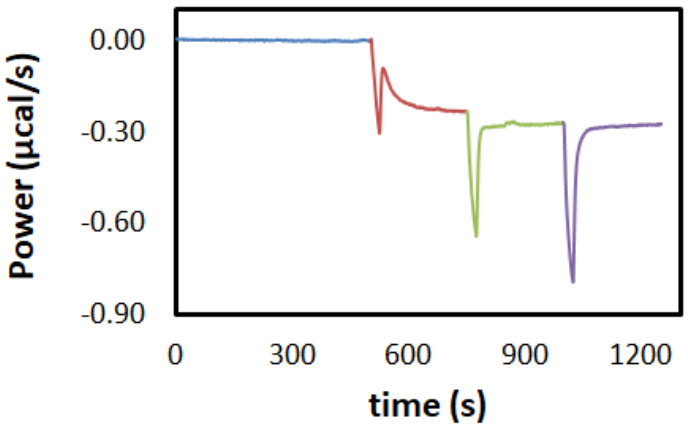

Figure S2.2. ITC saturation assay of *Ec*PanK. 3×12 µL volumes of a solution containing ATP (4mM) and pantothenate (4mM) were injected into a cell containing *Ec*PanK (100nM) and a large excess of pantothenate (3mM) at 250 second intervals. Red, green, and purple traces identify the first, second, and third injections, respectively.

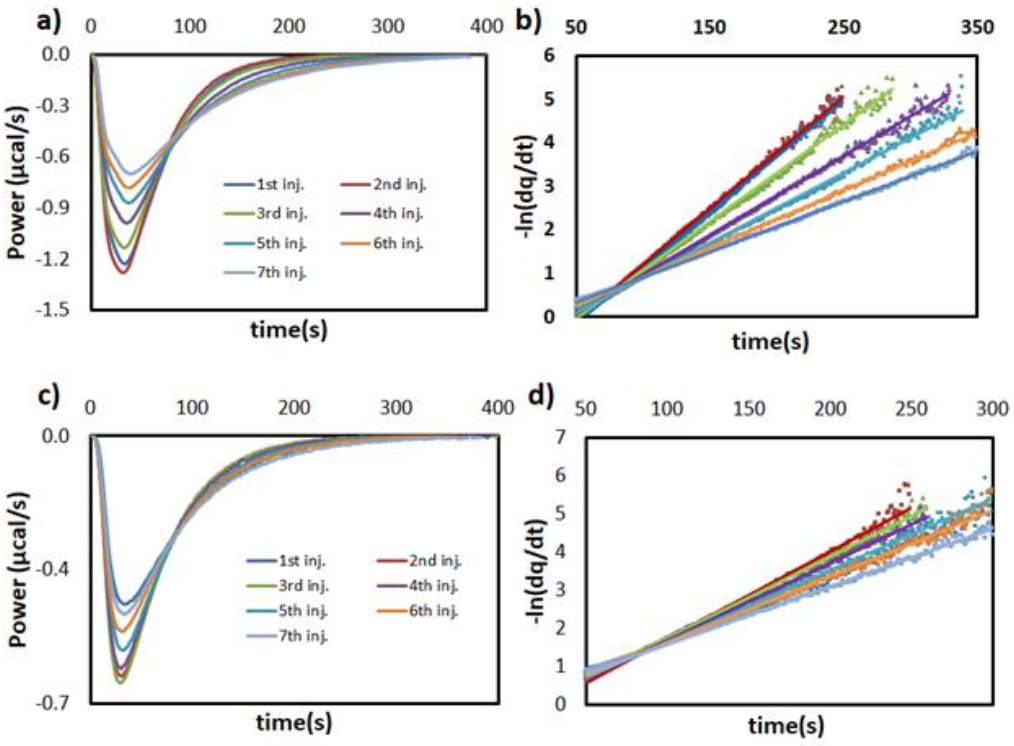

Figure S2.3. ITC transient assay of *Ec*PanK. a) Data for the first 0.2 µL injection were discarded. The subsequent 7×5 µL injections contained ATP (1.2 mM) and pantothenate (1.2 mM) were made every 800 seconds into a reaction cell containing *Ec*PanK (3.2 µM) and pantothenate (2 mM). **c)** Data for the first 0.2 µL injection were discarded. The subsequent 7×4 µL injections containing ATP (0.6 mM) and pantothenate (0.6 mM) were made every 800 seconds into a reaction cell containing *Ec*PanK (3.2 µM) and pantothenate (2 mM). Panels b and d show semi-logarithmic plots of the instrumental thermal power (dQ/dt (µcal/s)) versus time from panels a and c, respectively. Linear regression results (solid lines) are overlaid with the experimental data (solid circles), where the same colors are used to identify injection numbers in panels a, c and b, d respectively.

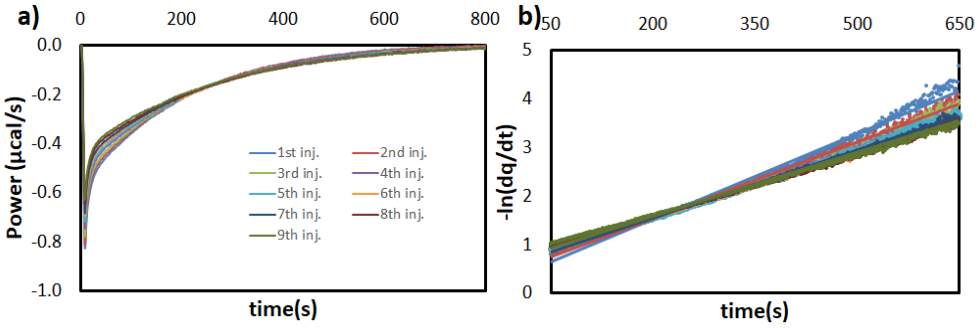

Figure S2.4. ITC transient assay of *Pa*PanK. a) Data for the first 0.2 µL injection were discarded. The subsequent 9×4 µL injections containing ATP (2.5 mM) and pantothenate (2.5 mM) were made every 1300 seconds into a reaction cell containing 11 µM *Pa*PanK and 1.8 mM pantothenate. **b)** semi-logarithmic plot of the instrumental thermal power (dQ/dt (µcal/s)) versus time from panels a. Linear regression results (solid lines) are overlaid with the experimental data (solid circles), where the same colors are used to identify injection numbers in panels a and b.

2.6.4 APH(3')-IIIa ITC Enzyme Assays

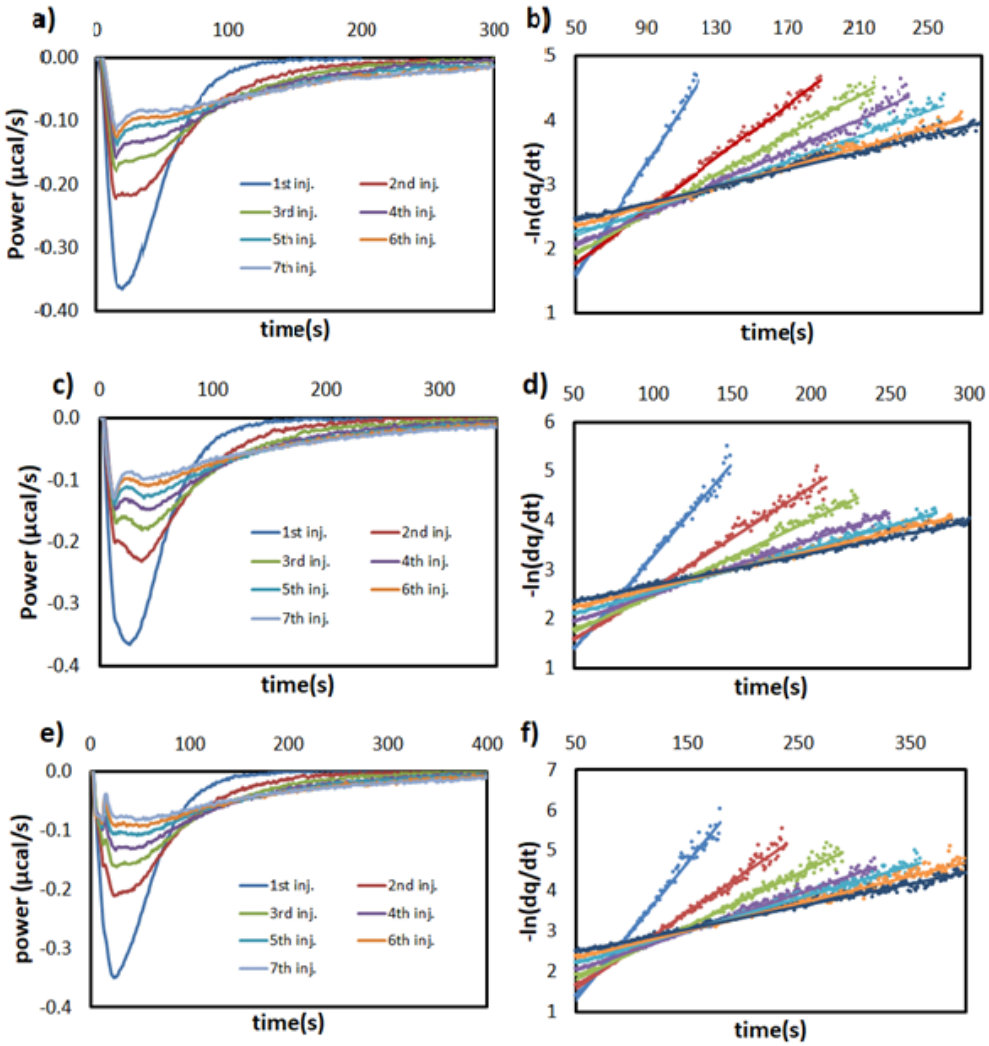

Figure S2.5. ITC transient assay of APH(3')-IIIa pre-saturated with Kanamycin A. Data for the first 0.2 µL injection were discarded. The subsequent 7×5 µL injections containing ATP (240 µM), kanamycin A (240 µM) and ADP (120 µM (a), 240 µM (c) and 360 µM (e) were made every 500 seconds into a reaction cell containing 2 µM APH(3')- IIIa and 120µM of kanamycin A. Panels b, d, f show semi-logarithmic plots of the instrumental thermal power (dQ/dt (µcal/s)) versus time from panels a, c, e respectively. Linear regression results (solid lines) are overlaid with the experimental data (solid circles), where the same colors are used to identify injection numbers in panels a, c, e, and b, d, f, respectively.

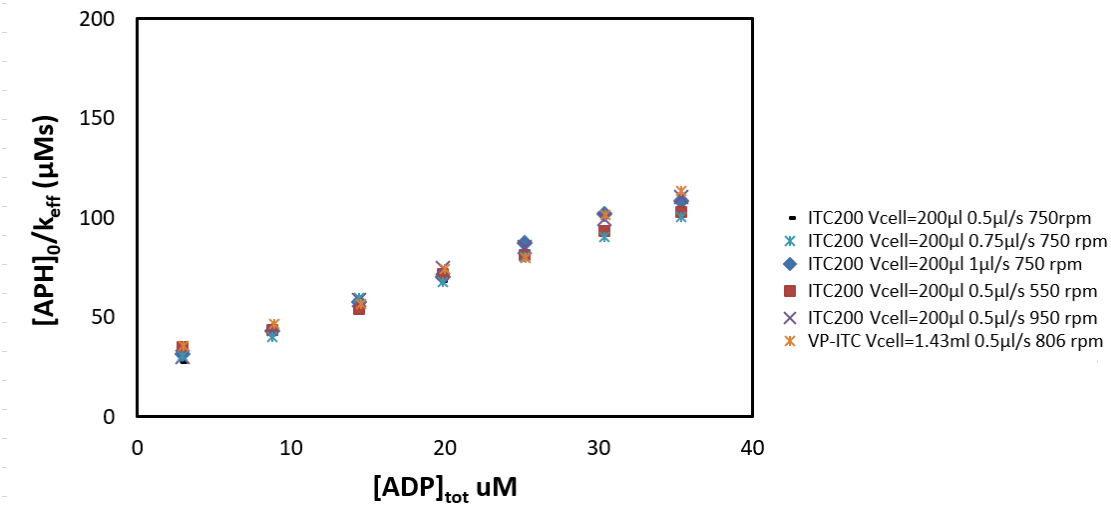

Figure S2.6. Plot of [APH]0/keff versus [ADP]tot with different ITC run parameters. ITC transient assay data for APH(3')-IIIa (**Figure 2.1a**) were reproduced using different stirring speeds (ranging from 550 to 950 rpm), injection rates (ranging from 0.5 µL/s to 1 µL/s) and reaction volumes (ITC200 ,Vcell=200 µL or VP-ITC, Vcell=1.43 mL).

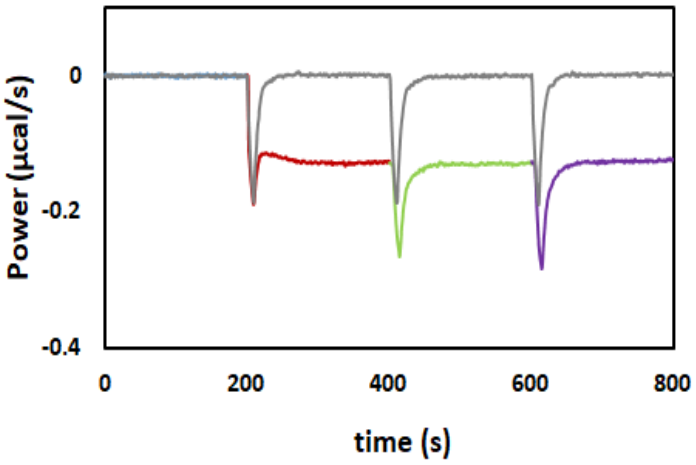

Figure S2.7. Overlay of blank and ITC saturation assay data for APH(3')-IIIa at 37°C. Red, green, and purple traces identify the first, second, and third injections, respectively. (3×10µL 2.5 mM ATP + 2.5 mM kanamycin A → 30 nM APH(3')-IIIa + 120 µM kanamycin A). The blank experiment (grey) was carried out under identical conditions in the absence of APH(3')-IIIa.

2.7 References

1. Cheek, S.; Zhang, H.; Grishin, N. V., Sequence and structure classification of kinases. *J Mol Biol* **2002,** *320* (4), 855-881.

2. Futreal, P. A.; Coin, L.; Marshall, M.; Down, T.; Hubbard, T.; Wooster, R.; Rahman, N.; Stratton, M. R., A census of human cancer genes. *Nat. Rev. Cancer* **2004,** *4* (3), 177-183.

3. Kotzbauer, P. T.; Truax, A. C.; Trojanowski, J. Q.; Lee, V. M. Y., Altered neuronal mitochondrial coenzyme A synthesis in neurodegeneration with brain iron accumulation caused by abnormal processing, stability, and catalytic activity of mutant pantothenate kinase 2. *J. Neurosci.* **2005,** *25* (3), 689-698.

4. Gloyn, A. L., Glucokinase (GCK) mutations in hyper- and hypoglycemia: maturity-onset diabetes of the young, permanent neonatal diabetes, and hyperinsulinemia of infancy. *Hum. Mutat.* **2003,** *22* (5), 353-362.

5. Shaw, K. J.; Rather, P. N.; Hare, R. S.; Miller, G. H., Molecular genetics of aminoglycoside resistance genes and familial relationships of the aminoglycoside-modifying enzymes. *Microbiol. Rev.* **1993,** *57* (1), 138-63.

6. Huynh, Q. K.; McKinsey, T. A., Protein kinase D directly phosphorylates histone deacetylase 5 via a random sequential kinetic mechanism. *Arch Biochem Biophys* **2006,** *450* (2), 141-8.

7. Park, I.; Ives, D. H., Kinetic mechanism and end-product regulation of deoxyguanosine kinase from beef liver mitochondria. *J. Biochem.* **1995,** *117* (5), 1058-61.

8. Peet, G. W.; Li, J., IkappaB kinases alpha and beta show a random sequential kinetic mechanism and are inhibited by staurosporine and quercetin. *J Biol Chem* **1999,** *274* (46), 32655-61.

9. Sobieszek, A., Regulation of smooth-muscle myosin-light-chain kinase. Steady-state kinetic studies of the reaction mechanism. *Eur. J. Biochem.* **1991,** *199* (3), 735-43.

10. Witt, J. J.; Roskoski, R., Jr., Rapid protein kinase assay using phosphocellulose-paper absorption. *Anal. Biochem.* **1975,** *66* (1), 253-8.

11. Hastie, C. J.; McLauchlan, H. J.; Cohen, P., Assay of protein kinases using radiolabeled ATP: a protocol. *Nat. Protoc.* **2006,** *1* (2), 968-971.

12. Rhee, H.-W.; Lee, S. H.; Shin, I.-S.; Choi, S. J.; Park, H. H.; Han, K.; Park, T. H.; Hong, J.-I., Detection of Kinase Activity Using Versatile Fluorescence Quencher Probes. *Angew. Chem., Int. Ed.* **2010,** *49* (29), 4919-4923, S4919/1-S4919/11.

13. Seethala, R.; Menzel, R., A homogeneous, fluorescence polarization assay for Src-family tyrosine kinases. *Anal. Biochem.* **1997,** *253* (2), 210-218.

14. Jing, M.; Verardi, R.; Veglia, G.; Bowser, M. T., Development of a sensitive assay for SERCA activity using FRET detection of ADP. *Anal. Methods* **2014,** *6* (5), 1468-1474.

15. Hong, L.; Quinn, C. M.; Jia, Y., Evaluating the utility of the HTRF Transcreener ADP assay technology: A comparison with the standard HTRF assay technology. *Anal. Biochem.* **2009,** *391* (1), 31-38.

16. Srinivasan, J.; Cload, S. T.; Hamaguchi, N.; Kurz, J.; Keene, S.; Kurz, M.; Boomer, R. M.; Blanchard, J.; Epstein, D.; Wilson, C.; Diener, J. L., ADP-specific sensors enable universal assay of protein kinase activity. *Chem. Biol.* **2004,** *11* (4), 499-508.

17. Easterby, J. S., Coupled enzyme assays: a general expression for the transient. *Biochim Biophys Acta* **1973,** *293* (2), 552-8.

18. Di Trani, J. M.; Moitessier, N.; Mittermaier, A. K., Complete Kinetic Characterization of Enzyme Inhibition in a Single Isothermal Titration Calorimetric Experiment. *Anal. Chem. (Washington, DC, U. S.)* **2018,** *90* (14), 8430-8435.

19. Di, T. J. M.; De, C. S.; O'Leary, R.; Plescia, J.; do, N. C. J.; Moitessier, N.; Mittermaier, A. K.; do, N. C. J., Rapid measurement of inhibitor binding kinetics by isothermal titration calorimetry. *Nat Commun* **2018,** *9* (1), 893.

20. Todd, M. J.; Gomez, J., Enzyme kinetics determined using calorimetry: A general assay for enzyme activity? *Anal. Biochem.* **2001,** *296* (2), 179-187.

21. Di Trani, J. M.; Moitessier, N.; Mittermaier, A. K., Measuring Rapid Time-Scale Reaction Kinetics Using Isothermal Titration Calorimetry. *Anal. Chem. (Washington, DC, U. S.)* **2017,** *89* (13), 7022-7030.

22. Oezen, C.; Serpersu, E. H., Thermodynamics of Aminoglycoside Binding to Aminoglycoside-3'-phosphotransferase IIIa Studied by Isothermal Titration Calorimetry. *Biochemistry* **2004,** *43* (46), 14667-14675.

23. Cai, L.; Cao, A.; Lai, L., An Isothermal Titration Calorimetric Method to Determine the Kinetic Parameters of Enzyme Catalytic Reaction by Employing the Product Inhibition as Probe. *Anal. Biochem.* **2001,** *299* (1), 19-23.

24. Bianconi, M. L., Calorimetric determination of thermodynamic parameters of reaction reveals different enthalpic compensations of the yeast hexokinase isozymes. *J. Biol. Chem.* **2003,** *278* (21), 18709-18713.

25. Olsen, S. N., Applications of isothermal titration calorimetry to measure enzyme kinetics and activity in complex solutions. *Thermochim. Acta* **2006,** *448* (1), 12-18.
26. Rohatgi, N.; Gudmundsson, S.; Rolfsson, O., Kinetic analysis of gluconate phosphorylation by human gluconokinase using isothermal titration calorimetry. *FEBS Lett.* **2015,** *589* (23), 3548-3555.
27. McKay, G. A.; Thompson, P. R.; Wright, G. D., Broad Spectrum Aminoglycoside Phosphotransferase Type III from Enterococcus: Overexpression, Purification, and Substrate Specificity. *Biochemistry* **1994,** *33* (22), 6936-44.
28. Shi, K.; Caldwell, S. J.; Fong, D. H.; Berghuis, A. M., Prospects for circumventing aminoglycoside kinase mediated antibiotic resistance. *Front. Cell. Infect. Microbiol.* **2013,** *4* (June), 22.
29. Szychowski, J.; Kondo, J.; Zahr, O.; Auclair, K.; Westhof, E.; Hanessian, S.; Keillor, J. W., Inhibition of aminoglycoside-deactivating enzymes APH(3')-IIIa and AAC(6')-Ii by amphiphilic paromomycin O2''-ether analogues. *ChemMedChem* **2011,** *6* (11), 1961-6.
30. Mander, L. N.; Liu, H.-w., Comprehensive natural products II : chemistry and biology. Elsevier: Amsterdam ;, **2010**; pp. 355-403.
31. Moolman, W. J. A.; de Villiers, M.; Strauss, E., Recent advances in targeting coenzyme A biosynthesis and utilization for antimicrobial drug development. *Biochem. Soc. Trans.* **2014,** *42* (4), 1080-1086.
32. Spry, C.; Kirk, K.; Saliba, K. J., Coenzyme A biosynthesis: an antimicrobial drug target. *FEMS Microbiol. Rev.* **2008,** *32* (1), 56-106.
33. Spry, C.; van Schalkwyk, D. A.; Strauss, E.; Saliba, K. J., Pantothenate utilization by Plasmodium as a target for antimalarial chemotherapy. *Infect. Disord.: Drug Targets* **2010,** *10* (3), 200-216.
34. McKay, G. A.; Wright, G. D., Kinetic mechanism of aminoglycoside phosphotransferase type IIIa. Evidence for a Theorell-Chance mechanism. *J. Biol. Chem.* **1995,** *270* (42), 24686-92.
35. Leskovac, V., Comprehensive Enzyme Kinetics. Kluwer Academic Publishers: Boston, MA, **2004**; pp. 51-69.
36. Cornish-Bowden, A., *Fundamentals of enzyme kinetics*. 4th ed., rev. and enlarged. ed.; Wiley-VCH: Weinheim, **2012**; p 99-129.
37. Hong, B. S.; Yun, M. K.; Zhang, Y.-M.; Chohnan, S.; Rock, C. O.; White, S. W.; Jackowski, S.; Park, H.-W.; Leonardi, R., Prokaryotic Type II and Type III

Pantothenate Kinases: The Same Monomer Fold Creates Dimers with Distinct Catalytic Properties. *Structure (Cambridge, MA, U. S.)* **2006,** *14* (8), 1251-1261.

38. Song, W.-J.; Jackowski, S., Kinetics and regulation of pantothenate kinase from Escherichia coli. *J. Biol. Chem.* **1994,** *269* (43), 27051-8.

39. Ishikawa, H.; Ogino, H.; Oshida, H., Rates of reactions catalysed by a dimeric enzyme. Effects of the reaction scheme and the kinetic parameters on co-operativity. *Biochem J* **1991,** *280 (Pt 1)*, 131-7.

40. Freiburger, L.; Miletti, T.; Zhu, S.; Baettig, O.; Berghuis, A.; Auclair, K.; Mittermaier, A., Substrate-dependent switching of the allosteric binding mechanism of a dimeric enzyme. *Nature Chemical Biology* **2014,** *10*, 937.

41. Freiburger, L.; Auclair, K.; Mittermaier, A., Global ITC fitting methods in studies of protein allostery. *Methods* **2015,** *76*, 149-161.

42. Yaginuma, H.; Kawai, S.; Tabata, K. V.; Tomiyama, K.; Kakizuka, A.; Komatsuzaki, T.; Noji, H.; Imamura, H., Diversity in ATP concentrations in a single bacterial cell population revealed by quantitative single-cell imaging. *Sci. Rep.* **2014,** *4*, 6522.

43. Tran, Q. H.; Unden, G., Changes in the proton potential and the cellular energetics of Escherichia coli during growth by aerobic and anaerobic respiration or by fermentation. *Eur. J. Biochem.* **1998,** *251* (1/2), 538-543.

44. Smith, C. K.; Windsor, W. T., Thermodynamics of Nucleotide and Non-ATP-Competitive Inhibitor Binding to MEK1 by Circular Dichroism and Isothermal Titration Calorimetry. *Biochemistry* **2007,** *46* (5), 1358-1367.

45. Ravilious, G. E.; Westfall, C. S.; Jez, J. M., Redox-linked Gating of Nucleotide Binding by the N-terminal Domain of Adenosine 5'-Phosphosulfate Kinase. *J. Biol. Chem.* **2013,** *288* (9), 6107-6115.

46. Skjærven, L.; Cuellar, J.; Martinez, A.; Valpuesta, J. M., Dynamics, flexibility, and allostery in molecular chaperonins. *FEBS Letters* **2015,** *589* (19, Part A), 2522-2532.

47. Liu, C.-W.; Li, X.; Thompson, D.; Wooding, K.; Chang, T.-l.; Tang, Z.; Yu, H.; Thomas, P. J.; DeMartino, G. N., ATP binding and ATP hydrolysis play distinct roles in the function of 26S proteasome. *Mol. Cell* **2006,** *24* (1), 39-50.

48. Palmgren, M. G.; Nissen, P., P-Type ATPases. *Annual Review of Biophysics* **2011,** *40* (1), 243-266.

49. Champoux, J. J., DNA Topoisomerases: Structure, Function, and Mechanism. *Annual Review of Biochemistry* **2001,** *70* (1), 369-413.

50. Vale, R. D.; Reese, T. S.; Sheetz, M. P., Identification of a novel force-generating protein, kinesin, involved in microtubule-based motility. *Cell (Cambridge, Mass.)* **1985,** *42* (1), 39-50.
51. Kad, N. M.; Ranson, N. A.; Cliff, M. J.; Clarke, A. R., Asymmetry, commitment and inhibition in the GroE ATPase cycle impose alternating functions on the two GroEL rings. *J Mol Biol* **1998,** *278* (1), 267-78.
52. Xu, Z.; Sigler, P. B., GroEL/GroES: Structure and Function of a Two-Stroke Folding Machine. *Journal of Structural Biology* **1998,** *124* (2), 129-141.
53. Jackson, G. S.; Staniforth, R. A.; Halsall, D. J.; Atkinson, T.; Holbrook, J. J.; Clarke, A. R.; Burston, S. G., Binding and hydrolysis of nucleotides in the chaperonin catalytic cycle: Implications for the mechanism of assisted protein folding. *Biochemistry* **1993,** *32* (10), 2554-2563.
54. Panaretou, B.; Prodromou, C.; Roe, S. M.; O'Brien, R.; Ladbury, J. E.; Piper, P. W.; Pearl, L. H., ATP binding and hydrolysis are essential to the function of the Hsp90 molecular chaperone in vivo. *EMBO J.* **1998,** *17* (16), 4829-4836.
55. Cicenas, J.; Zalyte, E.; Bairoch, A.; Gaudet, P., Kinases and cancer. *Cancers* **2018,** *10* (3), 63/1-63/7.
56. Hon, W.-C.; McKay, G. A.; Thompson, P. R.; Sweet, R. M.; Yang, D. S. C.; Wright, G. D.; Berghuis, A. M., Structure of an enzyme required for aminoglycoside antibiotic resistance reveals homology to eukaryotic protein kinases. *Cell (Cambridge, Mass.)* **1997,** *89* (6), 887-895.
57. Maldonado, E. N.; Lemasters, J. J., ATP/ADP ratio, the missed connection between mitochondria and the Warburg effect. *Mitochondrion* **2014,** *19* (Part_A), 78-84.
58. Pace, C. N.; Vajdos, F.; Fee, L.; Grimsley, G.; Gray, T., How to measure and predict the molar absorption coefficient of a protein. *Protein Sci.* **1995,** *4* (11), 2411-23.
59. Leonardi, R.; Chohnan, S.; Zhang, Y.-M.; Virga, K. G.; Lee, R. E.; Rock, C. O.; Jackowski, S., A pantothenate kinase from Staphylococcus aureus refractory to feedback regulation by coenzyme A. *J. Biol. Chem.* **2005,** *280* (5), 3314-3322.
60. Nazi, I.; Koteva, K. P.; Wright, G. D., One-pot chemoenzymatic preparation of coenzyme A analogues. *Anal. Biochem.* **2004,** *324* (1), 100-105.
61. Kruger, N. J., The Bradford Method For Protein Quantitation. In *The Protein Protocols Handbook*, Walker, J. M., Ed. Humana Press: Totowa, NJ, 2009; pp 17-24.

3. Allosteric interactions in a kinase active site modulate background ATP hydrolysis

3.1 Introduction

Kinases are a class of ubiquitous enzymes that catalyze the transfer of the terminal γ-phosphoryl group from a nucleotide cofactor, usually ATP (or GTP), to a range of substrates, including proteins, lipids, and small molecules, generating phosphorylated products and ADP (or GDP). These enzymes are essential to many fundamental cellular processes such as cell signaling, metabolism, protein regulation, and intracellular transport,[1] and are implicated in a variety of diseases including cancer[2], neurodegeneration[3], diabetes,[4] and antibiotic resistant infections.[5] In addition to catalyzing phosphoryl transfer to the relevant substrate, many kinases also show substantial ATP hydrolytic activity, cleaving the terminal phosphate of ATP to produce ADP and inorganic phosphate (Pi) when the native substrate is absent.[6] In most cases, this activity of kinases can be considered detrimental to the organism since it represents a "futile expenditure of cellular ATP supplies".[7] It is therefore functionally significant that the hydrolysis of ATP generally is much slower than the native phosphotransfer reaction.[8-13] The molecular underpinnings of these large differences in catalytic efficiency are of great interest. Firstly, understanding how kinases regulate the background hydrolysis of ATP helps to shed light on how these crucial enzymes work at a fundamental level. Furthermore, stimulating ATP hydrolysis by a particular kinase

using a small molecule effector could represent an avenue towards the specific therapeutic targeting of cells that express the enzyme.[14]

There are a number of ways in which kinases can suppress ATP hydrolysis while preserving efficient phosphotransferase activity. Cooperative substrate/ATP interactions have been observed for several kinases, such that substrate binding increases the affinity for ATP, leading to more efficient catalysis when ATP is present at sub-saturating concentrations.[15, 16] In addition, for many enzymes the maximum turnover rate, k_{cat}, for the native reaction is orders of magnitude greater than that of hydrolysis.[8-13, 17] The origin of this difference in k_{cat} is not well understood. Most kinases form a ternary enzyme/ATP/substrate Michaelis complex and follow a dissociative mechanism, such that the bond between the γ-phosphorus atom and ADP is largely broken before a bond starts to form with the incoming oxygen atom of the substrate.[18, 19] According to the general reaction scheme for a dissociative ligand substitution, this gives[20]

$$ATP + S \underset{k_{-1}}{\overset{k_1}{\rightleftarrows}} ADP + PO_3^- + S \xrightarrow{k_2} ADP + pS \qquad (3.1)$$

where S is either the native substrate (phosphotransfer) or water (hydrolysis), PO_3^- is the metaphosphate intermediate, pS is the phosphorylated product (phosphotransfer) or Pi

(hydrolysis), and charge balance and proton release have been neglected in the interests of simplicity. The rate of the chemical step of catalysis, k_{chem}, within the active site, i.e. excluding substrate binding and product release steps, is therefore

$$k_{\text{chem}} = \frac{k_1 k_2}{k_{-1}+k_2} \tag{3.2}$$

The difference in catalytic rates for the phosphotransfer vs hydrolytic reactions could simply be due to k_2 (capture of the PO_3^- intermediate) being much larger for the native substrate than it is for water. Studies have suggested that k_2 acceleration can be promoted by both positioning [18, 19] and electrostatic activation [18, 21, 22] of the substrate, so it is perhaps unsurprising that the hydrolysis side-reaction with water generally occurs more slowly. On the other hand, there is at least one example of a kinase (MEK) in which ATP hydrolysis is more than an order of magnitude faster than the native reaction,[7] so the preference for phosphotransfer is not an absolute feature of the chemistry. This raises the intriguing possibility that substrate binding could allosterically activate the enzyme towards the nucleotide cofactor. In other words, substrate binding could produce an increase in the rate of γ-phosphate bond scission (higher k_1) and/or stabilize the metaphosphate intermediate (higher k_1/k_{-1}). There is structural evidence to support this idea. Many kinases are tightly regulated by a variety of allosteric effectors that drive

conformational shifts between active and inactive conformations.[14, 23-25] In one example, the bound GTP cofactor was observed to adopt two different poses in the active site: an active one in which the γ-phosphate was positioned for transfer and inactive one in which it was oriented away from catalytic residues.[14] Substrate binding drove a conformational rearrangement from the inactive towards the active pose. Nevertheless, there is currently little functional data to accompany the structural evidence. It remains largely unknown to which extent and by which mechanism substrate-induced conformational changes actually influence the catalytic activity of kinases towards the ATP or GTP cofactor.

We have studied the process of ATP hydrolysis in the bacterial kinase aminoglycoside-3'-phosphotransferase-IIIa (APH(3')-IIIa) which phosphorylates 4,6-disubstututed aminoglycosides at the 3'-hydroxyl and 4,5-disubstututed aminoglycosides at the 3'- and/or 5"- hydroxyls.[26] APH(3')-IIIa is carried by enterococcal and staphylococcal opportunistic pathogens where it confers resistance to a broad spectrum of aminoglycoside (Amg) antibiotics including the clinically important drug amikacin.[27] The enzyme follows an ordered Bi-Bi mechanism in which ATP binds before the Amg substrate, and ADP dissociates after the phospho-Amg (pAmg) product.[28] X-ray crystallographic structures of APH(3')-IIIa have been determined for the apo state, as well as for binary and ternary complexes with substrates and cofactors,[21, 22, 27, 29

revealing striking similarities to eukaryotic protein kinases.[27, 29, 30] We have measured the rates of background ATP hydrolysis by APH(3')-IIIa, both in the presence and absence of non-substrate aminoglycosides (nsAmgs) that are chemically similar to the native substrates but lack the 3' hydroxyl required to receive the phosphoryl group. Previous work showed that nsAmgs can increase the rate of background ATP hydrolysis in another bacterial phosphotransferase, but there is little information on the underlying mechanism.[17] To better understand this phenomenon in APH(3')-IIIa, we developed a suite of Isothermal Titration Calorimetry (ITC) experiments to measure the rate of ATP hydrolysis under both steady-state and single-turnover conditions and to characterize the affinities, and association and dissociation rates of nsAmgs. ITC measures in real time the heat released or absorbed when one solution (in a syringe) is titrated into another (in the sample cell). The technique has typically been used to study host/guest binding interactions but has recently been gaining popularity as a general enzyme kinetic assay.[31, 32] Since most chemical reactions are either exothermic or endothermic, ITC can be applied to virtually any enzymatic reaction. We have previously used ITC to quantify ADP inhibition of APH(3')-IIIa and to measure enzyme inhibitor association and dissociation rates.[33, 34] In the present work, we found using ITC that binding of an nsAmg to APH(3')-IIIa accelerates the chemical step of ATP hydrolysis by at least 10- to 20-

fold. This is a direct demonstration of allosteric communication between the Amg- and ATP-binding pockets of the active site, such that the presence of a substrate substantially increases the activity of the enzyme towards cleaving the ADP/γ-phosphate bond. These results are consistent with substrate-induced rearrangements of the nucleotide positioning loop that have been observed crystallographically. [19, 21]

3.2 Methods

3.2.1 Reagents

The enzyme APH(3')-IIIa was expressed and purified as described previously.[33, 35] Purified APH(3')-IIIa was stored in buffer A (50mM Tris-HCl, pH 7.5, 40mM KCl and 10mM $MgCl_2$) at -80°C. The concentration of the enzyme was determined using spectroscopic absorption at 280nm and an extinction coefficient ε = 48735 M^{-1} cm^{-1}. Stock solutions of tobramycin (Sigma-Aldrich), gentamicin C (Sigma-Aldrich), and ATP (Chem-Implex) were prepared in buffer A.

3.2.2 ITC Experimental Conditions

The ITC assays were carried out with a MicroCal iTC_{200} (MicroCal, Northampton, MA, USA) with a stirring speed of 750 rpm in high gain mode with a filter time of 1 s. All

solutions were degassed for 3 minutes using a GE MicroCal ThermoVac Degassing Station before being loaded into the ITC. All experiments were performed in triplicate in buffer A at 37°C.

3.2.3 ITC Continuous assays

[ATP → APH(3')]: Cell: (4 µM APH(3')-IIIa), Syringe: (1mM ATP), 1×0.1 µL injection (data discarded) followed by 4×9 µL injections every 3000 seconds.

[ATP → APH(3') + tobramycin]: Cell: (4 µM APH(3')-IIIa + 200µM tobramycin), Syringe: (1mM ATP), 1×0.1 µL injection (data discarded) followed by 4×9 µL injections every 1000 seconds.

[ATP → APH(3') + gentamicin C]: Cell: (3 µM APH(3')-IIIa + 200µM gentamicin C), Syringe: (1mM ATP), 1×0.1 µL injection (data discarded) followed by 4×9 µL injections every 1200 seconds.

3.2.4 ITC Activation Assays

[tobramycin → APH(3') + ATP]: Cell: (3 µM APH(3')-IIIa + 1 mM ATP), Syringe: (80 µM tobramycin), 6×5 µL injections every 110 seconds.

[gentamicin C → APH(3') + ATP]: Cell: (3 μM APH(3')-IIIa + 1 mM ATP), Syringe: (120 μM gentamicin C), 7×5 μL injections every 180 seconds.

[streptomycin → APH(3')+ ATP]: Cell: (3 μM APH(3')-IIIa + 1 mM ATP), Syringe: (800 μM streptomycin), 7×5 μL injections every 150 seconds.

3.2.5 ITC Single-Turnover Assays

[ATP → APH(3')]: Cell: (30 μM APH(3')-IIIa), Syringe: (200 μM ATP), 5 μL injection at 700 seconds interval.

[ATP → APH(3') +tobramycin]: Cell: (10 μM APH(3')-IIIa + 200μM tobramycin), Syringe: (200 μM ATP), 5 μL injection at 120 seconds interval.

[ATP → APH(3') + gentamicin C]: Cell: (30 μM APH(3')-IIIa+ 200μM gentamicin C), Syringe: (200 μM ATP), 5 μL injection at 80 seconds interval.

3.2.6 ITC Data Analysis

The velocities of the enzyme-catalyzed reactions (v) were calculated from the displacements of the ITC signals from the initial baselines, measured in energy per unit time (dQ/dt), according to

$$v = \frac{d[P]}{dt} = -\frac{1}{V_{cell}\Delta H_{react}}\frac{dQ}{dt}, \quad (3.3)$$

where [P] is the concentration of product (ADP), V_{cell} is the volume of the sample cell in the ITC instrument (200 μL), and ΔH_{react} is the reaction enthalpy. The reaction enthalpy was calculated from the total area of a peaks from "continuous" ITC experiments according to

$$\Delta H_{react} = \frac{-1}{[P]_{final}V_{cell}}\int_{t=0}^{t=\infty}\frac{dQ}{dt}dt, \quad (3.4)$$

where $[P]_{final}$ is the total concentration of product formed. For multiple-turnover experiments, reaction rates thus obtained were fitted to the Michaelis Menten equation, taking into account competitive product inhibition by ADP, according to

$$v = \frac{k_{cat}[APH][ATP]}{K_m\left(1+\frac{[ADP]}{K_i^{ADP}}\right)+[ATP]} \quad (3.5)$$

where the concentration of [ATP] was calculated from partial integrals of each ITC peak according to

$$[ATP](t) = \frac{\int_t^{\infty}\frac{dQ}{dt}dt}{\int_0^{\infty}\frac{dQ}{dt}dt}[ATP](t=0) \quad (3.6)$$

and [ADP] was treated as a constant parameter for each peak, equal to the total amount of ATP contained in all previous injections plus the ATP of the current injection.

Finally, the ITC instrument detects the heat generated in the sample cell with a delay on the order of seconds. For ITC signals that vary more slowly (minutes timescale), such as the multiple-turnover "continuous" assays, this delay can be ignored in the analysis. For rapidly-varying signals, such as the single-turnover and activation assays, this delay must be quantitatively accounted for. The ITC signal, g(t), can be described mathematically as the convolution of the instantaneous heat signal, h(t), with an instrument response function, *f*(*t*), which defines the lag in detection [34, 36]

$$g(t) = f(t) \otimes h(t) = \int_0^t f(\tau)g(t-\tau)d\tau, \quad (3.7)$$

where $\otimes$ indicates the convolution. The response function can be well-approximated by the ITC signal resulting from a very short (0.1 s) injection in a calibration reaction (eg Ca^{2+}/EDTA). A short injection produces an instantaneous burst of heat, which makes h(t) close to a Dirac delta function and g(t)≈f(t). Instantaneous heat profiles can be deconvoluted from experimental ITC data using the convolution theorem which states that

$$\mathcal{F}\big(g(t)\big) = \mathcal{F}\big(f(t)\big) \cdot \mathcal{F}\big(h(t)\big) \quad (3.8)$$

where $\mathcal{F}$ indicates the Fourier transform, giving

$$h(t) = \mathcal{F}^{-1}\left(\frac{\mathcal{F}(g(t))}{\mathcal{F}(f(t))}\right). \quad (3.9)$$

ITC signals were deconvoluted where indicated, using Equation and filtering noise in the frequency (transformed) domain as described previously [36].

3.3 Results

3.3.1 ATP Hydrolysis by APH(3')-IIIa

We first quantified the kinetic parameters of ATP hydrolysis by APH(3')-IIIa using a "continuous" ITC assay as described by Todd and Gomez.[32] The sample cell contained the apo-enzyme (in the absence of non-substrate aminoglycosides) and series of injections were made from a syringe containing an ATP solution. The resulting heat flow is plotted as a function of time in **Figure 3.1a** with different colors used for different injections. Each injection produced a downward deflection of the ITC signal, corresponding to an exothermic reaction occurring in the sample cell when the ATP and enzyme were mixed. The signal returned to baseline over periods of about 2500 s, during which the ATP was completely converted to ADP and Pi. Note that blank injections of ATP into buffer produced minimal perturbations of the ITC signal, so the peaks truly reflect APH(3')-IIIa-catalyzed hydrolysis. The absolute integrated area of each peak is equal to the total

amount of heat released when all of the injected ATP is hydrolysed. The fraction of ATP remaining at a time point, *t*, after an injection can be calculated by taking the area to the right of *t* and dividing by the total area of the peak. Furthermore, the velocity of the enzyme at time=*t* is directly proportional to the magnitude of the deflection of the ITC signal (see Methods Section). Therefore each ITC peak can be converted directly into a Michaelis-Menten (MM) plot of reaction velocity, v, versus [ATP] (**Figure 3.1b**).[32] A complication arises from the fact that ADP is a competitive inhibitor of APH(3')-IIIa. It accumulates in the cell with each injection, slowing the enzyme and making each peak slightly broader than one before. Nevertheless, the set of four MM curves can be globally fit to yield the Michaelis constant, K_m, the turnover number, k_{cat}, and the inhibition coefficient K_i^{ADP}, listed in **Table 3.1**. Notably, the k_{cat} we measured for ATP hydrolysis (0.01 s^{-1}) is more than 140-fold slower than the k_{cat} for the native reaction with kanamycin as a substrate (1.42 s^{-1}).[33] Thus APH(3')-IIIa represents typical example of a kinase with far less efficient hydrolytic compared to phosphotransfer activities.

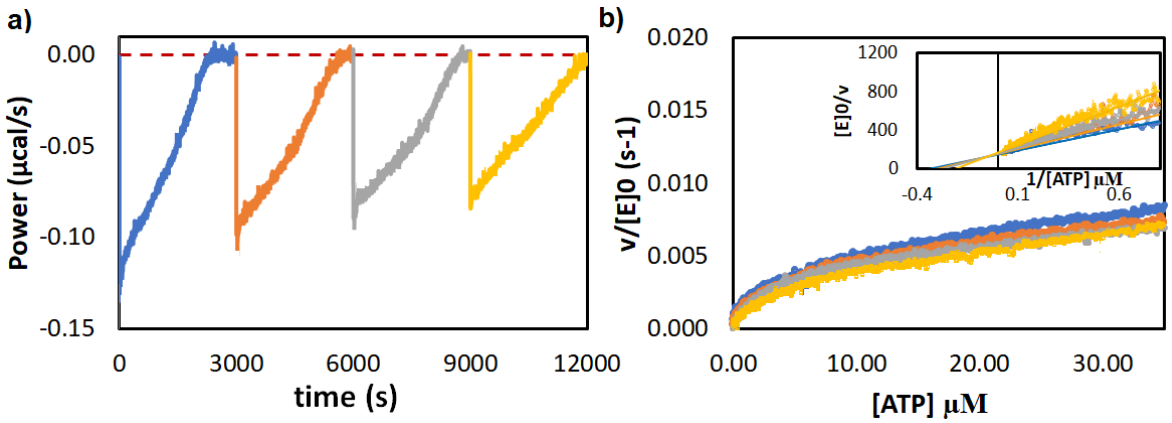

Figure 3.1. Hydrolysis of ATP by APH(3')-IIIa. a) ITC continuous assay data for multiple injections of ATP into APH(3')-IIIa (4×9 µL 1mM ATP → 200 µL 4 µM APH(3')-IIIa). b) Reaction rates plotted as a function of [ATP] calculated from a. The inset shows a double reciprocal plot of the same data.

3.3.2 Non-substrate Aminoglycosides (nsAmgs) Enhance ATP Hydrolysis by APH(3')-IIIa

To probe allosteric communication between the Amg and ATP binding pockets of APH(3')-IIIa, we repeated the ITC kinetics experiments described above, this time in the presence of two nsAmgs, tobramycin and gentamicin C. These are 4,6-disubstututed aminoglycosides that lack the 3'-OH group targeted by APH(3')-IIIa and are therefore not substrates for this enzyme (as verified below). Apart from the lack of the 3' OH group, tobramycin and gentamicin C are virtually identical to the APH(3')-IIIa substrates kanamycin B, and gentamicin B, respectively. A series of injections of an ATP solution

was made into a sample containing APH(3')-IIIa and either tobramycin or gentamicin C (**Figure 3.2c, e**). The resulting ITC signals from the tobramycin experiment are overlaid with those of enzyme in the absence of nsAmgs in **Figure 3.2a**. The deflection of the ITC signal was initially much greater in the presence of tobramycin, indicated a higher enzyme velocity, and the peak was much narrower implying that all of the injected ATP was hydrolyzed in less time. The MM plots calculated from the raw ITC data (**Figure 3.2b**) exhibited a larger k_{cat} (higher asymptote) and lower K_m (sharper increase) when tobramycin was present. Recurrent injections of ATP into the enzyme with tobramycin and gentamicin C (**Figure 3.2c, e**), showed competitive inhibition by accumulating ADP (**Figure 3.2d, f**), similarly to the apo-enzyme. Values of k_{cat}, K_m, and K_i^{ADP} were extracted and are listed in **Table 3.1**. The presence of nsAmgs increased k_{cat} by factors of about 2 and 4, indicating faster turnover, and reduced K_m by factors of 8 and 2, indicating tighter interactions with ATP, for gentamicin C and tobramycin, respectively. Mass spectrometry was used to analyze the contents of the sample cell after completion of the ITC experiments. These showed complete conversion of ATP to ADP while tobramycin and gentamicin C remained completely unmodified, confirming that the ITC signals obtained for the enzyme with tobramycin and gentamicin C indeed corresponded to the heat generated by enhanced ATP hydrolysis (**Figure. S3.1**).

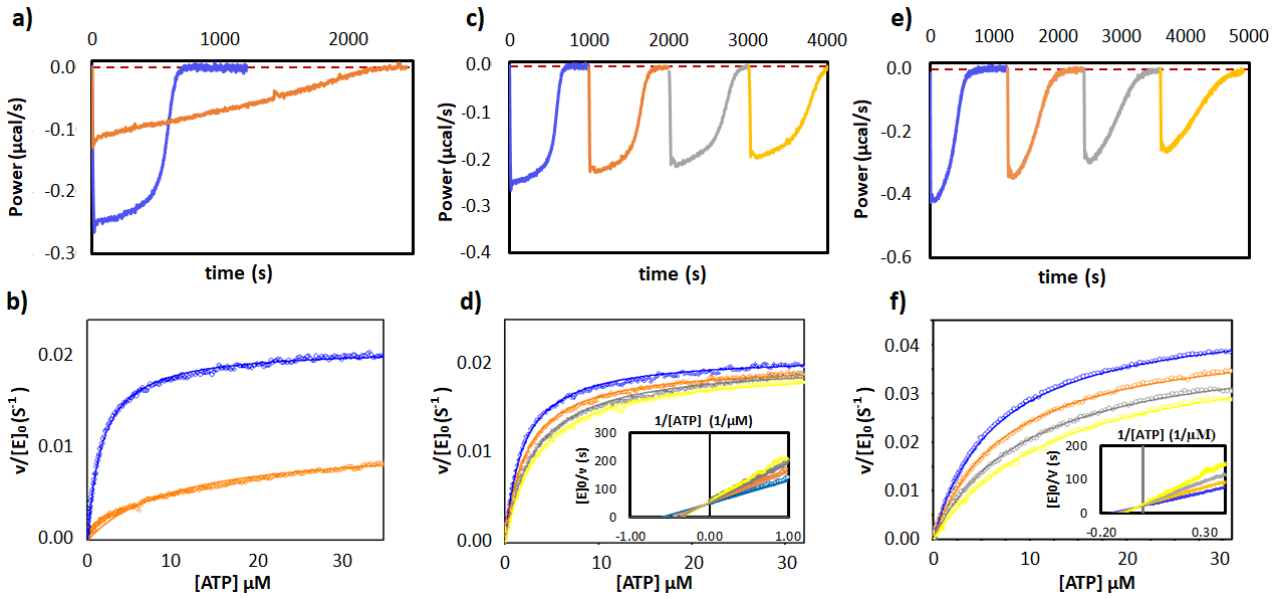

Figure 3.2. Activation of APH(3')-IIIa by non-substrate aminoglycosides tobramycin and gentamicin C. a) Raw ITC traces for the APH(3')-IIIa-catalysed ATP hydrolysis reaction in the presence (blue) and absence (orange) of 200 µM tobramycin, (9 µl of 1 mM ATP → 200 µL 4 µM APH(3')-IIIa ± 200 µM tobramycin). **b)** Reaction rates plotted as a function of [ATP] calculated from a. Experimental data are shown as points and fits to the Michaelis-Menten equation are shown as solid lines. **c)** ITC continuous assay data for APH(3')-IIIa presaturated with tobramycin (4×9 µL 1mM ATP → 200 µL 4 µM APH(3')-IIIa + 200 µM tobramycin). **d)** Reaction rates plotted as a function of [ATP] calculated from c. The inset shows a double reciprocal plot of the same data **e)** ITC continuous assay data for APH(3')-IIIa presaturated with gentamicin C (4×9 µL 1mM ATP → 200 µL 3 µM APH(3')-IIIa + 200 µM gentamicin C). **f)** Reaction rates plotted as a function of [ATP] calculated from e. The inset shows a double reciprocal plot of the same data

Table 3.1. Summary the reaction entropy and kinetic parameters for the APH(3')-IIIa background hydrolysis

AMGs	**ΔH (kcal/mol)**	**K_m (μM)**	**k_{cat} (s^{-1})**	**K_i^{ADP} (μM)**	**k_{obs} (s^{-1})**	**k_{on}^{ATP} ($M^{-1}s^{-1}$)**	**k_{chem} (s^{-1})**	**k_{diss}^{ADP} (s^{-1})**	**k_{ass}^{ADP} (M^{-1} s^{-1})**
Native Rx (kanamycinA)	-14.9 ± 0.1 [a]	26.3 ± 0.9[a]	1.42 ± 0.06[a]	7.3 ± 0.2[a]	NA	6.35×10^{4} [b]	7.1[c]	1.42[d]	1.9×10^{5} [e]
No AMGs	-15.6 ± 0.8	6.75 ± 2.76	0.011 ± 0.001	73.8 ± 11.9	0.010 ± 0.001	6.35×10^{4} [f]	0.012 ± 0.002[g]	1.42[f]	1.9×10^{4} [e]
Tobramycin	-15.5 ± 0.4	0.82 ± 0.08	0.021 ± 0.001	47.8±4.5	0.09 ± 0.01	0.9×10^{4} [h]	≥0.10 ± 0.01[i]	≤0.027[j] ≥0.021[k]	5.6×10^{2} [e] 4.4×10^{2} [e]
Gentamicin C	-15.4 ± 0.3	3.70 ± 0.57	0.047 ± 0.007	44.3 ± 2.9	0.19 ± 0.03	0.6×10^{4} [h]	≥0.21 ± 0.03[i]	≤0.061[j] ≥0.047[k]	1.4×10^{3} [e] 1.1×10^{3} [e]

[a]From reference [33]. [b]From reference [37] . [c]From reference [38]. [d]$k_{diss}^{ADP}=k_{cat}$. [e]$k_{ass}^{ADP}= k_{diss}^{ADP}/ K_i^{ADP}$. [f]Assumed identical to native reaction. [g]According to **Equation 3.20**. [h]Assuming $k_{obs}=k_{on}[E]$. [i]Lower limit for k_{chem} according to **Equations 3.14** and **3.20**. [j]According to **Equations 3.14** and **3.20** (upper limit). [k]Assuming $k_{diss}^{ADP}=k_{cat}$ (lower limit).

We hypothesized that nsAmgs enhance the ATP hydrolytic activity of APH(3')-IIIa by binding in the Amg pocket of the active site and inducing a rearrangement of the ATP pocket that promotes γ-phosphate cleavage. If that is the case, an observed enzyme kinetic parameter (such as the ITC signal, dQ/dt) should be a population-weighted average of the values for the free and nsAmg-bound forms of the enzyme and should show an asymptotic dependence on nsAmg concentration according to:

$$\left(\frac{dQ}{dt}\right)_{obs} = \left(\frac{dQ}{dt}\right)_{free} + f_{bound}\left(\left(\frac{dQ}{dt}\right)_{bound} - \left(\frac{dQ}{dt}\right)_{free}\right). \quad (3.10)$$

f_{bound} is the fraction of protein bound to nsAmg,

$$f_{bound} = \frac{1}{2}\left(1 + \chi_r + \frac{1}{c} - \sqrt{\left(1 + \chi_r + \frac{1}{c}\right)^2 - 4\chi_r}\right) \quad (3.11)$$

where χ_r = [nsAmg]/[APH(3')-IIIa], c=[APH(3')-IIIa]/K_d, and K_d is the equilibrium dissociation constant for the nsAmg.[39] In order to test this hypothesis, we designed an ITC experiment to measure the [nsAmg]-dependence of catalytic enhancement directly, similar to an approach we previously developed for measuring enzyme inhibition.[34] A saturating amount of ATP was placed in the sample cell with dilute enzyme at a high enough concentration to produce a measurable heat signal from hydrolysis, but not high enough to appreciably consume the ATP, leading to a steady rate of hydrolysis and a

horizontal ITC signal (**Figure 3.3a,c**). Tobramycin and gentamicin C were added to the sample cell in a series of injections. Each injection led to an acceleration in enzyme activity and increase in the rate of heat production, producing a series of downward steps. The magnitudes of the deflections were proportional to the enhancements in reaction velocity and asymptotically approached a maximum enhancement as the nsAmg concentrations increased in the sample cell. The enhancements were fit using **Equations 3.10** and **3.11**, varying $\left(\frac{dQ}{dt}\right)_{free}$, $\left(\frac{dQ}{dt}\right)_{bound}$, and K_d, giving excellent agreement with the calculated curves and yielding the equilibrium dissociation constants for gentamicin C (K_d^{genC}=1.85 ± 0.05 μM, **Figure 3.3b**) and tobramycin (K_d^{tob}=0.89 ± 0.03 μM, **Figure 3.3e**), close to the previously reported value of K_d^{tob}=0.8 μM.[40] In addition, we tested streptomycin (**Figure 3.3f**), an aminoglycoside that does not match the substrate profile of APH(3')-IIIa. It lacks the 2-deoxystreptamine moiety and contains two bulky guanidino groups, likely preventing it from binding in the active site. Additions of concentrated streptomycin failed to produce any shift in the ITC signal except for injection artifacts (**Figure 3.3f**), suggesting that nsAmgs must resemble the natural substrates of APH(3')-IIIa in order to enhance ATP hydrolysis.

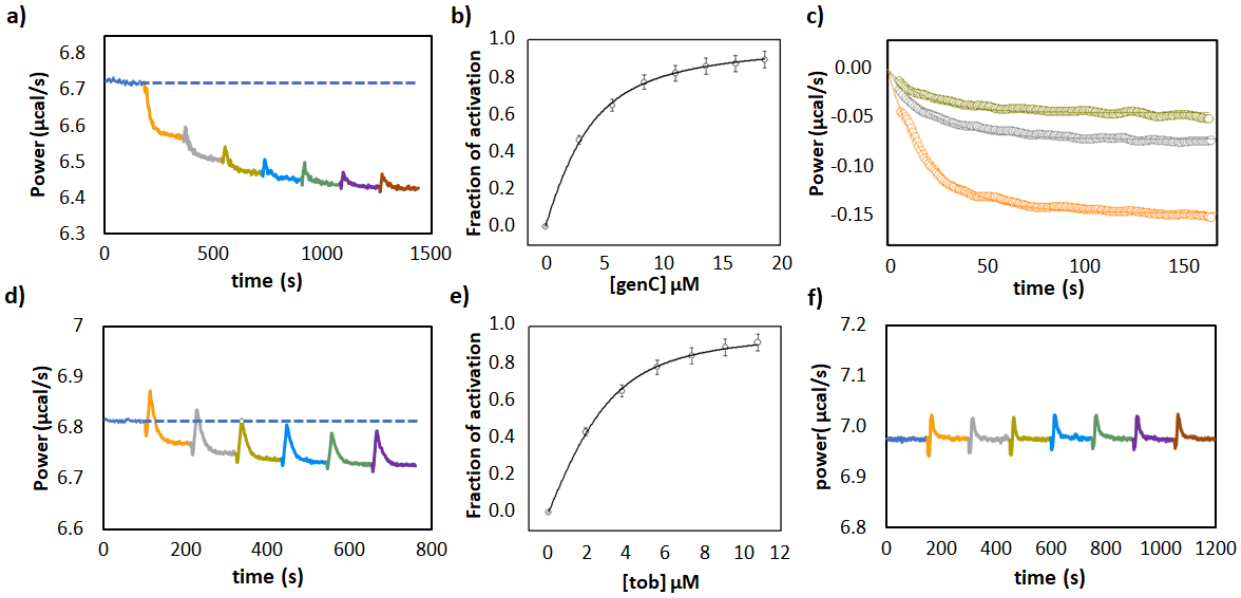

Figure 3.3. APH(3')-IIIa activation kinetics experiments. a) Raw ITC data for multiple injections of gentamicin C into APH(3')-IIIa saturated with ATP (7×5 µL 120 µM gentamicin C → 200 µL 3 µM APH(3')-IIIa + 1mM ATP). **b)** Fractional change in enzyme activation plotted as a function of gentamicin c concentration. **c)** Overlay of data for injections 1,2 and 3 (orange, grey and green open circles) with fits to second-order binding kinetics (solid lines). **d)** Raw ITC data for multiple injections of tobramycin into APH(3')-IIIa saturated with ATP (6×5 µL 80 µM tobramycin → 200 µL 3 µM APH(3')-IIIa + 1mM ATP). **e)** Fractional change in enzyme activation plotted as a function of tobramycin concentration. **f)** Raw ITC data for multiple injections of streptomycin into APH(3')-IIIa saturated with ATP (7×5 µL 800 µM streptomycin → 200 µL 3 µM APH(3')-IIIa + 1mM ATP).

3.3.3 Gentamicin C Exhibits Slow Binding Kinetics

Additional information can be gained from a closer inspection of **Figure 3.3a**. Each injection of gentamicin C led to a downward shift in the ITC signal, presumably due to its binding in the active site and enhancing ATP hydrolysis. However these downward shifts did not happen instantaneously, and instead occurred over periods of about 50 seconds after each injection (after deconvolution of the ITC signal as described in the Methods Section), as highlighted in **Figure 3.3c**. We hypothesized that these delays were due to slow kinetics of binding. To test this idea, we globally fit the ITC traces to an equation describing association kinetics[41, 42]

$$[\mathrm{APH}]^{\mathrm{free}}(\mathrm{t}) = \frac{\mathrm{E+D-e^{-2D}}k_{\mathrm{on}}\mathrm{t+}\varphi\mathrm{(E-D)}}{\mathrm{1-e^{-2D}}k_{\mathrm{on}}\mathrm{t+}\varphi} \qquad (3.12)$$

$$\varphi = \ln|[\mathrm{APH}]^0 - \mathrm{E} - \mathrm{D}| - \ln|[\mathrm{APH}]^0 - \mathrm{E} + \mathrm{D}|$$

$$\mathrm{D} = \sqrt{\mathrm{E}^2 + [\mathrm{APH}]^{\mathrm{tot}}\mathrm{K_d}}$$

$$\mathrm{E} = \frac{1}{2}([\mathrm{APH}]^{\mathrm{tot}} - [\mathrm{nsAmg}]^{\mathrm{tot}} - \mathrm{K_d})$$

where $[\mathrm{APH}]^{\mathrm{free}}$ is the concentration of enzyme not bound to nsAmg, $[\mathrm{APH}]^0$ is the value of $[\mathrm{APH}]^{\mathrm{free}}$ at t=0, and $[\mathrm{APH}]^{\mathrm{tot}}$ and $[\mathrm{nsAmg}]^{\mathrm{tot}}$ are the total concentrations of enzyme and nsAmg. Fits using this equation and fixing the K_d to the value extracted in **Figure 3.3b** (1.85 μM), and calculating ITC signals according to **Equation 3.12** were in excellent agreement with the experimental data points, as shown in **Figure 3.3c**. In these plots, the

x-axis shows the length of time evolved after the end of each injection and the ITC signals have been shifted in the vertical dimension so that each begins with a power of zero. The extracted association rate constant k_{on}^{genC}= 0.69 × 10^4 $M^{-1}s^{-1}$ is slower than the rate of Amg binding estimated from steady state kinetics (1.4 × 10^5 M^{-1} s^{-1}) and smaller than typical values for small molecule association rates, which are usually on the order of 10^5 to 10^9 $M^{-1}s^{-1}$.[34, 43, 44] Slow association rates can reflect coupling between the binding event and protein conformational changes, as we believe may be the case here.[37] X-ray crystal structures show that Amg binding is associated with rearrangements of both the Amg and nucleotide binding pockets(See Supporting Information).[21, 22, 29] Enzyme conformational changes can lead to discrepancies between apparent steady-state and rapid-mixing kinetics, which could explain why the ITC activation kinetics do not match the steady-state estimates.[37, 45] We calculated the dissociation rate as k_{off}^{genC} = K_d^{genC}×k_{on}^{genC} = 0.013 s^{-1}, which is much slower than the turnover rate for ATP hydrolysis in the presence of gentamicin C (k_{cat}^{genC} = 0.05 s^{-1}). This implies that on average, about 4 molecules of ATP are hydrolyzed for each gentamicin C dissociation event. In other words, the same molecule of nsAmg is usually present in the active site during ATP binding, hydrolysis, and ADP release. Ideally, we could have performed a similar treatment of the tobramycin binding profiles. However the overall enhancement produced

by tobramycin is about 2.5-fold less than that of gentamicin C, leading to much smaller changes in the ITC signal (**Figure 3.3a** versus **3.3d**) and hindering such an analysis.

3.3.4 nsAmgs Accelerate the Chemical Step of Catalysis

The rate of enzyme catalytic turnover, k_{cat}, can be separated into at least two sequential components: k_{chem}, the rate at which the chemical transformation takes place in the active site and k_{diss}, the dissociation rate for the product. For the Uni-Uni ATP hydrolysis reaction, this gives:

$$E{:}\,ATP \overset{k_{\mathrm{chem}}}{\rightarrow} E{:}\,ADP \overset{k_{\mathrm{diss}}}{\rightarrow} E + ADP \tag{3.13}$$

The macroscopic k_{cat} is related to these two microscopic rates according to

$$k_{\mathrm{cat}} = \frac{k_{\mathrm{chem}} k_{\mathrm{diss}}}{k_{\mathrm{chem}} + k_{\mathrm{diss}}} \tag{3.14}$$

If the chemical step is much slower than dissociation ($k_{chem} << k_{diss}$), it becomes rate limiting and $k_{cat}=k_{chem}$. Conversely, if $k_{diss} << k_{chem}$, then $k_{cat}=k_{diss}$. Under multiple turnover conditions, where $[E]_{tot} << [ATP]$ and every molecule of APH(3')-IIIa hydrolyzes many molecules of ATP, it is not possible to distinguish whether either of these situations apply, or alternatively if $k_{chem} \approx k_{diss}$. This ambiguity can be resolved by single-turnover enzyme

kinetic experiments in which $[E]_{tot}>>[ATP]$ and each enzyme molecule hydrolyzes either one or zero molecules of ATP during the course of the reaction.[46] The effective scheme for hydrolysing ATP to ADP with a large excess of enzyme becomes

$$ATP \underset{k_{off}}{\overset{k_{on}[E]}{\rightleftarrows}} E{:}ATP \xrightarrow{k_{chem}} E{:}ADP \tag{3.15}$$

where the concentration of free enzyme, [E], is nearly constant, and $k_{on}[E]$ is a pseudo-first order rate constant. In general, the concentration of E:ADP grows in a bi-exponential manner according to[46]

$$[ADP](t) = C\left(1 - (Ae^{-k_a t} + Be^{-k_b t})\right) \tag{3.16}$$

Where C is the final concentration of ADP (and initial concentration of ATP) and

$$k_{a,b} = \frac{k_{on}[E]+k_{off}+k_{chem}}{2}\left(1 \pm \sqrt{1 - \frac{4k_{chem}k_{on}[E]}{(k_{on}[E]+k_{off}+k_{chem})^2}}\right). \tag{3.17}$$

According to the boundary conditions ([ADP](t=0) = 0 and d[ATP]/dt(t=0) = 0),

$$A = \frac{k_b}{k_b - k_a} \text{ and } B = 1 - A. \tag{3.18}$$

If the chemical step is much slower than association ($k_{chem}<<k_{on}[E]$), then the binding step rapidly equilibrates and the appearance of ADP becomes nearly mono-exponential

$$[ADP](t) = C(1 - e^{-k_{obs} t}) \tag{3.19}$$

with a single rate constant, k_{obs}, close in value to k_{chem} [46]

$$k_{obs} = k_{chem} \frac{[E]}{[E]+K_d^{ATP}} \quad (3.20)$$

where $K_d^{ATP} = k_{off}/k_{on}$. If the association step is rate limiting ($k_{on}[E] << k_{chem}$), then the kinetics are also mono-exponential (**Equation 3.19**) with a rate constant close to $k_{on}[E]$,

$$k_{obs} = k_{on}[E] \frac{k_{chem}}{k_{chem}+k_{off}} . \quad (3.21)$$

In either case, k_{obs} is always less than or equal to k_{chem} and can be interpreted as a lower bound for the rate of the chemical step of catalysis.

We have developed an approach for performing single-turnover enzyme kinetics experiments by ITC. To our knowledge, ITC has not been used in this fashion before. The sample cell contained a solution of APH(3')-IIIa at a concentration of 30 μM which is 4.5-fold higher than the K_m for the enzyme in the absence of nsAmgs. ATP was then rapidly injected to a concentration of 5 μM, and the resulting heat trace was recorded. We performed a control experiment injecting instead AMP-PCP, a non-hydrolysable analog of ATP that binds in a similar manner to the cofactor. The total heat evolved in these experiments was 10-fold less than those performed with ATP, indicating that the heat of hydrolysis is much higher than the heat of binding. Therefore the ITC traces we

observed in the single-turnover experiments predominantly reported the kinetics of catalysis, i.e. the rate of ADP production. They were deconvoluted and used to calculate [ADP] as a function of time, as given by **Equations 3.9** and **3.6** in the Methods Section. The resulting data were indeed well fit by a mono-exponential curve (**Figure 3.4a**). ATP is in rapid equilibrium with the apo-enzyme [37], therefore we used **Equation 3.20** and the extracted value of k_{obs}^{apo}=0.010 ± 0.001s^{-1} to calculate k_{chem}^{apo}= 0.012 ± 0.002s^{-1} which is very close to the steady-state turnover rate k_{cat}^{apo} =0.011 ± 0.001s^{-1}. The close agreement of k_{chem}^{apo} and k_{cat}^{apo} implies that k_{chem}^{apo} is rate-limiting and k_{diss}^{apo}>>k_{chem}^{apo}. This is consistent with the turnover rate for the native reaction with kanamycin A as a substrate (1.42 s^{-1}); both the native reaction and ATP hydrolysis have dissociation of the binary E:ADP complex as the last step of the catalytic cycle[28, 37]. In the native reaction, ADP dissociation is rate-determining, thus k_{diss}^{apo}=1.42 s^{-1}, which is much faster than the measured value of k_{chem}^{apo}. The experiment was then repeated for APH(3')-IIIa saturated with tobramycin or gentamicin C, and at enzyme concentrations 8- and 12-fold greater than the K_m. The single-turnover ITC heat traces were again well-fit by mono-exponential kinetics (**Figure 3.4b,c**) and yielded rate constants, k_{obs}^{tob}= 0.10±0.01 s^{-1} and k_{obs}^{genC}= 0.21±0.03 s^{-1}. If one again assumes a rapid pre-equilibrium with ATP, then k_{chem}^{nsAmg}≈k_{obs}^{nsAmg} and the chemical step of ATP hydrolysis is accelerated by at least 10-

to 20-fold when an nsAmg is present in the active site. Furthermore, the single-turnover k_{chem} values were about 5-fold faster than the steady-state k_{cat}, which indicates that ADP dissociation has become largely rate limiting in the presence of nsAmgs. ADP dissociation rates calculated using **Equation 3.14** ($k_{diss}^{ADP,tob}$=0.027 s^{-1} $k_{diss}^{ADP,genC}$=0.061 s^{-1}) were up to 50-fold slower than for the apo enzyme, which makes sense, since the presence of a substrate or analog in the aminoglycoside binding pocket largely blocks access to and from the ATP binding pocket.[28]

The slow access to the ATP site reveals an inconsistency in the analysis above, namely the assumption of rapid pre-equilibration of ATP in the presence of nsAmgs and the use of **Equation 3.20** to interpret k_{obs} values above. If ADP access is significantly reduced, then presumably so is that of the ATP co-factor. A more self-consistent interpretation is as follows: Firstly, steric hindrance by the nsAmg slows ATP binding to the point that association governs the single-turnover kinetics, **Equation 3.21** applies, and $k_{obs} \approx k_{on}[E]$. Using the experimental k_{obs} values and [E]=10 μM or [E]=30 μM, this gives $k_{on}^{ATP,tob}$=0.9×10^4 $M^{-1}s^{-1}$ and $k_{on}^{ATP,genC}$=0.6×10^4 $M^{-1}s^{-1}$, respectively. Secondly, the 10- to 20-fold acceleration of k_{chem} estimated above is very possibly an underestimation. For the native reaction, single-turnover kinetics give $k_{chem} \approx 7.1$ s^{-1} [38]. Such a rapid chemical step would be consistent with our data for the nsAmg-bound enzyme as well, assuming

that ADP dissociation becomes completely rate determining under multiple turnover conditions and k_{diss}=k_{cat}, (giving k_{diss}^{ADP} values about 15% slower than those calculated above). Overall, the data unambiguously show that for apo-enzyme, k_{chem} is rate-determining under multiple turnover conditions and is about 700-fold slower than for the native reaction. For nsAmg-bound enzyme, k_{chem} is at least 10-fold faster than for the apo-enzyme (likely much more) and ADP release is slowed at least 25-fold, becoming rate-determining.

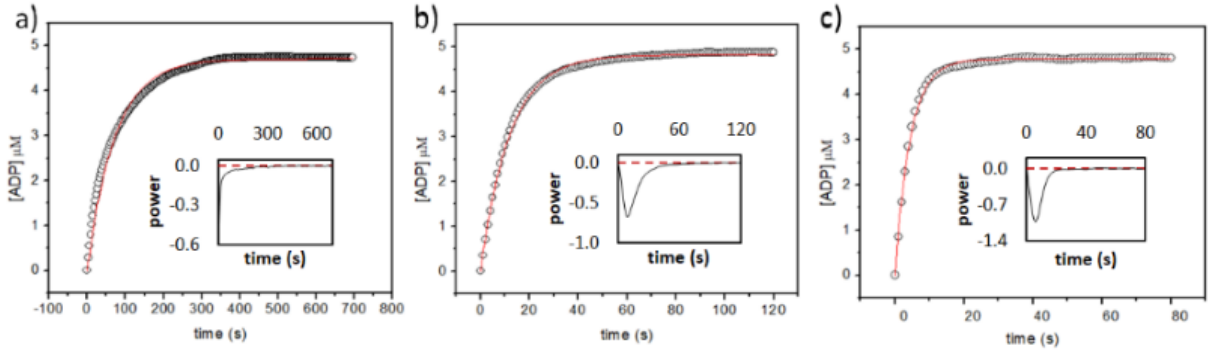

Figure 3.4. ITC-derived single-turnover kinetics of ATP hydrolysis by APH(3')-IIIa. ADP concentrations calculated from deconvoluted ITC data (insets) obtained **a)** in the absence of Amgs, and saturated with **b)** tobramycin and **c)** gentamicin C.

3.4 Discussion

3.4.1 Structural Basis of APH(3')-IIIa Activation by Amgs

Our results show that the presence of an nsAmg in the active site accelerates that cleavage of the ATP γ-phosphate by at least 10- to 20-fold. Fortunately, there exists structural and mutational data to explain how this allosteric activation may be achieved. X-ray crystal structures of APH(3')-IIIa in the apo form and in complex with various combinations of aminoglycosides and nucleotides have been reported by Berghuis and co-workers. [21, 22, 27, 29] The enzyme has a bilobal structure with the nucleotide binding pocket in a deep cleft between the two lobes and the aminoglycoside binding site near to the C-terminus. An approximately ten-residue region, referred to as the nucleotide positioning loop (NPL), has structural homology to the activation loop of eukaryotic protein kinases[29] and is strongly implicated in the chemical step of the native reaction. [19, 29] The structure of a binary complex of APH(3')-IIIa with an ATP analog (AMP-PNP) [PDB:1J7U] has a hydrogen bond between the hydroxyl of Ser27 in the NPL and an oxygen of the nucleotide β-phosphate, however there are no interactions between the protein and γ-phosphate.[19, 29] Binding of an Amg (butirosin A) induces a conformational change in the NPL such that the main chain amide of Met26 forms a new hydrogen bond with the nucleotide γ-phosphate. This interaction was proposed to stabilize the meta-

phosphate intermediate during phosphoryl transfer (**Figure 3.5**).[21, 29] The key roles played by Met26 and Ser27 were confirmed by mutagenesis. Substitutions with Ala or Pro at either location slowed k_{cat} by 3- to 40-fold, and reduced k_{chem} to the point that it became rate-determining, in contrast to the wild-type enzyme where k_{cat} is limited by ADP dissociation.[19] We propose that nsAmg binding induces the same allosteric transition in the NPL as is seen in the X-ray crystal structures, and that this conformational change produces the acceleration in ATP hydrolysis that we observe experimentally. Furthermore, it seems likely that this allosteric linkage between Amg binding and the activation of γ-phosphate cleavage evolved specifically to prevent the enzyme from performing unwanted ATP hydrolysis in the absence of substrate.

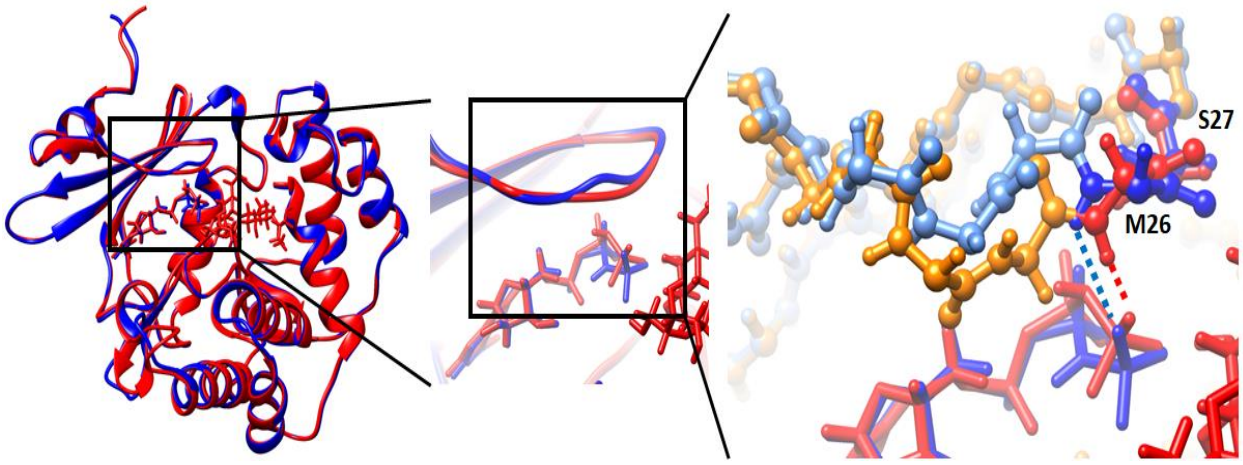

Figure 3.5. Overlay the crystal structures in the NPL region of APH(3')-IIIa AMPPNP binary complex (blue; PDB 1J7U) with of APH(3')-IIIa AMPPNP Butirosin A ternary complex (red; PDB 3TM0). Upon binding with the AMG, the

additional interaction is observed between the main chain amide of Met26 and a γ-phosphate oxygen, as shown in the right panel.

3.4.2 Towards Therapeutic Activation of ATP Hydrolysis

The rate of background hydrolysis by APH(3')-IIIa is roughly 140-fold lower than the rate of phosphoryl transfer to Amgs. Even so, it is likely the presence of the enzyme is metabolically costly to bacteria in the absence of antibiotic substrates. Mobashery and co-workers[17] studied a related enzyme, APH(3')-Ia, which phosphorylates kanamycin A and hydrolyzes ATP (k_{cat}^{kan}=1.7 s^{-1}, k_{cat}^{hyd}=0.02 s^{-1}, respectively), with similar rates to APH(3')-IIIa (k_{cat}^{kan}=1.4 s^{-1}, k_{cat}^{hyd}=0.011 s^{-1}). Based on APH(3')-Ia expression levels, they calculated that background ATP hydrolysis by the enzyme could consume as much as sevenfold the existing pool of ATP during a single bacterial doubling time. They then cultured *E. coli* bacteria over many doubling times and compared the loss of plasmids harboring the APH(3')-Ia gene versus otherwise identical plasmids encoding instead a β-lactamase enzyme that does not have a detrimental background activity. They found that after 1500 generations, 50% of bacteria had lost the APH(3')-Ia-bearing plasmids compared to only 10% loss of the β-lactamase-bearing plasmid. This shows that even relatively low background ATP hydrolytic activity can generate negative selective

pressure. Faster background ATP hydrolysis would likely be far more deleterious and could potentially be exploited to treat infections. It has been suggested that small molecules that allosterically activate nucleotide triphosphate hydrolysis by antibiotic resistance phosphotransferases could trap bacteria in a check-mate situation, in which they must either wastefully consume large amounts of their energy stores or lose resistance.[14] Such a strategy could also apply to cancer therapeutics, where over-expression and dysregulation of kinases is often linked to malignant transformation.[47] Our results suggest that the idea of stimulating ATP-hydrolysis with small molecules is realistic, at least in the case of APH(3')-IIIa. In fact, non-substrate aminoglycosides have precisely this effect on APH(3')-IIIa, increasing the k_{cat} for hydrolysis by 2- to 4-fold. Furthermore, we find that much larger accelerations are likely feasible. The chemical step of ATP hydrolysis is increased by at least 10- to 20-fold and possibly much more. This large acceleration in k_{chem} is mostly obscured by the fact that the presence of an nsAmg blocks access to the nucleotide pocket, slowing ADP binding kinetics by at least 13-fold, likely with similar effects on ATP binding. If a small molecule could be identified that induces the allosteric activation of the NPL loop while preserving the access of ATP and ADP, it is likely that acceleration of k_{cat}^{hyd} up to the ADP dissociation rate, i.e. by more than two orders of magnitude, are within reach. Furthermore, many other kinases follow

random bi-bi mechanisms in which the substrates bind and products dissociate with no preferred order.[48-51] Presumably, the presence of substrate analogs in the active sites of these enzymes would not block ATP binding or ADP release. Therefore such systems could be especially attractive targets for small molecules that allosterically induce background ATP hydrolysis.

3.4.3 The Native Reaction Mechanism

Our investigation of nsAmg-activated ATP hydrolysis also sheds new light on the nature of the native aminoglycoside phosphotransferase mechanism. APH(3')-IIIa has been extensively studied using classic enzymology approaches, including steady-state[28, 35, 37] and pre-steady state[38] kinetics assays, dead end inhibitor, substrate, and product inhibition studies, and thio and viscosity effect measurements.[28, 35, 37, 38] Together, these studies indicate that the enzyme follows a Theorell-Chance mechanism in which ATP binds first, followed by rapid Amg binding, phosphoryl transfer, and pAmg release. ADP dissociation is slower and rate-determining, as illustrated in **Figure 3.6**. The structural basis of the ordered mechanism is evident from X-ray crystal structures of the ternary complexes of APH(3')-IIIa with Amg and ADP or AMP-PNP.[19, 21, 22] The Amg partially

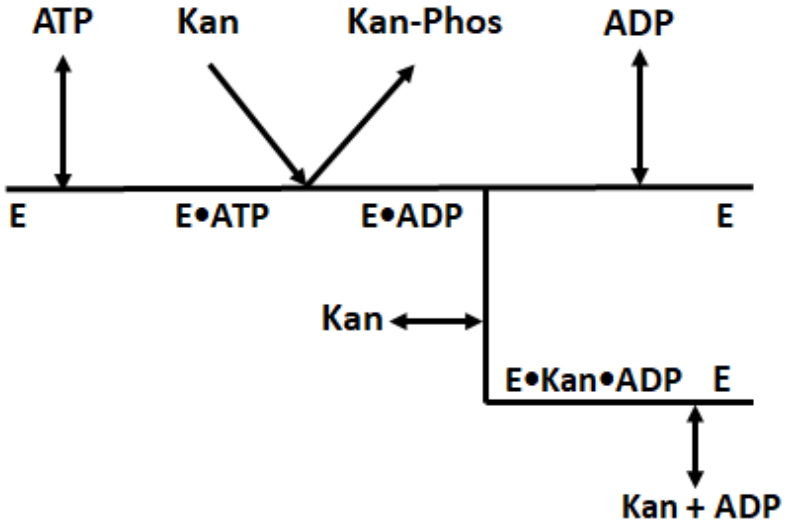

Figure 3.6. Theorell-Chance kinetic mechanism of APH(3')-IIIa.

blocks access to the nucleotide binding site, presumably impeding ingress and egress of ATP and ADP. However, our kinetics results suggest that this blockage is not absolute, and provide some quantitative values for the rates of nucleotide binding with an Amg already present in the active site. Using the ADP dissociation rates, k_{diss}, determined in the single-turnover experiments and the values of K_i^{ADP} from the steady-state measurements, we calculated ADP association rates as $k_{ass}=k_{diss}/K_i^{ADP}$, as listed in **Table 3.1**. Dissociation was slowed by about 25- to 50-fold while association was slowed about 35- and 15-fold with tobramycin and gentamicin C bound, respectively, compared to the apo-enzyme. Furthermore, given a classic Theorell-Chance mechanism, the ATP association rate for the apo-enzyme is $k_{on}^{ATP}=k_{cat}^{native}/K_m^{ATP,native}=6.35\times10^4$ M^{-1} s^{-1}.[37] If we assume that ATP binding was rate-limiting in the single turnover experiments (as

discussed above), this gives k_{on}^{ATP}=0.9×10^4 M^{-1} s^{-1} and k_{on}^{ATP}=0.6 ×10^4 M^{-1} s^{-1}, for the tobramycin- and gentamicin C-bound enzymes, respectively, corresponding to 6- and 9-fold slower association rates. These numbers help to explain why the macroscopic mechanism is ordered: ATP association is about an order of magnitude slower if the Amg binds first. However, our results also suggest that this ordering is not unconditional. Amgs readily form non-productive binary (E:Amg) and ternary (E:ADP:Amg) complexes[28]. Nucleotide access to the active site in the presence of bound Amgs is sufficiently rapid such that escape of ADP from E:ADP:Amg and entry of ATP into E:Amg could become kinetically relevant at very high Amg concentrations.

3.4.4 Enzyme Kinetics by ITC

Although ITC has been used to study enzyme kinetics for almost two decades [32], recognition of the distinct advantages it offers is still not widespread. It is therefore worthwhile discussing several aspects of the study that were uniquely enabled by this technique. Firstly, we analyzed ITC experiments in which multiple injections of ATP were made into a sample cell containing APH(3')-IIIa with and without nsAmgs. The reaction became slower with each injection due to competitive inhibition by the reaction

product, ADP, which accumulated throughout the course of the experiment. This allowed us to measure the inhibition constant, K_i^{ADP}, in addition to k_{cat} and K_m. It is not possible to study ADP inhibition of kinases using the standard pyruvate kinase/lactate dehydrogenase coupled enzyme assay, since this approach relies on converting all ADP into ATP as quickly as it is produced.[33, 52] The ITC-derived K_i^{ADP} values were useful here, as they allowed us to calculate ADP association rates, given the experimentally-determined rates of dissociation. Secondly, we measured the enhancement of the hydrolysis reaction as we injected nsAmgs into a sample cell containing APH(3')-IIIa and ATP, extracting binding affinities for tobramycin and gentamicin C. The gradual response of the ITC signal also allowed us to determine how quickly gentamicin C entered the active site and stimulated hydrolysis. This approach is very similar to our recent ITC-based investigation of enzyme inhibitor binding kinetics,[34] and takes advantage of the fact that ITC detects the rate of catalysis directly, thus time-dependent changes in reaction velocity are straightforward to measure. In contrast, traditional enzyme assays measure the concentrations of products and/or substrates over time, and changes in reaction velocity appear only as curvature in the data.[34] The gentamicin C binding kinetics established that ATP association and ADP association occur while the nsAmg remains in place and were crucial for formulating the model of the APH(3')-IIIa reaction mechanism

presented here. Our results illustrate the utility and versatility of using ITC to measure the binding kinetics of inhibitors and allosteric effectors. Finally, we performed ITC enzyme kinetics experiments under single turnover conditions, which, to our knowledge, is the first example ITC being used in this manner. Notably, this experiment detected on-enzyme ATP hydrolysis in real-time, in contrast to all previous single-turnover kinase studies in which discontinuous methods were employed, for instance quenching the reaction in acid by rapid mixing and quantifying the amount of ADP at various time points by HPLC.[53] Since most on-enzyme chemical steps are expected to release or absorb heat, in principal, ITC could be used as a general method for real-time detection of single-turnover kinetics. The main drawback is that the kinetics of the reaction must be slower than the response time of the instrument ($\tau_{response} \approx$ 8 to 20 seconds [54, 55]), otherwise they become completely obscured by internal heat flow and electronic processes occurring within the instrument during the measurements. This limits the scope of the method to systems where k_{obs} (**Equation 3.19**) is less than or equal to about 0.1 s^{-1}. Fortunately, this is the case for ATP hydrolysis by APH(3')-IIIa, and the single-turnover measurements were essential to one of the main findings of the study, that k_{chem} is dramatically enhanced by nsAmg binding.

3.5 Conclusion

The mechanisms by which kinases avoid background ATP hydrolysis while maintaining phosphoryl transfer activity towards their substrates are important for explaining their cellular function but remain poorly understood. Structural studies have implicated allosteric communication between the substrate and nucleotide binding pockets, such that enzymatic catalysis is activated only (or mainly) when a substrate is present to receive the γ-phosphoryl group.[14] This idea was supported by observations that substrate analogs induced ATP hydrolysis in a bacterial kinase,[17] but detailed kinetic information has been largely lacking. Here we show that the presence of non-substrate analogs in the active site of APH(3')-IIIa accelerates the chemical step of ATP hydrolysis by a minimum of 10- to 20-fold, presumably through allosteric rearrangement of the nucleotide binding loop. It is likely that a similar transition activates the enzyme towards its natural substrates. This study provides some of the first kinetic information on allosteric interactions within a kinase that modulate background ATP hydrolysis. For APH(3')-IIIa, a bound nsAmg molecule substantially blocks access of ADP (and probably ATP) to the active site, consistent with the enzyme's Theorell Chance mechanism.[28] This slows steady-state ATP hydrolysis in the presence of nsAmgs to the extent that the acceleration of the chemical step is largely hidden. It is worth noting that if the nucleotide

binding pocket (and positioning loop) adopted the active conformation constitutively in the absence of substrate, the rate of background ATP hydrolysis would be at least 10- to 20-fold greater than it is in the wild-type enzyme, since nucleotide access to the active site would be unhindered. This provides compelling evidence that APH(3')-IIIa, and likely other kinases, have evolved specific mechanisms to avoid ATP hydrolysis when substrates are absent. These same mechanisms could be exploited to allosterically induce background ATP hydrolysis by kinases expressed in pathogens or cancers in order apply negative selective pressure. We arrived at these conclusions using a suite of ITC experiments that measured both steady state and single-turnover enzyme kinetic parameters as well as the affinities and binding rates of nsAmg allosteric effectors. This study demonstrates the versatility of ITC as an enzyme kinetic technique and highlights its potential for better understanding this important and largely overlooked aspect of kinase activity.

3.6 Supporting Information

3.6.1 ESI-MS Data

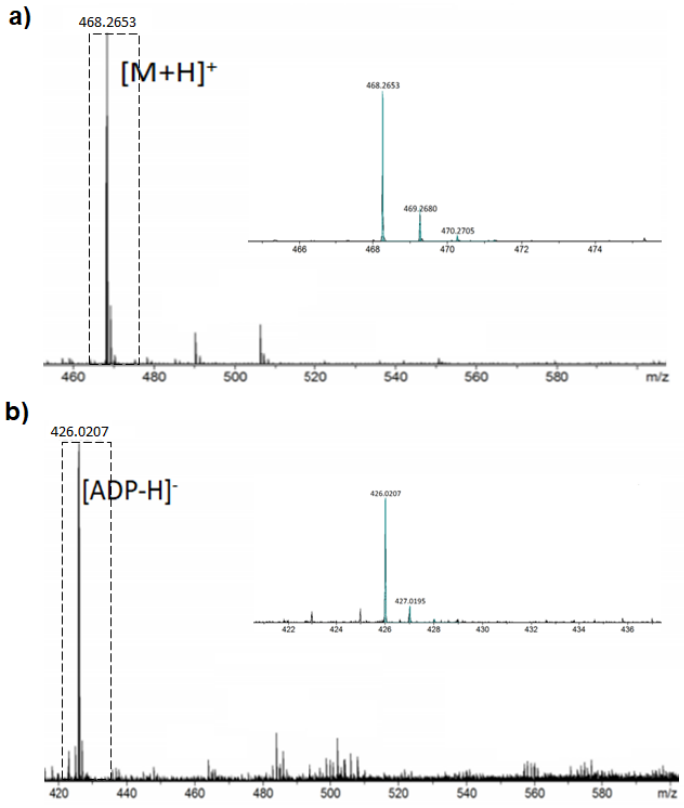

Figure S3.1. ESI Mass spectra of non-substrate tobramycin after APH(3')-IIIa catalyzed background hydrolysis of ATP. a) non-substrate tobramycin remains unphosphorylated after reaction. Positive mode. The peak at 468.2653 is due to $[Tob+H]^+$=468.2699. b) ATP was converted to ADP by APH(3')-IIIa catalyzed background hydrolysis. Negative mode. The peak at 426.0207 is due to $[ADP-H]^-$=426.0215. No phosphorylated product was detected around 547.

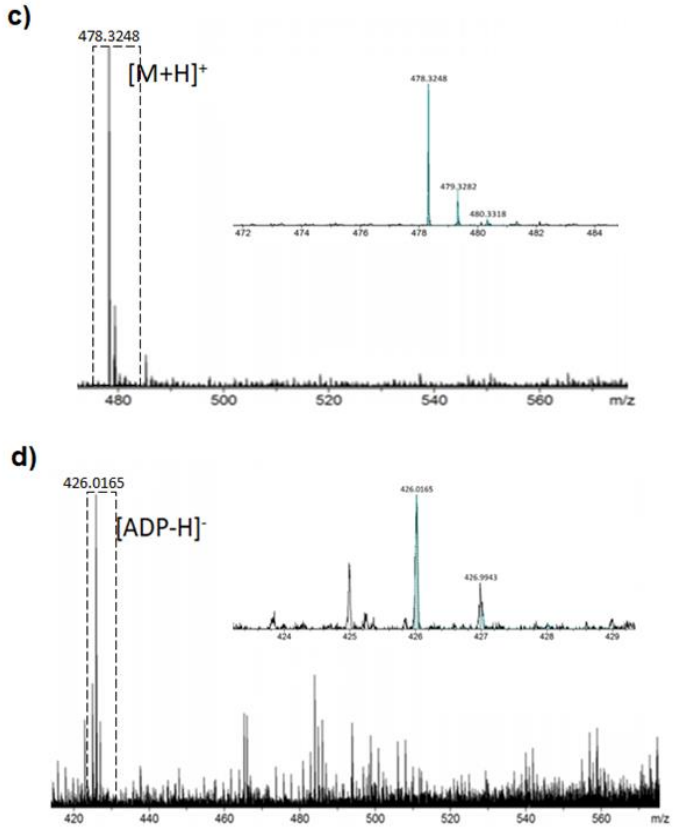

Figure S3.1 c) and d). ESI Mass spectra analysis of unphosphorylated non-substrate gentamicin C after APH(3')-IIIa catalyzed background hydrolysis of ATP. c)non-substrate gentamicin C remain unphosphorylated forms after reaction complete. Positive mode. The peak at 478.3248 is due to $[Gen+H]^{+}$= 478.3241. d) ATP was converted to ADP by APH(3')-IIIa catalyzed background hydrolysis. Negative mode. The peak at 426.0165 is due to $[ADP-H]^{-}$= 426.0215. No phosphorylated product was detected around 557.

3.6.2 Amg binding Induced Conformational Change on APH(3')-IIIa

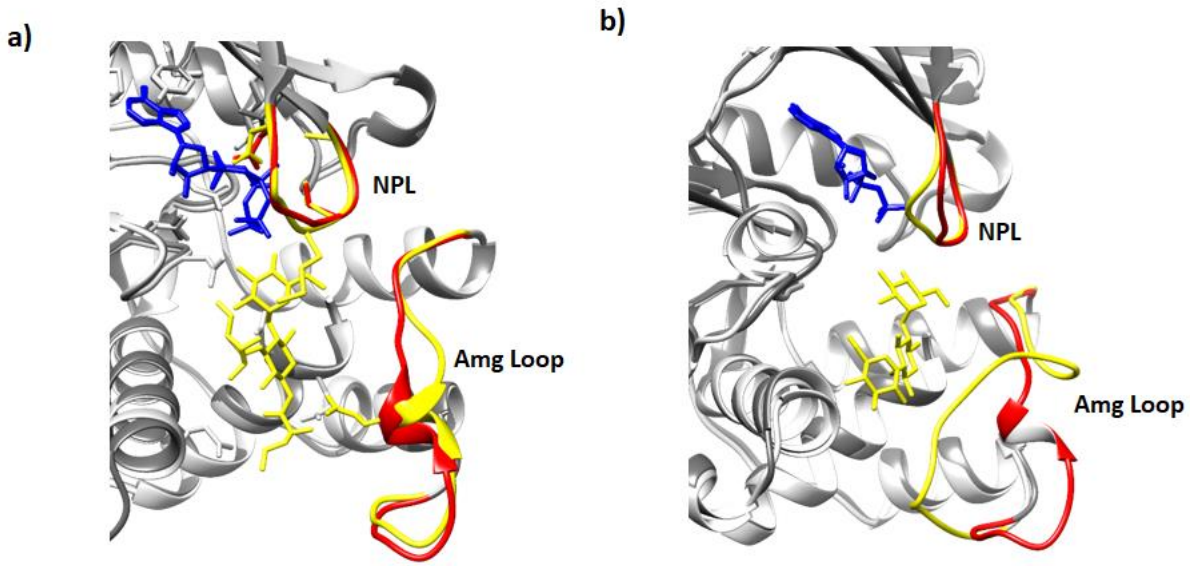

Figure S3.2. APH(3')-IIIa conformation changes observed on both NPL and Amg loop upon Aminoglycoside binding. a) The APH(3')-IIIa • butirosin A •AMPPNP ternary complex [PDB:3TM0] is shown in light gray/yellow, and the APH(3')-IIIa•AMPPNP [PDB:1J7U] is shown in dark gray/red. b) The APH(3')-IIIa •kanamycin A•ADP ternary complex [PDB:1L8T] is shown in light gray/yellow, and the APH(3')-IIIa•ADP [PDB:1J7L] is shown in dark gray/red.

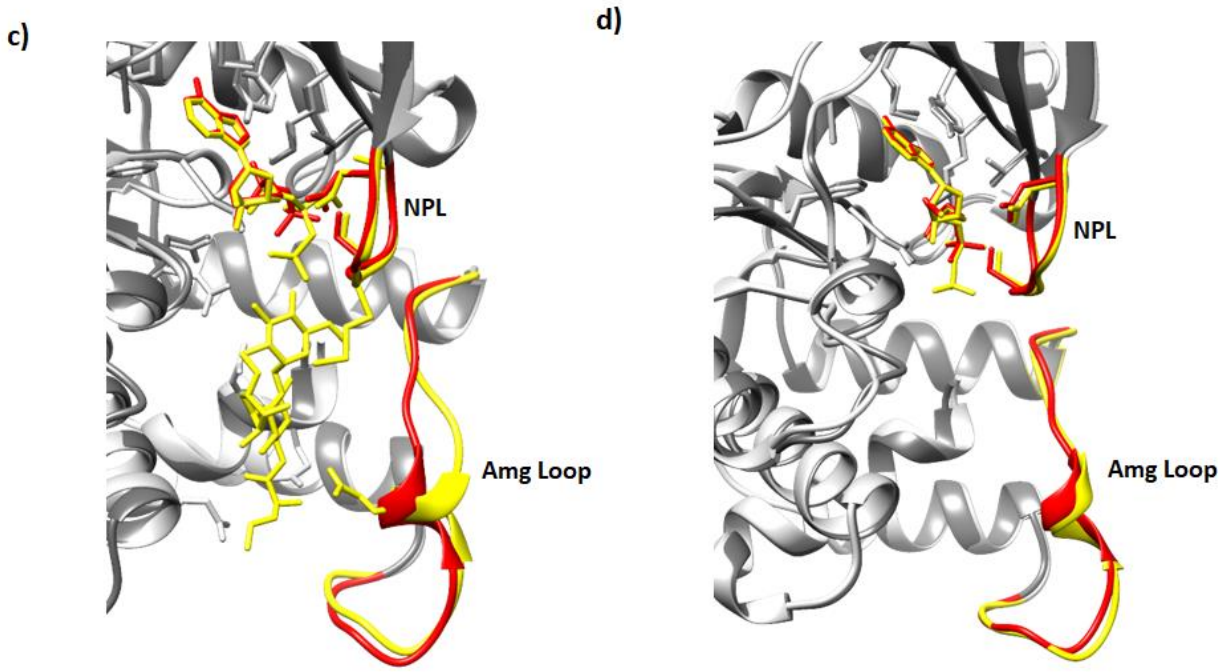

Figure S3.2. c) The APH(3')-IIIa • butirosin A •AMPPNP ternary complex [PDB:3TM0] is shown in light gray/yellow, and the APH(3')-IIIa•ADP [PDB: 1J7L] is shown in dark gray/red. d) The APH(3')-IIIa •AMPPNP complex [PDB: 1J7U] is shown in light gray/yellow, and the APH(3')-IIIa•ADP [PDB: 1J7L] is shown in dark gray/red.

3.7 References

1. Cheek, S.; Zhang, H.; Grishin, N. V., Sequence and structure classification of kinases. *J Mol Biol* **2002,** *320* (4), 855-881.

2. Futreal, P. A.; Coin, L.; Marshall, M.; Down, T.; Hubbard, T.; Wooster, R.; Rahman, N.; Stratton, M. R., A census of human cancer genes. *Nat. Rev. Cancer* **2004,** *4* (3), 177-183.

3. Kotzbauer, P. T.; Truax, A. C.; Trojanowski, J. Q.; Lee, V. M. Y., Altered neuronal mitochondrial coenzyme A synthesis in neurodegeneration with brain iron accumulation caused by abnormal processing, stability, and catalytic activity of mutant pantothenate kinase 2. *J. Neurosci.* **2005,** *25* (3), 689-698.

4. Gloyn, A. L., Glucokinase (GCK) mutations in hyper- and hypoglycemia: maturity-onset diabetes of the young, permanent neonatal diabetes, and hyperinsulinemia of infancy. *Hum. Mutat.* **2003,** *22* (5), 353-362.

5. Shaw, K. J.; Rather, P. N.; Hare, R. S.; Miller, G. H., Molecular genetics of aminoglycoside resistance genes and familial relationships of the aminoglycoside-modifying enzymes. *Microbiol. Rev.* **1993,** *57* (1), 138-63.

6. Jencks, W. P., Binding Energy, Specificity, and Enzymic Catalysis: The Circe Effect. In *Adv Enzymol Relat Areas Mol Biol*, 1975; Vol. 43, pp 219-410.

7. Rominger, C. M.; Schaber, M. D.; Yang, J.; Gontarek, R. R.; Weaver, K. L.; Broderick, T.; Carter, L.; Copeland, R. A.; May, E. W., An intrinsic ATPase activity of phospho-MEK-1 uncoupled from downstream ERK phosphorylation. *Arch. Biochem. Biophys.* **2007,** *464* (1), 130-137.

8. Chen, G.; Porter, M. D.; Bristol, J. R.; Fitzgibbon, M. J.; Pazhanisamy, S., Kinetic Mechanism of the p38-α MAP Kinase: Phosphoryl Transfer to Synthetic Peptides. *Biochemistry* **2000,** *39* (8), 2079-2087.

9. Di Luccio, E.; Petschacher, B.; Voegtli, J.; Chou, H.-T.; Stahlberg, H.; Nidetzky, B.; Wilson, D. K., Structural and Kinetic Studies of Induced Fit in Xylulose Kinase from Escherichia coli. *J Mol Biol* **2007,** *365* (3), 783-798.

10. Paudel, H. K.; Carlson, G. M., The ATPase activity of phosphorylase kinase is regulated in parallel with its protein kinase activity. *J. Biol. Chem.* **1991,** *266* (25), 16524-9.

11. DelaFuente, G.; Lagunas, R.; Sols, A., Induced fit in yeast hexokinase. *Eur. J. Biochem.* **1970,** *16* (2), 226-33.

12. Fromm, H. J.; Zewe, V., Kinetic studies of yeast hexokinase. *J. Biol. Chem.* **1962,** *237*, 3027-32.

13. Prowse, C. N.; Lew, J., Mechanism of activation of ERK2 by dual phosphorylation. *J. Biol. Chem.* **2001,** *276* (1), 99-103.

14. Caldwell, S. J.; Huang, Y.; Berghuis, A. M., Antibiotic Binding Drives Catalytic Activation of Aminoglycoside Kinase APH(2'')-Ia. *Structure (Oxford, U. K.)* **2016,** *24* (6), 935-945.

15. Masterson, L. R.; Mascioni, A.; Traaseth, N. J.; Taylor, S. S.; Veglia, G., Allosteric cooperativity in protein kinase A. *Proc Natl Acad Sci U S A* **2008,** *105* (2), 506-511.

16. Wu, L.; Serpersu, E. H., Deciphering interactions of the aminoglycoside phosphotransferase(3′)-IIIa with its ligands. *Biopolymers* **2009,** *91* (9), 801-809.

17. Kim, C.; Cha, J. Y.; Yan, H.; Vakulenko, S. B.; Mobashery, S., Hydrolysis of ATP by Aminoglycoside 3'-Phosphotransferases. An Unexpected Cost to Bacteria for Harboring an Antibiotic Resistance Enzyme. *J. Biol. Chem.* **2006,** *281* (11), 6964-6969.

18. Matte, A.; Tari, L. W.; Delbaere, L. T. J., How do kinases transfer phosphoryl groups? *Structure (London)* **1998,** *6* (4), 413-419.

19. Thompson, P. R.; Boehr, D. D.; Berghuis, A. M.; Wright, G. D., Mechanism of Aminoglycoside Antibiotic Kinase APH(3')-IIIa: Role of the Nucleotide Positioning Loop. *Biochemistry* **2002,** *41* (22), 7001-7007.

20. Benson, D., *Mechanisms of inorganic reactions in solution: an introduction*. McGraw-Hill: London, 1968.

21. Fong, D. H.; Berghuis, A. M., Structural basis of APH(3')-IIIa-mediated resistance to N1-substituted aminoglycoside antibiotics. *Antimicrob. Agents Chemother.* **2009,** *53* (7), 3049-3055.

22. Fong, D. H.; Berghuis, A. M., Substrate promiscuity of an aminoglycoside antibiotic resistance enzyme via target mimicry. *EMBO J.* **2002,** *21* (10), 2323-2331.

23. Xiao, B.; Sanders, M. J.; Carmena, D.; Bright, N. J.; Haire, L. F.; Underwood, E.; Patel, B. R.; Heath, R. B.; Walker, P. A.; Hallen, S.; Giordanetto, F.; Martin, S. R.; Carling, D.; Gamblin, S. J., Structural basis of AMPK regulation by small molecule activators. *Nature Communications* **2013,** *4* (1), 3017.

24. Cheng, X.; Shaltiel, S.; Taylor, S. S., Mapping substrate-induced conformational changes in cAMP-dependent protein kinase by protein footprinting. *Biochemistry* **1998,** *37* (40), 14005-14013.

25. Vonrhein, C.; Schlauderer, G. J.; Schulz, G. E., Movie of the structural changes during a catalytic cycle of nucleoside monophosphate kinases. *Structure* **1995,** *3* (5), 483-90.

26. Wright, G. D.; Thompson, P. R., Aminoglycoside phosphotransferases: proteins, structure, and mechanism. *Front. Biosci.* **1999,** *4*, D9-D21.

27. Hon, W.-C.; McKay, G. A.; Thompson, P. R.; Sweet, R. M.; Yang, D. S. C.; Wright, G. D.; Berghuis, A. M., Structure of an enzyme required for aminoglycoside antibiotic resistance reveals homology to eukaryotic protein kinases. *Cell (Cambridge, Mass.)* **1997,** *89* (6), 887-895.

28. McKay, G. A.; Wright, G. D., Kinetic mechanism of aminoglycoside phosphotransferase type IIIa. Evidence for a Theorell-Chance mechanism. *J. Biol. Chem.* **1995,** *270* (42), 24686-92.

29. Burk, D. L.; Hon, W. C.; Leung, A. K. W.; Berghuis, A. M., Structural Analyses of Nucleotide Binding to an Aminoglycoside Phosphotransferase. *Biochemistry* **2001,** *40* (30), 8756-8764.

30. Daigle, D. M.; McKay, G. A.; Thompson, P. R.; Wright, G. D., Aminoglycoside antibiotic phosphotransferases are also serine protein kinases. *Chem. Biol.* **1999,** *6* (1), 11-18.

31. Wang, Y.; Wang, G.; Moitessier, N.; Mittermaier, A. K., Enzyme kinetics by isothermal titration calorimetry: allostery, inhibition, and dynamics. *Frontiers in Molecular Biosciences* **2020,** *7*, 285.

32. Todd, M. J.; Gomez, J., Enzyme kinetics determined using calorimetry: A general assay for enzyme activity? *Anal. Biochem.* **2001,** *296* (2), 179-187.

33. Wang, Y.; Guan, J.; Di Trani, J. M.; Auclair, K.; Mittermaier, A. K., Inhibition and Activation of Kinases by Reaction Products: A Reporter-Free Assay. *Analytical chemistry* **2019,** *91* (18), 11803-11811.

34. Di, T. J. M.; De, C. S.; O'Leary, R.; Plescia, J.; do, N. C. J.; Moitessier, N.; Mittermaier, A. K.; do, N. C. J., Rapid measurement of inhibitor binding kinetics by isothermal titration calorimetry. *Nat Commun* **2018,** *9* (1), 893.

35. McKay, G. A.; Thompson, P. R.; Wright, G. D., Broad Spectrum Aminoglycoside Phosphotransferase Type III from Enterococcus: Overexpression, Purification, and Substrate Specificity. *Biochemistry* **1994,** *33* (22), 6936-44.

36. Di Trani, J. M.; Moitessier, N.; Mittermaier, A. K., Measuring Rapid Time-Scale Reaction Kinetics Using Isothermal Titration Calorimetry. *Anal. Chem. (Washington, DC, U. S.)* **2017,** *89* (13), 7022-7030.

37. McKay, G. A.; Wright, G. D., Catalytic Mechanism of Enterococcal Kanamycin Kinase (APH(3‘)-IIIa): Viscosity, Thio, and Solvent Isotope Effects Support a Theorell−Chance Mechanism. *Biochemistry* **1996,** *35* (26), 8680-8685.

38. Lallemand, P.; Leban, N.; Kunzelmann, S.; Chaloin, L.; Serpersu, E. H.; Webb, M. R.; Barman, T.; Lionne, C., Transient kinetics of aminoglycoside phosphotransferase(3′)-IIIa reveals a potential drug target in the antibiotic resistance mechanism. *FEBS Letters* **2012,** *586* (23), 4223-4227.

39. Beckett, D., Chapter one - Measurement and Analysis of Equilibrium Binding Titrations: A Beginner's Guide. In *Methods Enzymol*, Johnson, M. L.; Holt, J. M.; Ackers, G. K., Eds. Academic Press: 2011; Vol. 488, pp 1-16.

40. Ozen, C.; Serpersu, E. H., Thermodynamics of aminoglycoside binding to aminoglycoside-3'-phosphotransferase IIIa studied by isothermal titration calorimetry. *Biochemistry* **2004,** *43* (46), 14667-75.

41. Lauffenburger, D. A.; Linderman, J., Receptors : Models for Binding, Trafficking, and Signaling. Oxford University Press: New York, 1996.

42. contributors, W., Receptor–ligand kinetics. *In Wikipedia, The Free Encyclopedia, https://en.wikipedia.org/w/index.php?title=Receptor%E2%80%93ligand_kinetics&oldid=840646302* **2018**.

43. Meneses, E.; Mittermaier, A., Electrostatic interactions in the binding pathway of a transient protein complex studied by NMR and isothermal titration calorimetry. *J. Biol. Chem.* **2014,** *289* (40), 27911-27923.

44. Alsallaq, R.; Zhou, H. X., Electrostatic rate enhancement and transient complex of protein–protein association. *Proteins: Structure, Function, and Bioinformatics* **2008,** *71* (1), 320-335.

45. Szabo, A.; Shoup, D.; Northrup, S. H.; McCammon, J. A., Stochastically gated diffusion-influenced reactions. *The Journal of Chemical Physics* **1982,** *77* (9), 4484-4493.

46. Fierke, C. A.; Hammes, G. G., [1] Transient kinetic approaches to enzyme mechanisms. In *Methods Enzymol*, Academic Press: 1995; Vol. 249, pp 3-37.

47. Faust, R. A.; Gapany, M.; Tristani, P.; Davis, A.; Adams, G. L.; Ahmed, K., Elevated protein kinase CK2 activity in chromatin of head and neck tumors: association with malignant transformation. *Cancer Letters* **1996,** *101* (1), 31-35.

48. Wu, H.; Zheng, Y.; Wang, Z.-X., Evaluation of the catalytic mechanism of the p21-activated protein kinase PAK2. *Biochemistry* **2003,** *42* (4), 1129-1139.

49. Waas, W. F.; Dalby, K. N., Transient protein-protein interactions and a random-ordered kinetic mechanism for the phosphorylation of a transcription factor by extracellular-regulated protein kinase 2. *Journal of Biological Chemistry* **2002,** *277* (15), 12532-12540.

50. Boerner, R. J.; Barker, S. C.; Knight, W. B., Kinetic mechanisms of the forward and reverse pp60c-src tyrosine kinase reactions. *Biochemistry* **1995,** *34* (50), 16419-16423.

51. Trauger, J. W.; Lin, F.-F.; Turner, M. S.; Stephens, J.; LoGrasso, P. V., Kinetic mechanism for human Rho-Kinase II (ROCK-II). *Biochemistry* **2002,** *41* (28), 8948-8953.

52. Easterby, J. S., Coupled enzyme assays: a general expression for the transient. *Biochim Biophys Acta* **1973,** *293* (2), 552-8.

53. Lallemand, P.; Chaloin, L.; Roy, B.; Barman, T.; Bowler, M. W.; Lionne, C., Interaction of human 3-phosphoglycerate kinase with its two substrates: is substrate antagonism a kinetic advantage? *J Mol Biol* **2011,** *409* (5), 742-757.

54. TA, MICROCALORIMETRY: ITC & DSC. **2019**.

55. Malvern, MICROCAL ITC SYSTEMS:UNDERSTANDING BIOMOLECULAR INTERACTIONS. **2016**.

4. Rapid characterization of Bi-substrate enzymes by 2D-ITC

4.1 Introduction

Enzymes are among the most common drug targets in pharmaceutical research.[1] Characterizing enzyme kinetics, can reveal mechanistic and functional information, which can be critical to the drug design process. The simplest mechanisms involve a single substrate converting to reaction products, for example the Uni-Uni reaction: S → P. Uni-substrate enzymes typically follow the Michaelis-Menten/Briggs-Haldane (MM/BH) mechanism with characteristic hyperbolic saturation kinetics (**Equation 4.1**).

$$v = \frac{V_{max}[S]}{K_m + [S]} \tag{4.1}$$

The reaction velocity, v, can measured as a function of substrate concentration [S] and analyzed by regression of the linearized data (Lineweaver-Burk or Eadie Hofstee plots)[2, 3] or non-linear least-squares fitting to the raw data, yielding the Michaelis constant (K_m) and turnover number ($k_{cat}=V_{max}/[E]$) thereby providing a quantitative description of the enzymatic reaction.[4] However, most biological reactions are catalyzed by Bi-substrate enzymes, as epitomized by the Bi-Bi reaction, A + B → P + Q, with >60% of all known enzymatic reactions belonging to this type.[3] There are several different possible mechanisms that all fall into the Bi-Bi category, as illustrated in **Figure 4.1**

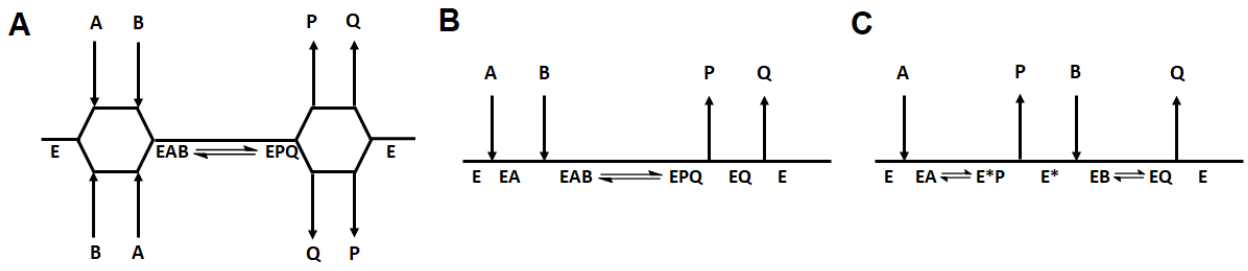

Figure 4.1. Bi-substrate enzymatic reaction models.[5] **A)** random sequential, **B)** ordered sequential, and **C)** ping-pong mechanisms.

In a sequential mechanism (also known as a ternary complex mechanism), both substrates A and B bind to the enzyme simultaneously to form the Michaelis complex and both products P and Q must dissociate before another round of catalysis can begin (**Figure 4.1A,B**). This mechanism can be further categorized as either ordered sequential (**Figure 4.1B**), where A binds before B and P dissociates before Q, or random sequential (**Figure 4.1A**), where A and B bind and P and Q dissociate in either order. In both cases, the rate equation is given by[3, 6]

$$v = \frac{V_{max}[A][B]}{K_m^B[A]+K_m^A[B]+[A][B]+K_i^A K_m^B} \quad (4.2)$$

Note that the ordered and random sequential mechanisms are kinetically indistinguishable in the absence of product inhibition since they both follow **Equation 4.2**. However, the two mechanisms differ kinetically when P or Q act as inhibitors, allowing them to be differentiated, as detailed below.[3]

In a ping-pong mechanism (also known as a substituted enzyme or double substitution mechanism), the enzyme, E, reacts with substrate A to form the first product, P and a chemically modified form of the enzyme E*. E* then reacts with the second substrate, B, producing the second product Q and regenerating the enzyme, E (**Figure 4.1C**), and giving the rate equation [3, 6]

$$v = \frac{V_{max}[A][B]}{K_m^B[A]+K_m^A[B]+[A][B]} \quad (4.3)$$

For both sequential and ping-pong mechanisms, the enzyme follows simple MM/BH kinetics if the concentration of one of the substrates is fixed while the concentration of the other one is varied. Furthermore, the apparent values of K_m and k_{cat} for the varied substrate can change depending on the concentration of the fixed substrate. For example, in a sequential reaction, the apparent K_m for substrate A varies between K_i^A at vanishingly low [B] and K_m^A at saturating [B]. For a ping-pong mechanism, both k_{cat} and K_m for substrate A increase with increasing [B], such that their ratio is constant. Thus by measuring the reaction velocity as a function of both substrate concentrations, it is possible to gain detailed mechanistic information into Bi-Bi enzymes.[2]

A variety of experiments have been developed to quantity enzyme-catalyzed reaction kinetics. In general, these can be classified as continuous (real-time) and discontinuous

assays.[7] In a continuous assay, the concentration of the substrate or product in a reaction mixture is measured in real time during the catalytic reaction, typically spectroscopically, such as with fluorimetry, UV/vis absorption, or nuclear magnetic resonance, and relying on the different spectroscopic signatures of substrates and products.[8-10] In some special cases, substrates and products are clearly distinguishable by spectroscopy. In general however, chemical modification of the substrate is required for direct spectroscopic quantification.[9] The drawbacks of this approach include the need for different customized substrates for different enzymes and the fact that substrate analogs do not necessarily follow the same reaction kinetics as the natural substrates. Alternatively, coupled enzyme assays employ a reaction mixture with a secondary enzyme which can rapidly react with the reaction product to produce a spectroscopically active substance.[11, 12] This approach allows native substrates to be used, but accurate results depend on choosing appropriate concentrations of the coupled enzymes and secondary substrates.[13] When it is not possible to monitor substrate or product concentrations in real time, discontinuous enzyme assays must be used. In these experiments, the reaction is quenched at various time points after initiation and the substrates and products are separated by an ancillary technique.[14-19] These additional steps add time, expense, and uncertainty to the characterization process.

Isothermal titration calorimetry (ITC) is primarily used to study protein/ligand binding reactions but is increasingly gaining popularity as a general assay for enzyme kinetics. [20, 21] ITC measures the heat released or absorbed by a reaction in real time. Since most chemical reactions are either exothermic or endothermic, ITC can be universally applied to almost any enzymatic reaction, without the need for customized reporter molecules, additional coupled enzymes, or post-reaction separation. Furthermore, ITC experiments can be performed with conventional dilute enzymatic reaction mixtures, even with opaque samples or suspensions.[20] There are several examples of Bi-substrate enzymes without facile conventional assays whose reactions were successfully analyzed using ITC.[20-30] However, traditional ITC assays require maintaining a constant concentration of one substrate while collecting the kinetics data by varying the concentrations of the other substrates. This requires setting up and running multiple (minimum 5) separate ITC experiments, making it a costly process in terms of both time and material.[22-24, 26] Even more ITC experiments are required when product inhibition is present.[25] Thus, complete kinetic characterization of Bi-substrate enzymes is difficult using current ITC kinetics methods.

Here, we present a simple ITC assay which can completely kinetically characterize Bi-substrate enzymes in a single, (2 hour) experiment. It measures the reaction velocity

as the concentrations of both substrates are systematically varied, generating a full two dimensional map of ν as a function of both [A] and [B], identifying the type of Bi-Bi mechanism (sequential or ping-pong) and yielding the values of quantitative kinetic parameters in **Equations 4.2-4.3**. In favourable cases, the same ITC experiment also allows discrimination of ordered versus random sequential mechanisms, based on their different behaviors with respect to product inhibition. As a proof-of-concept, we applied this approach to pyruvate kinase from rabbit muscle (rMPK), which transfers of phosphate group from phosphoenolpyruvate (PEP) to ADP, generating pyruvate and ATP in the last step of glycolysis, following a random Bi-Bi mechanism.[31, 32] The enzyme is homotetramer with 4 identical active sites.[33, 34] Interestingly, the amino acid phenylalanine (Phe) binds to allosteric sites each of the subunits, leading to weaker substrate affinity and positively cooperative, non-MM/BH kinetics for PEP.[35-38] Our ITC method correctly identified the random-BiBi mechanism for rMPK in a single experiment. When we repeated the measurements in the presence of the Phe allosteric modifier, sigmoidal, non-MM/BH behavior was clearly evident for PEP, in good agreement with previous reports.

4.2 Methods

4.2.1 Materials

Pyruvate kinase from rabbit muscle (ammonium sulfate suspension) and ADP were purchased from Sigma-Aldrich. Phosphoenolpyruvate (PEP) was purchased from Chem-Impex. L-phenylalanine was purchased from Fisher Scientific. rMPK in ammonium sulfate solution was centrifuged (11,000×g for 10 minutes); the enzyme pellet was dissolved in buffer A (pH 7.5, 50 mM Tris buffer, 100 mM KCl, 10 mM $MgCl_2$). The enzyme solution was then dialyzed against buffer A to remove the remaining ammonium sulfate. The concentration of the enzyme stock solution was measured using a Bradford protein assay (see SI).[39] The stock solutions of ADP, phosphoenolpyruvate (PEP) and L-phenylalanine were prepared in buffer A.

4.2.2 Experimental Section

All ITC experiments were performed on a MicroCal iTC_{200} (MicroCal, Northampton, MA, USA) with a stirring speed of 750 rpm in high gain mode with a filter time of 1 s. All solutions were degassed for 3 minutes using a Malvern MicroCal ThermoVac Degassing Station before being loaded into the ITC. The ITC experiments were performed in triplicate in buffer A at 25°C. The data were analysed after blank subtraction.

Recurrent Single Injection of PEP into Enzyme and ADP: rMPK (8nM) and ADP (3.1mM) were placed in the sample cell with PEP (40mM) in syringe. 1×0.1 µL injection (data discarded) followed by 15 ×1 µL injections were made. The blank experiment was carried out under the same conditions in the absence of the enzyme.

Recurrent Single Injection of PEP into Enzyme, ADP and Phenylalanine: rMPK (8nM), ADP (3.1mM) and Phe (50mM) were placed in the sample cell with PEP (40mM) in syringe. 1×0.1 µL injection (data discarded) followed by 15 ×1 µL injections were made. The blank experiments were carried out under the same conditions in the absence of the enzyme.

4.2.3 ITC Data Analysis

ITC measures the amount of heat (dQ) produced by converting substrates to products per unit time (dt), which is directly proportional to the reaction rate as described in **Equation (4.4)**:

$$\text{Power} = \frac{dQ}{dt} = -V_{cell}\Delta_r H \frac{d[P]_t}{dt} \quad (4.4)$$

where dQ/dt is the rate of heat flow, V_{cell} is the sample cell volume, $\Delta_r H$ is the reaction enthalpy and $(d[P]_t)/dt$ is the concentration of the product over time. The reaction enthalpy can be determined by integration of the peak as showed in **Equation (4.5)**:

$$\Delta_r H = \frac{-1}{[P]_{final} V_{cell}} \int_{t=0}^{t=\infty} \frac{dQ}{dt} dt \quad (4.5)$$

where $[P]_{final}$ is the total concentration of product formed. The rate of catalysis at any time (t) can be calculated according to:

$$v = \frac{d[P]_t}{dt} = \frac{-1}{V_{cell} \Delta_r H} \frac{dQ}{dt} \quad (4.6)$$

and the remaining substrate concentration as function of time is determined from partial integrals of each ITC peak according to **Equation (4.7)**:

$$[S](t) = \frac{\int_t^\infty \frac{dQ}{dt} dt}{\int_0^\infty \frac{dQ}{dt} dt} [S](t = 0) \quad (4.7)$$

In order to quantitatively model the peaks produced by ITC, the ITC Empirical Response Model (ITC-ERM) was applied as described previously. [40, 41] The response function was measured by the ITC signal resulting from 0.1 s injection in a calibration reaction (Ca2+/EDTA) at 25°C.

The *v*([ADP,PEP]) datasets without the addition of the allosteric inhibitor, phenylalanine, were fitted by MATLAB using nonlinear least squares regression. The *v*([ADP,PEP]) datasets with phenylalanine were fitted by nonlinear least squares regression, using the SciPy set of scientific libraries for the Python programming language.

4.3 Results

4.3.1 The 2D-ITC Method

An ITC instrument measures the rate at which heat is produced or absorbed as a titrant solution in an injection syringe is gradually added to an analyte solution in the sample cell. Raw ITC data, therefore, consist of heat flow values (dQ/dt), plotted as a function of time. In the case of enzyme assays, the rate of heat generation is directly proportional to the velocity (-d[S]/dt) and the enthalpy ($\Delta_r H$) of the catalyzed reaction. Since the $\Delta_r H$ is easily extracted from ITC data as the total heat released per mol of product formed, the raw ITC signal thus gives a direct and quantitative readout of enzyme activity. Our new approach is based on the "single injection" experiment described by Todd and Gomez in 2001[21]. The reaction is initiated when a substrate in the syringe in injected into an enzyme solution in the cell. Immediately following the injection, the enzyme is nearly saturated with substrate and the magnitude of the heat signal is at a maximum (displaced downwards for exothermic and upwards for endothermic reactions). As the substrate is gradually converted to product, the reaction velocity and corresponding heat flow drop, until finally the signal returns to the baseline when all the substrate has consumed, producing peak in the ITC output. The velocity of the enzyme at any time, *t*, can be taken directly from the instantaneous value of the ITC signal ($\frac{\mathrm{dQ}}{\mathrm{dt}}(t)$) and the fraction of

substrate remaining at time *t* is given by the peak area lying to the right of *t* divided by the total peak area (See Methods). Thus a single ITC peak gives a complete ν versus [S] curve which can be fitted to extract the values of K_m and k_{cat}. One advantage of this approach is that several substrate injections can be performed in the same experiment, producing a series of peaks, something we refer to as recurrent single injection methods[20]. Recurrent single injection ITC experiments can give additional enzyme kinetic information. For instance, reaction products accumulate in the sample cell with each injection. If they modulate enzyme activity then each peak will yield different values of K_m and k_{cat} and the series of ITC peaks can be fitted to quantitative models describing product inhibition or activation[25, 42]. Alternatively, a mixture of substrate and inhibitor can be loaded into the injection syringe. Again, the inhibitor accumulates in the sample cell with each injection and the series of ITC peaks can be fitted to extract the strength and mode of inhibition, as well as the MM/BH parameters of the enzyme[41, 43].

Single-injection ITC kinetics experiments have primarily been used for Uni-substrate enzymes. In the few cases where they have been applied to Bi-substrate systems, they have mostly been used to probe the kinetic properties of only one substrate (determining k_{cat} and K_m), while the concentration of the other substrate was held effectively fixed[21, 23-25, 30]. In a few examples, these experiments were repeated at different fixed

concentrations of the second substrate[22, 26]. However, each experiment requires that the instrument be cleaned, loaded with fresh sample, and equilibrated, making the full kinetic characterization of Bi-substrate enzymes by ITC laborious and costly in terms of time and material.

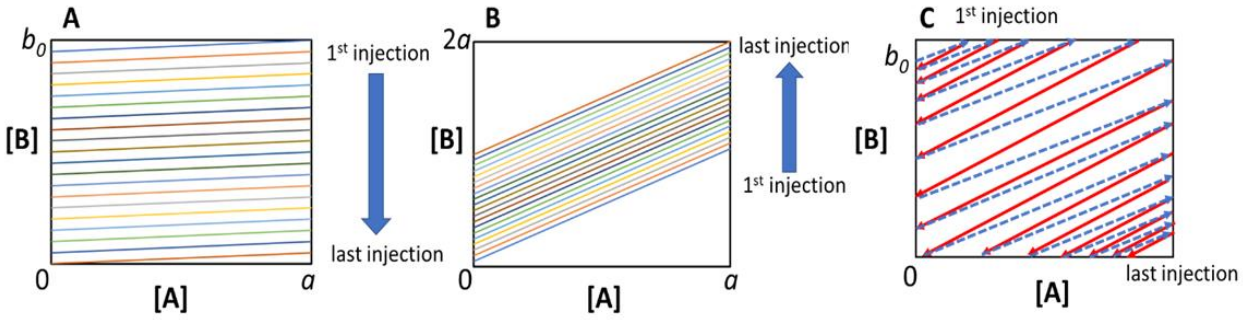

Figure 2. Sampling of substrate concentrations by different injection schemes in 2D-ITC experiments. Each solid line represents the set of concentrations of [A] and [B] sampled after a single ITC injection (typically sampled at about 100 to 1000 points, depending on the width of the peak). The lines have a slope of one and are sampled from top right to bottom left with increasing time. **A)** The syringe contains substrate A and the cell contains enzyme + substrate B**.** Prior to the first injection, [B]=b_0. Immediately after each injection, [A] = a = 0.05×b_0. **B)** The syringe contains both substrates with [A]=100a and [B]=105a and the cell initially contains enzyme alone. 100-fold dilutions are assumed for each injection. **C)** The syringe contains substrate A at a slightly higher concentration than substrate B and the cell initially contains enzyme + substrate B, initially at [B]=b_0. The solid lines have the same meaning as in the first two panels while dashed lines represent the concentrations of A and B in the cell during an injection and have a slope of $[B]_{syr}/[A]_{syr}$.

We have developed a simple variant of the recurrent single-injection ITC kinetics in which one fully maps the dependence of reaction velocity as a function of both substrate concentrations in a single experiment, allowing one to rapidly identify the Bi-substrate reaction mechanism and quantify deviations from classical MM/BH behavior. The resulting datasets comprise ν determined as a function of two concentration dimensions, [A] and [B], and we refer to this experiment as 2D-ITC. The approach is based on the idea that during the acquisition of a peak in a single-injection experiment, both A and B are consumed in equal proportion while the velocity of the reaction is detected as heat flow, typically at one second intervals. The set of concentrations sampled in a single peak can therefore be represented by a straight line with a slope of 1 on an [A] vs [B] plot. The second injection samples a new line in the plot, and after a series of injections, comprehensive sampling of the entire 2-dimensional concentration can be achieved (**Figure 4.2**). For example, if the sample cell initially contains the enzyme and substrate B at a concentration b_0, the reaction can be initiated by injecting substrate A at a concentration $a = 0.05 \times b_0$. After the first injection, the concentration of A in the cell varies from a to 0, while that of B varies from b_0 to $b_0 – a$. After the second injection, [A] again varies from a to 0 while [B] varies from $b_0 – a$ to $b_0 – 2a$. After the twentieth injection, [A] still varies from a to 0, while [B] varies from $b_0 – 19a$ to $b_0 – 20a = 0$ (**Figure 4.2A**).

Since we wish the sampled concentrations of A and B to extend from zero to roughly 5-fold their respective K_m values, this arrangement is suitable when $K_m^B >> K_m^A$. Many variations on this theme are possible. For instance, if the values of K_m are similar for the two substrates, then the syringe may be filled with a mixture of the two substrates where $[A]_{syr} = 100a$ and $[B]_{syr}=100(a + \Delta)$, $\Delta=.05a$. After the first injection (assuming 100-fold dilution into the cell), [A] varies from a to 0 while [B] varies from $a + \Delta$ to Δ. After the second, [A] varies from a to 0 while [B] varies from $a + 2\Delta$ to 2Δ. After the twentieth injection, [A] again varies from a to 0 while [B] varies from $a + 20\Delta$ to 20Δ, which is equal to $2a$ to a (**Figure 4.2B**). A wide variety of other scenarios are also possible. In general, when sample cell initially contains the enzyme and substrate B at a concentration b_0, the syringe contains A and B at concentrations of a and b, then the injections themselves can be represented as lines with slope b/a whose lengths are defined by the sizes of the injections, and the reactions as lines with slopes of 1 which continue until either [A]=0 or [B]=0 (**Figure 4.2C**). In other words, there are many options for performing series of injections that finely sample [A], [B] space. One aspect of this method that cannot be ignored is that the reaction products (P and Q for a Bi-Bi reaction) accumulate throughout the experiment. If product inhibition or activation is present, then the velocity of the enzyme catalyzed reaction will depend not only on the variations in

[A] and [B], but also on the gradually increasing values of [P] and [Q]. While this adds a level a complexity to the analysis of the data, it offers some advantages to the method. Random and ordered sequential mechanisms are indistinguishable based on variation in [A] and [B] alone (**Equation 4.2**). However, their patterns of product inhibition are quite different. For the random sequential mechanism with product inhibition and assuming rapid equilibrium, the reaction velocity is given by [6]

$$v = \frac{V_{max}[A][B]}{K_m^B[A]+K_m^A[B]+[A][B]+K_i^A K_m^B\left(1+\frac{[P]}{K_i^P}+\frac{[Q]}{K_i^Q}+\frac{[P][Q]}{K_m^P K_i^Q}+\frac{[B][Q]}{K_i^B K_{ii}^Q}+\frac{[A][P]}{K_i^A K_{ii}^P}\right)} \quad (4.8)$$

where K_i^P, K_m^P, and K_{ii}^P are dissociation constants for P binding to E, EQ, and EA, while K_i^Q and K_{ii}^Q are for Q binding to E and EB. For the ordered sequential mechanism, the expression is

$$v = \frac{V_{max}[A][B]}{K_m^B[A]+K_m^A[B]+[A][B]+K_i^A K_m^B\left(\begin{array}{c}1+\frac{K_m^Q[P]}{K_m^P K_i^Q}+\frac{[Q]}{K_i^Q}+\frac{[P][Q]}{K_m^P K_i^Q}+\frac{K_m^Q[A][P]}{K_i^A K_m^P K_i^Q} \\ +\frac{K_m^A[B][Q]}{K_i^A K_m^Q K_i^Q}+\frac{[A][B][P]}{K_i^A K_m^B K_i^P}+\frac{[B][P][Q]}{K_i^B K_m^P K_i^Q}\end{array}\right)} \quad (4.9)$$

where the definitions of the steady-state kinetic constants are given in Cornish-Bowden [3]. This can lead to sufficiently different sets of calculated curves when fitting 2D-ITC kinetics datasets that the random and ordered sequential mechanisms can be distinguished

while at the same time extracting kinetic parameters for the correct model. For the sake of comparison, the kinetics of a ping-pong enzyme with product inhibition follow

$$v = \frac{V_{max}[A][B]}{K_m^B[A]+K_m^A[B]+[A][B]+K_i^A K_m^B\left(\frac{[P]}{K_i^P}+\frac{K_m^P[Q]}{K_m^Q K_i^P}+\frac{[P][Q]}{K_i^P K_m^Q}+\frac{K_m^A[B][Q]}{K_i^A K_m^B K_i^Q}+\frac{[A][P]}{K_i^A K_i^P}\right)} \quad (4.10)$$

again taken from Cornish-Bowden [3].

4.3.2 Enzyme Kinetics of Rabbit Muscle Pyruvate Kinase

We performed ITC kinetic analysis of rMPK with enzyme (16 nM) and ADP (3.1 mM) in the sample cell and PEP (40 mM) in the injection syringe. As an initial test, we made 3 equal injections of PEP over a period of about 5000 seconds (1.5 hours) (**Figure 4.3A**). Each injection was accompanied by a heat artefact due to slight buffer mismatch, appearing as a sharp spike in the ITC output. This was immediately followed by an upward deflection of the signal, corresponding to an endothermic enzymatic reaction. The signal gradually returned to the baseline over the next 500 to 1000 seconds, as the PEP was completely converted to pyruvate with concomitant equimolar conversion of ADP to ATP. Each peak was lower and broader than the one preceding it, implying that the enzyme velocity was slower and required more time to completely consume the same

amount of PEP. Note that the areas of all three peaks were identical, as expected, since this depends only the total amount of PEP injected and the enthalpy of the reaction. The gradual slowdown of the enzyme could be due to the consumption of ADP (since reducing the concentration of one substrate reduces the apparent k_{cat} for the other substrate). It could also be due to product inhibition by the reaction products ATP and pyruvate which accumulate with each injection. In order to test this second possibility, we repeated the experiment with a mixture of PEP (40 mM) and pyruvate (40 mM) in the syringe, such that accumulation of this product would be enhanced. Nevertheless, the peaks thus obtained were identical to those without pyruvate (**Figure 4.3B**). We then repeated the experiment a third time, with PEP (40 mM) and ATP (40 mM) in the syringe. In this case, the peaks broadened to much greater extent than in the previous two experiment, even though the consumption of ADP was identical in all three cases. This conclusively shows that the enzyme is inhibited by the product ATP, but not by pyruvate, in agreement with previous studies[32, 44]. This makes sense, as PEP binding is largely driven by the phosphate group, which is absent from pyruvate.[34, 45] Since enzyme activity is not affected by pyruvate, it will be ignored in what follows and the reaction will be discussed in terms of [PEP], [ADP], and [ATP].

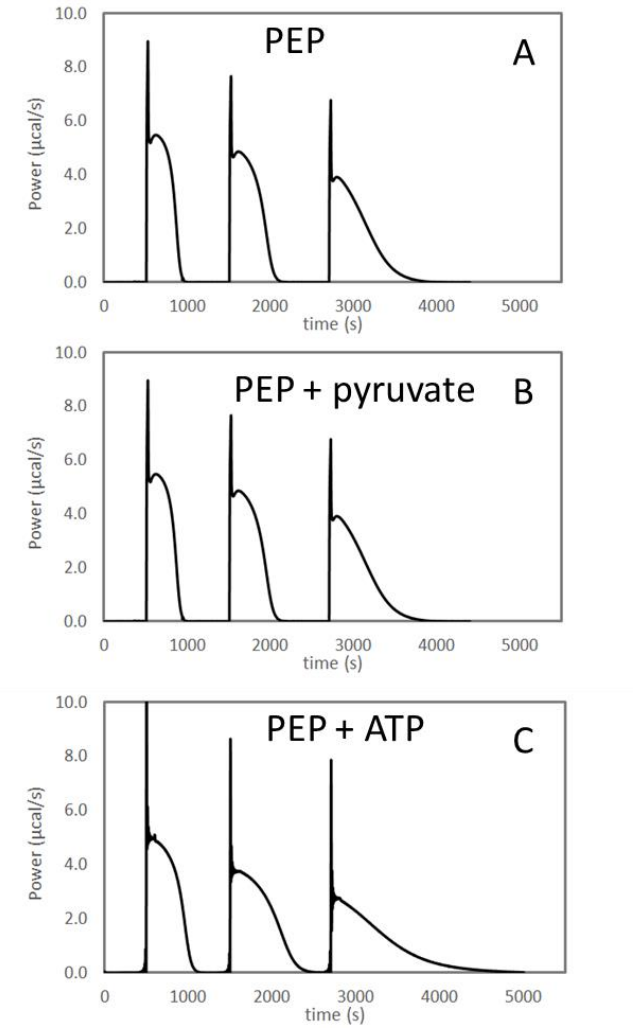

Figure 4.3. Product inhibition of rMPK by ATP. A) Recurrent single injection of PEP into enzyme and ADP. rMPK (16nM) and ADP (3.1mM) were placed in the sample cell with PEP (40mM) in syringe. 1×0.1 µL injection (data discarded) followed by 3×5 µL injections. **B)** Recurrent single injection of PEP and Pyruvate into enzyme and ADP. rMPK (16nM) and ADP (3.1mM) were placed in the sample cell with PEP (40mM) and Pyruvate (40mM) in syringe. 1×0.1 µL injection (data discarded) followed by 3×5 µL injections. **C)** Recurrent single injection of PEP and ATP into enzyme and ADP: rMPK (16nM) and ADP (3.1mM) were placed in the sample cell with PEP (40mM) and ATP (40mM) in syringe. 1×0.1 µL injection (data discarded) followed by 3×5 µL injections.

We then performed the experiment as a 2D-ITC measurement, carefully mapping the reaction velocity as a function of both PEP and ADP concentration. 15 injections of PEP were made into a sample cell containing rMPK and ADP, such that the concentration of PEP in the cell varied between 0 and 0.2 mM after each injection, while the concentration of ADP varied between 0.1 and 3.1 mM over the course of the experiment, in a scheme similar to **Figure 4.2A** (the [B] vs [A] lines). As shown in the overlay in **Figure 4.4A**, each peak was broader than the previous one due to consumption of ADP and accumulation of ATP in the cell with each injection. As described above, the Power values in **Figure 4.4A** are proportional to the reaction velocity, ν, while the total amount of PEP present at each time *t* can be calculated by integrating the peak from *t* to ∞, dividing by the total integral of the peak from 0 to ∞, and multiplying by the concentration of PEP present in cell immediately after the injection (**Equation 4.7**). Thus the ITC data could be easily converted to a series of ν versus [PEP] plots, with one curve obtained for each injection. Just as the ITC peaks became broader during the course of the experiment, the enzyme velocity plots became lower (smaller V_{max}) and broader (larger K_m), since each peak was obtained with lower [ADP] and higher [ATP] than the previous one. When plotted in double-reciprocal (Lineweaver-Burk) form, data for each peak gave a straight line, confirming that they followed MM/BH kinetics. This graph

must be interpreted with care for a number of reasons. Firstly, both [ADP] and [ATP] are different for each line on the graph, therefore **Figure 4.4C** combines the effects of substrate depletion and product inhibition in a single series of lines. There will be substantially difference for the patterns of lines in double-reciprocal plots. For instance, ping-pong enzymes give characteristic series of parallel lines in the absence of product inhibition, but when product inhibition is present, this mechanism gives series of intersecting lines, more typical of sequential mechanisms (**Figure S4.2**) Another important caveat is that ADP reacts with PEP during collection of the ITC peak producing ATP, therefore [ATP], [ADP], and [PEP] vary while an ITC peak is being measured. In the current experiment [PEP] varies over 100% of its range during a single peak, while [ADP] and [ATP] vary only over about 7% of theirs, so [ADP] and [ATP] can be thought of as nearly constant for each curve in **Figure 4.4B** and line in **Figure 4.4C**. However in other 2D-ITC schemes (eg **Figure 4.2B,C**), the relative variations of both substrates [A] and [B] can be similarly large during peak collection and this approximation would break down. We find that a more rigorous way to present the 2D-ITC data is in the form of a $\nu([A],[B])$ or $\nu([PEP],[ADP])$ surface, since it is straightforward to take the simultaneous variation of concentrations into account. Each ITC peak is converted into a series of closely spaced ν values, extending across the full range of [PEP] values. Due to the

consumption [ADP] during peak collection, the curves are diagonal to [PEP] (as in **Figure 4.2A**). Note that although the concentration of ATP is not explicitly plotted here, its value can be easily calculated since $[ADP]+[ATP]=[ADP]_{init}$.

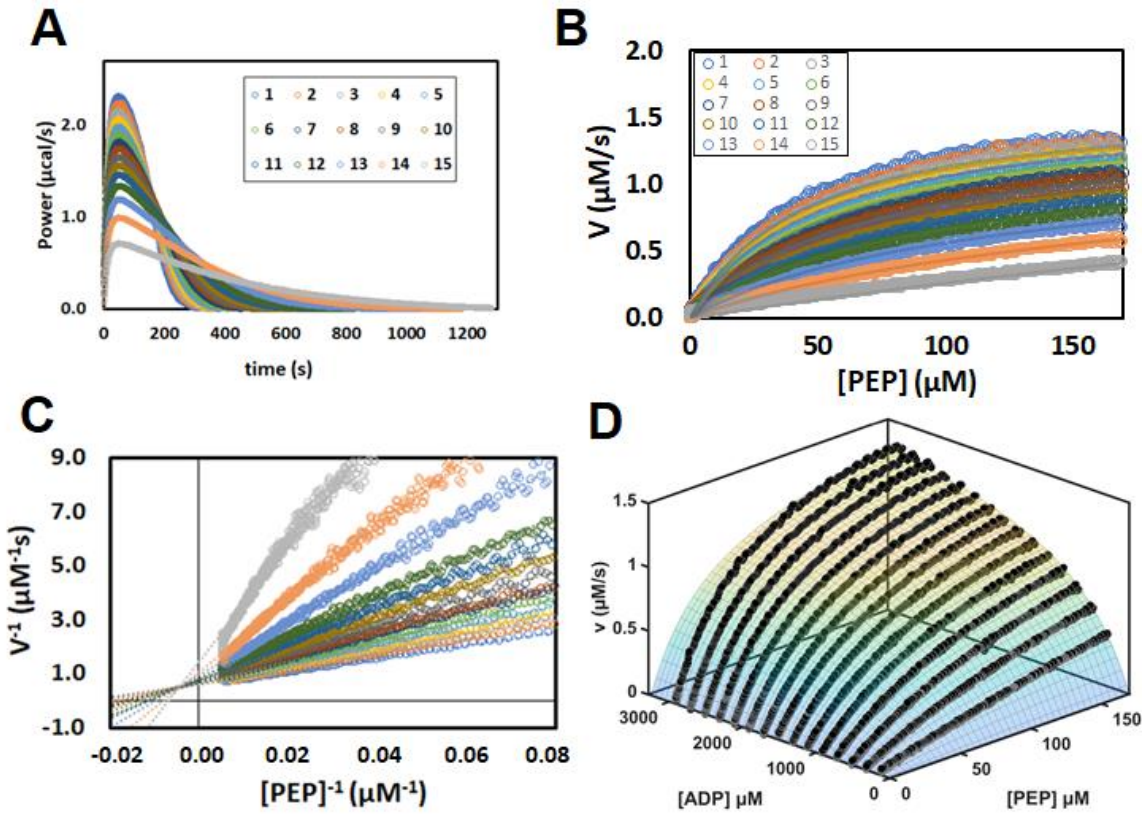

Figure 4.4. 2D-ITC measurement of apo-rMPK. A) Overlay the ITC traces from recurrent single injections of PEP into rMPK and ADP mixture. The order of each injection was presented in different colors as indicated in the figure legend. **B)** The plot of ν versus substrate concentration (circles) with best fits (solid lines). **C)** The Lineweaver-Burk plot from B), the dot lines correspond to the best linear fits. **D)** The plot of ν versus [PEP] and [ADP] (circles) with best fit (mesh surface).

Importantly the ν([PEP],[ADP]) surfaces can be fitted directly to kinetic **Equations 4.8 to 4.10** to identify the enzyme mechanism and extract the parameters of interest, since the values of [ADP], [PEP], [ATP], and [pyruvate] are known for each measured ν value. A complication arises from the need to assign the identities of substrates and products to A, B, P, and Q (in **Figure 4.1**) in **Equations 4.8** to **4.10**. For the ping-pong mechanism, PEP must be A and pyruvate must be P, since the catalyzed reaction involves the transfer of a phosphate group from PEP to ADP. In contrast for the ordered sequential mechanism, there are 4 different ways to fit the equation to the data with PEP as either A or B and pyruvate as either P or Q. The random sequential equation is symmetrical in [A], [B], [P], and [Q], so PEP, ADP, ATP, and pyruvate can be arbitrarily assigned to A, B, P, and Q in **Equation 4.8**. This equation was fit to the 2D-ITC dataset with terms involving [Pyruvate] set to zero since pyruvate does not inhibit the enzyme. The resulting fit (mesh surface in **Figure 4.4D**) gave excellent agreement with the experimental data with a residual sum of squared errors (RSSE) of 0.67. We then repeated the fits with the ping-pong equation (**Equation 4.10**, with [P]=0), obtaining an RSSE value of 6.65 and all 4 permutations of the ordered sequential equation (**Equation 4.9**, with [pyruvate]=0), which gave RSSE values between 2.72 and 6.89 (**Table 4.1**). Thus the random sequential model clearly matches the experimental data better than either the ping-pong or ordered

sequential mechanism, in agreement with the reported mechanism for this enzyme[32, 38]. Furthermore, the large value of K_{ii}^{ATP} indicates that the dead-end complex rMPK:PEP:ATP does not readily form. Thus **Equation 4.8** can be simplified to

$$v = \frac{V_{max}[A][B]}{K_m^A K_i^B\left(1+\frac{[P]}{K_i^P}\right)+[A]K_m^B+[B]K_m^A+[A][B]} \quad (4.11)$$

The extracted values of k_{cat} = 240±20 s^{-1}, K_m^{PEP} = 45±3 µM, K_m^{ADP} =0.52±0.03 mM, K_i^{PEP} = 42±3 µM, , K_i^{ADP} = 0.51±0.03 mM, and K_i^{ATP} = 1.1±0.2 mM, are close to published values.[23, 31] There is no cooperative interactions between PEP and ADP since K_m and K_i for PEP or those of ADP are identical. These results further imply that the rMPK phosphorylation reaction follows a random mechanism.[2]

Table 4.1. The Goodness of fit (residual sum of squared errors, RSSE) for various of Bi-Bi mechanisms.

Entry	Mechanism	RSSE
random	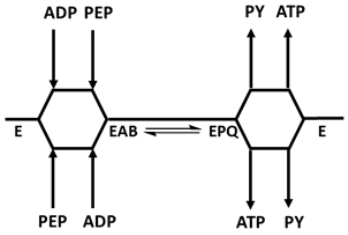	0.67
ordered	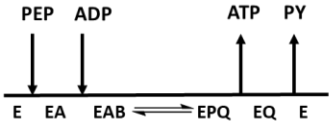	4.07
	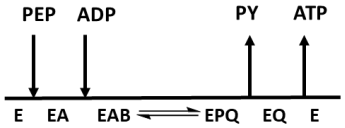	2.72
	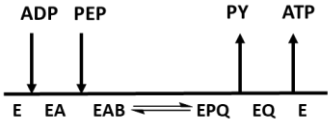	6.89
	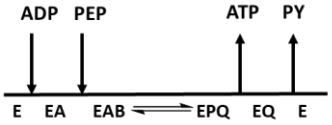	4.08
ping-pong	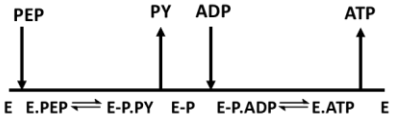	6.65

4.3.3 Cooperative Kinetics of rMPK with Phenylalanine

The amino acid phenylalanine is known to allosterically modulate rMPK activity, reducing catalysis and introducing cooperativity into the enzyme kinetics.[35, 38] In order to see how these effects manifested the 2D-ITC method, we repeated the experiments detailed above, in the presence of 50 mM Phe. The first peaks (after injecting PEP) of the raw ITC traces, obtained in the presence and absence of Phe, are overlaid in **Figure 4.5A**. The peak is clearly lower and broader in the presence of Phe, as expected for a negative effector. We then converted the ITC traces to ν vs [PEP] plots (**Figure 4.5B**). In the absence of Phe, the curve follows the classical hyperbolic shape of the MM/BH equation. In the presence of Phe, the curve exhibits pronounced sigmoidal character, indicative of positively cooperative interactions when PEP binds the four active sites of the tetrameric enzyme. Alternatively, plotting the values of ν obtained for maximum [PEP] in different injections allows one to reconstruct ν vs [ADP] curves (complicated somewhat by the fact that [ATP] increases as [ADP] decreases). The data thus obtained in the presence and absence of Phe are overlaid in **Figure 4.5C**. The curves show typical hyperbolic shapes in both cases, although the reaction velocities are scaled lower when Phe is present, as expected. A 2D-ITC surface plot of ν([PEP],[ADP]) (circles) superimposed on the results

obtained in the absence of Phe (mesh) clearly show a reduction in reaction rate and sigmoidal character along the [PEP] dimension (**Figure 4.5D**).

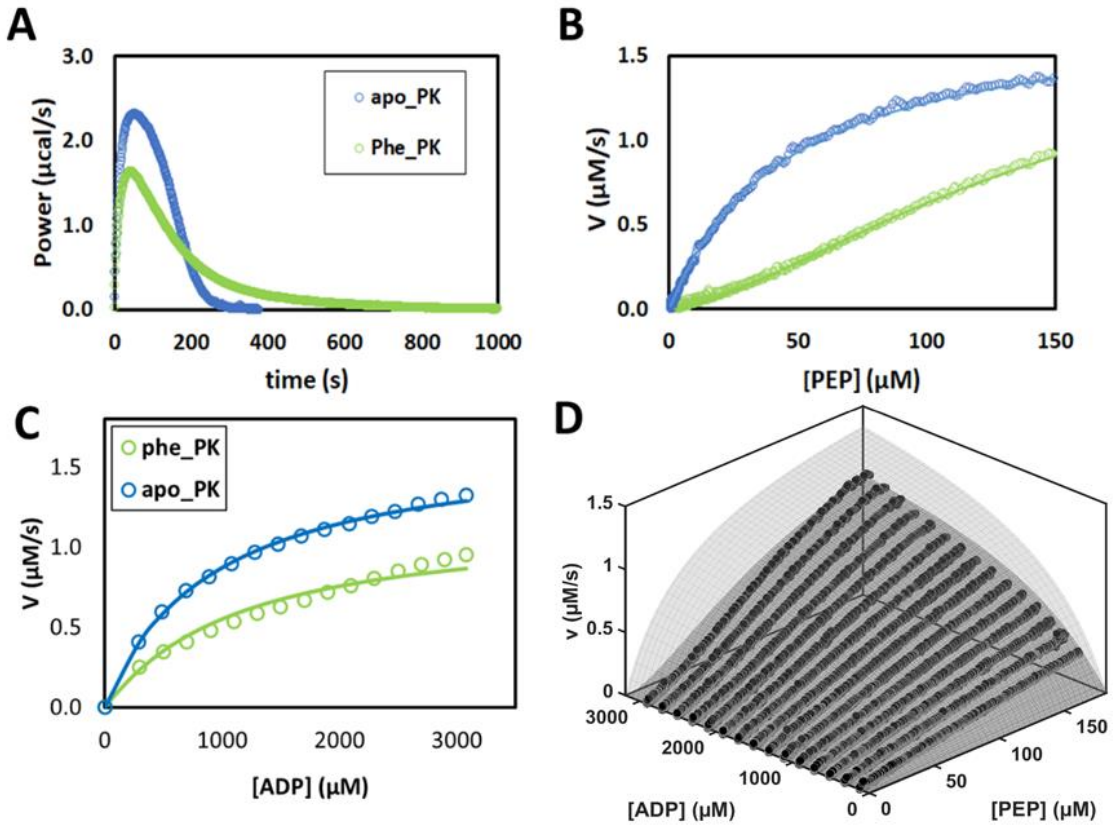

Figure 4.5. Kinetic analysis of rMPK in the presence of phenylalanine. A) Overlay the first ITC trace from recurrent single injection experiments in the absence (blue) and the presence of phenylalanine (green). **B)** The plot of reaction velocity versus PEP concentration (open circles) with best fits (solid lines). **C)** The plot of reaction velocity versus ADP concentration (open circles) with best fits (solid lines). **D)** 2D-ITC surface plot of *v*([PEP],[ADP]) (circles) in the presence of Phe superimposed on the results obtained in the absence of Phe (mesh).

Enzyme kinetic cooperativity can be described in terms of the Hill coefficient (n). For Uni-substrate enzymes with multiple active sites, cooperative enzyme kinetics often empirically follow the relationship

$$\nu = \frac{V_{max}[S]^n}{(K_m)^n + [S]^n} \quad (4.12)$$

Values of n > 1 are consistent with binding of substrate at one active site in the enzyme increasing the affinity at the other sites. Values of n < 1 are consistent with binding substrate at one active site decreasing the affinity of the other sites. When n=1, substrates interact with active sites independently and **Equation 4.12** reduces to the simple MM/BH equation (**Equation 4.1**). The situation is clearly more complicated for a Bi-Bi random sequential mechanism with product inhibition, as is the case here. Nevertheless, when only one of the substrate shows kinetic cooperativity a similar equation can be written in analogy to **Equation 4.12**, assuming A (PEP) binds cooperatively, B (ADP) and P (ATP) bind with simple Langmuir-type or MM/BH saturation curves, Q (pyruvate) does not bind at all, and the dead-end complex AP does not form (as determined above):[37, 46, 47]

$$\upsilon = \frac{V_{max}^{app}[A]^n}{\left(K_m^{app}\right)^n + [A]^n} \quad (4.13)$$

V_{max}^{app} and K_m^{app} are the maximum velocity and the concentration of A required to reach 50% of the maximum velocity, at a fixed value of [B]. Rearrangement of **Equation 4.11** gives:

$$V_{max}^{app} = \frac{V_{max}[B]}{(K_m^B + [B])} \quad (4.14)$$

$$K_m^{app} = \frac{K_m^A[B] + K_m^A K_m^B\left(1 + \frac{[P]}{K_i^P}\right)}{(K_m^B + [B])} \quad (4.15)$$

This equation was fitted to the 2D-ITC dataset, giving good agreement with experimental reaction velocities over the entire [PEP],[ADP] surface (**Figure 4.5D**). The extracted value of k_{cat}, 187±19 s^{-1}, was about 20% slower than that of apo(Phe-free)-rMPK. The extracted value of K_m^{PEP} was 126±5 μM, about 3-fold higher than that of apo-rMPK (K_m^{PEP}= 45±3 μM), indicating the binding of Phe reduces the affinity of enzyme for PEP. The extracted Hill coefficient was n=1.5±0.1, which agrees with previous reports. [35, 37] In addition, the inhibition constant was increased by about a factor of 2 (K_i^{ATP}= 2.5±0.1 mM) for phenylalanine bound enzyme compare with that of the apo-PK.

4.4 Discussion

The 2D-ITC method presented here represents a versatile approach to studying the kinetics of Bi-substrate enzymes using ITC. As described above and elsewhere[42], ITC

represents a powerful and nearly universal, real-time enzyme assay that can applied under conditions where spectroscopic methods fail (eg solutions that strongly scatter or absorb light). Previous ITC studies of Bi-substrate enzymes required a series of separate experiments to be performed at different substrate concentrations. In an example involving rMPK, one ITC experiment was performed per ν data-point, with 52 points reported in the study[24]. In contrast, a single one of the 2D-ITC experiments described here gives 3000 to 7000 separate velocity measurements in just 2 hours of experiment time. The bulk of the time required to perform ITC analyses is consumed with cleaning, filling the syringe and cell with fresh sample, and equilibrating the instrument, with actual run-time representing a relatively small fraction. Therefore the 2D-ITC method presented here increases the efficiency ITC-based Bi-substrate enzyme assays by as much as several orders of magnitude. In principle, the numbers of data points produced in these experiments even exceeds those produced by high-throughput spectroscopic approaches, which would require on the order of 70 separate 96-well plates to achieve the same coverage.[11, 31] It must be noted that the 2D-ITC experiment samples the injected substrate dimension ([PEP] in this case) much more finely (200-400 increments collected once per second) than it does the indirectly observed dimension ([ADP], 15 increments). Nevertheless, 2D-ITC provides at least as detailed kinetic information as the best high-

throughput spectroscopic techniques and also enjoys all the benefits of near universality that all ITC enzyme kinetics experiments deliver.

The main drawback to this approach is that the analysis is more complicated than for traditional enzyme assays for two reasons. Firstly, because both [A] and [B] are different for every measured value of the reaction velocity, traditional analyses in which one substrate concentration is fixed and the other varied cannot strictly be applied. For substrates with very different K_m values, this approximation largely holds, but in general, and for full rigor, 2D-ITC data sets should be fitted as ν([A],[B]) surfaces (**Figure 4.4D and 4.5D**). Secondly the accumulation of products throughout the experiment means that product inhibition must be addressed explicitly, leading to lengthier equations with more adjustable parameters. We note that all of the kinetic parameters were precisely defined in our fits here, despite the larger number of adjustable parameters. This aspect of the approach has advantages as well, as it can allow one to differentiate between random and ordered sequential mechanisms, which is not possible from a simple analysis of the substrate concentration dependence of enzyme activity. Also, because of the influence that product inhibition can have in 2D-ITC, it is highly advisable to perform control experiments in which the injectant includes extra product (ATP and pyruvate in this case). rMPK was inhibited by only one of the products, which simplified the kinetic equations

by eliminating terms in [pyruvate]. For an enzyme inhibited by both products, it would likely be necessary to repeat the 2D-ITC experiment several times, with one or the other or neither product in the syringe, along with substrates, and to globally fit the experiment data, although this is beyond the scope of this work. Finally, we note that for enzyme-catalyzed reactions that lack easily available purified products, it is still possible to check for the presence of product inhibition. Different injection schemes (**Figure 4.2**) will lead to different amounts of products being present as the same regions of [A],[B] space are being sampled. If the measured reaction velocities differ, then product inhibition is present. This is not generally sufficient information to perform full kinetic fits including product inhibition. When produced exclusively by the reaction itself, [P]=[Q] and the concentrations of the two products cannot be varied independently. The random sequential kinetic model is symmetrical in [P] and [Q] when dead-end complexes are absent, and thus separate inhibition constants for the two products cannot be determined unless they can be added separately to the syringe. However, if different injection schemes all give the same rates within the same regions of [A],[B] space, then the 2D-ITC dataset can be fitted with the simpler **Equations 4.2** to **4.3** that lack product inhibition terms.

Finally, even though rMPK was primarily selected as a previously well characterized model system with which to test the 2D-ITC method, our study nevertheless improves our understanding of this enzyme. Firstly, previous studies of apo-rMPK had employed coupled enzyme assay and measured reaction velocities for roughly 25 different [PEP], [ADP] values. The fact that fits to data obtained from a very different modality (ITC) sampling [PEP], [ADP] space at 2000 to 3000 locations gave very similar kinetic parameters both validates the 2D-ITC methodology and confirms the kinetic properties of the enzyme. Secondly, the kinetic behavior of rMPK in the presence of Phe had previously been characterized in much less detail than that of apo-rMPK. Previous studies had measured the kinetic parameters for PEP with saturating ADP and vice versa.[36, 38] The 2D-ITC provides systematically mapped the $\nu([PEP], [ADP])$. Finally, to our knowledge, this is the first study to measure rMPK product inhibition in the presence of Phe. Phe is largely thought to down regulate rMPK catalysis by reducing V_{max} (by a factor of 20%) and increasing K_m^{PEP} (by a factor of 3-fold). However the concentration of ATP in muscle cells, about 4mM, is roughly 3-fold larger than K_i^{ATP}, which means that enzyme activity is suppressed by product inhibition under physiological conditions. However, we found that Phe increased K_i^{ATP} by a factor of 2, which reduces product inhibition (assuming [ATP] is constant), and could offset the reduction in activity towards PEP. In

fact, the apparent K_m^{app} (**Equation 4.15**) decrease about 40% when K_i^{ATP} increases from 1.1 to 2.5 mM ([Phe] equals to 50 mM). In other words, Phe allosterically produces a variety of effects on rMPK activity that partly cancel each other out. The functional significance of these opposing changes remains an open question, but they highlight the importance of full kinetic characterization of enzymes. Overall, this proof-of-principle study demonstrates that 2D-ITC can rapidly provide highly detailed and accurate information on Bi-substrate enzyme kinetics. Given the ubiquity of Bi-substrate enzymes and challenges associated with designing efficient enzymatic assays, together with the near-universality of ITC-based enzyme kinetics assays and wide availability of suitable instrumentation, this method is a potentially powerful addition to the enzymologist's toolkit.

4.5 Conclusion

In this study, a simple 2D-ITC assay was developed to characterize the kinetic property of a Bi-substrate enzymes in a single experiment. The reaction velocity was measured when the concentrations of both substrates were systematically varied. The resulting full two dimensional map of ν as a function of both [A] and [B] can be resolved

by global fitting to identify the type of Bi-Bi mechanism (sequential or ping-pong), as well as yield the values of quantitative kinetic parameters. rMPK phosphorylation reaction was applied as the model system. The 2D-ITC method correctly identified the random Bi-Bi mechanism for rMPK in a single experiment. In addition, a systematically mapped ν([PEP],[ADP]) was generated in the presence of an allosteric inhibitor phenylalanine. Phenylalanine binds to rMPK, leading to weaker substrate affinity and positively cooperative for PEP, in good agreement with previous reports. This 2D-ITC is ideal for resolving the kinetic properties of Bi-substrate enzymes and is a potentially powerful assay for enzymologists.

4.6 Supporting Information

4.6.1 Determination the stocking rMPK solution concentration.

The concentration of the stocking rMPK solution was determined using Bradford protein assay. The Pierce™ Coomassie Plus (Bradford) Assay Kit was purchased from ThermoFisher. Bradford protein assay was performed in 96 well microplate format following the standard procedure: combine a small amount of protein sample with the assay reagent, mix well, incubate briefly and measure the absorbance at 595nm. The

calibration curve was measured at 25°C, with six BSA standard solutions (0, 25,125, 250, 500 and 750µg/mL), as shown in **Figure S4.1**. The concentration of stocking rMPK was calculated from the standard curve.

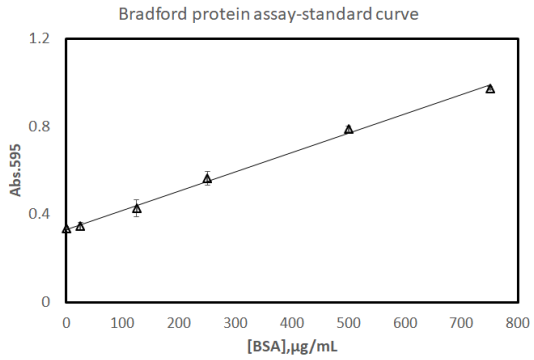

Figure S4.1. Bradford protein assay to evaluate the stocking concentration of rMPK.

4.6.2 Lineweaver-Burk (double-reciprocal) plot

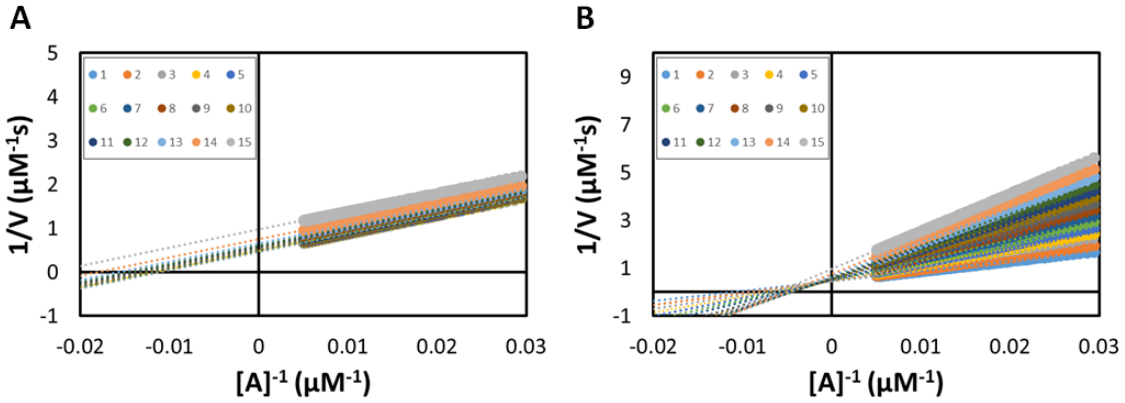

Figure S4.2. Simulation of double-reciprocal plot of ping-pong Bi-Bi mechanism A) in the absence, and **B)** in the presence of product inhibition.

4.7 Reference

1. Zheng, C. J.; Han, L. Y.; Yap, C. W.; Ji, Z. L.; Cao, Z. W.; Chen, Y. Z., Therapeutic targets: progress of their exploration and investigation of their characteristics. *Pharmacological reviews* **2006,** *58* (2), 259-279.
2. Bisswanger, H., *Enzyme kinetics: principles and methods*. John Wiley & Sons: 2017.
3. Cornish-Bowden, A., Chapter 6 - Two-substrate reactions. In *Fundamentals of Enzyme Kinetics*, Cornish-Bowden, A., Ed. Butterworth-Heinemann: 1979; pp 99-129.
4. Johnson, K. A.; Goody, R. S., The original Michaelis constant: translation of the 1913 Michaelis–Menten paper. *Biochemistry* **2011,** *50* (39), 8264-8269.
5. Cleland, W. W., The kinetics of enzyme-catalyzed reactions with two or more substrates or products: I. Nomenclature and rate equations. *Biochimica et Biophysica Acta (BBA) - Specialized Section on Enzymological Subjects* **1963,** *67*, 104-137.
6. Segel, I. H., *Enzyme kinetics: behavior and analysis of rapid equilibrium and steady state enzyme systems*. Wiley New York:: 1975; Vol. 115.
7. Harris, T. K.; Keshwani, M. M., Chapter 7 Measurement of Enzyme Activity. In *Methods in Enzymology*, Burgess, R. R.; Deutscher, M. P., Eds. Academic Press: 2009; Vol. 463, pp 57-71.
8. Seethala, R.; Menzel, R., A homogeneous, fluorescence polarization assay for Src-family tyrosine kinases. *Anal. Biochem.* **1997,** *253* (2), 210-218.
9. Reetz, M. T., Combinatorial and evolution-based methods in the creation of enantioselective catalysts. *Angew. Chem., Int. Ed.* **2001,** *40* (2), 284-310.
10. Shu, Q.; Frieden, C., Relation of Enzyme Activity to Local/Global Stability of Murine Adenosine Deaminase: 19F NMR Studies. *J Mol Biol* **2005,** *345* (3), 599-610.
11. McKay, G. A.; Wright, G. D., Kinetic mechanism of aminoglycoside phosphotransferase type IIIa. Evidence for a Theorell-Chance mechanism. *J. Biol. Chem.* **1995,** *270* (42), 24686-92.
12. Easterby, J. S., Coupled enzyme assays: a general expression for the transient. *Biochim Biophys Acta* **1973,** *293* (2), 552-8.
13. Bianconi, M. L., Calorimetry of enzyme-catalyzed reactions. *Biophys. Chem.* **2007,** *126* (1-3), 59-64.
14. Butler, J. E., Enzyme-Linked immunosorbent assay. *J. Immunoassay* **2000,** *21* (2 & 3), 165-209.

15. Hastie, C. J.; McLauchlan, H. J.; Cohen, P., Assay of protein kinases using radiolabeled ATP: a protocol. *Nat. Protoc.* **2006,** *1* (2), 968-971.
16. Kerner, J.; Hoppel, C. L., Radiochemical malonyl-CoA decarboxylase assay: Activity and subcellular distribution in heart and skeletal muscle. *Anal. Biochem.* **2002,** *306* (2), 283-289.
17. Witt, J. J.; Roskoski, R., Jr., Rapid protein kinase assay using phosphocellulose-paper absorption. *Anal. Biochem.* **1975,** *66* (1), 253-8.
18. Dann, L. G.; Britton, H. G., Kinetics and mechanism of action of muscle pyruvate kinase. *Biochemical Journal* **1978,** *169* (1), 39-54.
19. Fridland, A.; Connelly, M. C.; Robbins, T. J., Tiazofurin metabolism in human lymphoblastoid cells: evidence for phosphorylatin by adenosine kinase and 5'-nucleotidase. *Cancer Res.* **1986,** *46* (2), 532-7.
20. Wang, Y.; Wang, G.; Moitessier, N.; Mittermaier, A. K., Enzyme kinetics by isothermal titration calorimetry: allostery, inhibition, and dynamics. *Frontiers in Molecular Biosciences* **2020,** *7*, 285.
21. Todd, M. J.; Gomez, J., Enzyme kinetics determined using calorimetry: A general assay for enzyme activity? *Anal. Biochem.* **2001,** *296* (2), 179-187.
22. Rohatgi, N.; Gudmundsson, S.; Rolfsson, O., Kinetic analysis of gluconate phosphorylation by human gluconokinase using isothermal titration calorimetry. *FEBS Lett.* **2015,** *589* (23), 3548-3555.
23. Lonhienne, T. G. A.; Reilly, P. E. B.; Winzor, D. J., Further evidence for the reliance of catalysis by rabbit muscle pyruvate kinase upon isomerization of the ternary complex between enzyme and products. *Biophysical Chemistry* **2003,** *104* (1), 189-198.
24. Lonhienne, T. G. A.; Winzor, D. J., Calorimetric Demonstration of the Potential of Molecular Crowding To Emulate the Effect of an Allosteric Activator on Pyruvate Kinase Kinetics. *Biochemistry* **2002,** *41* (22), 6897-6901.
25. Wang, Y.; Guan, J.; Di Trani, J. M.; Auclair, K.; Mittermaier, A. K., Inhibition and Activation of Kinases by Reaction Products: A Reporter-Free Assay. *Analytical Chemistry* **2019,** *91* (18), 11803-11811.
26. Palmer, A.; Begres, B. N.; Van Houten, J. M.; Snider, M. J.; Fraga, D., Characterization of a putative oomycete taurocyamine kinase: Implications for the evolution of the phosphagen kinase family. *Comparative Biochemistry and Physiology Part B: Biochemistry and Molecular Biology* **2013,** *166* (3), 173-181.
27. Olsen, S. N., Applications of isothermal titration calorimetry to measure enzyme kinetics and activity in complex solutions. *Thermochim. Acta* **2006,** *448* (1), 12-18.

28. Szabó, K.; Kandra, L.; Gyémánt, G., Studies on the reversible enzyme reaction of rabbit muscle glycogen phosphorylase b using isothermal titration calorimetry. *Carbohydrate Research* **2019,** *477*, 58-65.
29. Méndez-Lorenzo, L.; Porras-Domínguez, J. R.; Raga-Carbajal, E.; Olvera, C.; Rodríguez-Alegría, M. E.; Carrillo-Nava, E.; Costas, M.; López Munguía, A., Intrinsic Levanase Activity of Bacillus subtilis 168 Levansucrase (SacB). *PloS one* **2015,** *10* (11), e0143394-e0143394.
30. Bianconi, M. L., Calorimetric determination of thermodynamic parameters of reaction reveals different enthalpic compensations of the yeast hexokinase isozymes. *J. Biol. Chem.* **2003,** *278* (21), 18709-18713.
31. Ainsworth, S.; Macfarlane, N., A kinetic study of rabbit muscle pyruvate kinase. *Biochemical Journal* **1973,** *131* (2), 223-236.
32. Reynard, A. M.; Hass, L. F.; Jacobsen, D. D.; Boyer, P. D., The correlation of reaction kinetics and substrate binding with the mechanism of pyruvate kinase. *Journal of Biological Chemistry* **1961,** *236* (8), 2277-2283.
33. Larsen, T. M.; Benning, M. M.; Rayment, I.; Reed, G. H., Structure of the Bis (Mg2+)− ATP− Oxalate Complex of the rabbit muscle pyruvate kinase at 2.1 Å resolution: ATP binding over a barrel. *Biochemistry* **1998,** *37* (18), 6247-6255.
34. Larsen, T. M.; Benning, M. M.; Wesenberg, G. E.; Rayment, I.; Reed, G. H., Ligand-Induced Domain Movement in Pyruvate Kinase: Structure of the Enzyme from Rabbit Muscle with Mg2+, K+, andl-Phospholactate at 2.7 Å Resolution. *Archives of biochemistry and biophysics* **1997,** *345* (2), 199-206.
35. Williams, R.; Holyoak, T.; McDonald, G.; Gui, C.; Fenton, A. W., Differentiating a ligand's chemical requirements for allosteric interactions from those for protein binding. Phenylalanine inhibition of pyruvate kinase. *Biochemistry* **2006,** *45* (17), 5421-5429.
36. Friesen, R. H. E.; Castellani, R. J.; Lee, J. C.; Braun, W., Allostery in rabbit pyruvate kinase: development of a strategy to elucidate the mechanism. *Biochemistry* **1998,** *37* (44), 15266-15276.
37. Carminatti, H.; de Asúa, L. J.; Leiderman, B.; Rozengurt, E., Allosteric properties of skeletal muscle pyruvate kinase. *Journal of Biological Chemistry* **1971,** *246* (23), 7284-7288.
38. Consler, T. G.; Jennewein, M. J.; Cai, G. Z.; Lee, J. C., Synergistic effects of proton and phenylalanine on the regulation of muscle pyruvate kinase. *Biochemistry* **1990,** *29* (48), 10765-10771.

39. Bradford, M. M., A rapid and sensitive method for the quantitation of microgram quantities of protein utilizing the principle of protein-dye binding. *Analytical Biochemistry* **1976,** *72* (1), 248-254.
40. Di Trani, J. M.; Moitessier, N.; Mittermaier, A. K., Measuring Rapid Time-Scale Reaction Kinetics Using Isothermal Titration Calorimetry. *Anal. Chem. (Washington, DC, U. S.)* **2017,** *89* (13), 7022-7030.
41. Di Trani, J. M.; Moitessier, N.; Mittermaier, A. K., Complete Kinetic Characterization of Enzyme Inhibition in a Single Isothermal Titration Calorimetric Experiment. *Anal. Chem. (Washington, DC, U. S.)* **2018,** *90* (14), 8430-8435.
42. Wang, Y.; Mittermaier, A. K., Allosteric interactions in a kinase active site modulate background ATP hydrolysis. *in preparation* **2021**.
43. Di, T. J. M.; De, C. S.; O'Leary, R.; Plescia, J.; do, N. C. J.; Moitessier, N.; Mittermaier, A. K.; do, N. C. J., Rapid measurement of inhibitor binding kinetics by isothermal titration calorimetry. *Nat Commun* **2018,** *9* (1), 893.
44. Boyer, P. D., The inhibition of pyruvate kinase by ATP: A Mg++ buffer system for use in enzyme studies. *Biochemical and Biophysical Research Communications* **1969,** *34* (5), 702-706.
45. Urness, J. M.; Clapp, K. M.; Timmons, J. C.; Bai, X.; Chandrasoma, N.; Buszek, K. R.; Fenton, A. W., Distinguishing the Chemical Moiety of Phosphoenolpyruvate That Contributes to Allostery in Muscle Pyruvate Kinase. *Biochemistry* **2013,** *52* (1), 1-3.
46. Faustova, I.; Jarv, J. In *Kinetic analysis of cooperativity of phosphorylated L-type pyruvate kinase*, 2006; TRUEKITUD OU: 2006; p 179.
47. Israelsen, W. J.; Vander Heiden, M. G. In *Pyruvate kinase: function, regulation and role in cancer*, 2015; Elsevier: 2015; pp 43-51.

5. Conclusions

5.1 Thesis conclusions and contributions

Enzymes play important roles in a variety of biological processes. The study of enzyme activity and regulatory mechanisms is important. ITC-based kinetic assays directly measure the heat released or absorbed during enzyme-catalyzed reactions in real time, thus becoming a powerful and universal technique. This thesis is focused on the development and application of ITC-based methods to study enzyme kinetic properties and understand their mechanistic details. Four novel customized ITC-based methods: the transient assay, the activation assay, the single turn-over assay, and the 2D-ITC assay were developed. These assays overcome limitations of previously developed ITC methods and extend the application of the approach. Detailed conclusions and contributions of this thesis are summarized in this chapter.

5.1.1 Inhibition and Activation of Kinases by Reaction Products: A Reporter-Free Assay

In Chapter 2, we developed a transient ITC assay to measure the effect of the product ADP on kinase activity. This is a challenge to measure by other conventional enzyme assays. Using our ITC assay, we studied the inhibition and activation effects of the

product ADP with three bacterial kinases: aminoglycoside phosphotransferase [APH(3')-IIIa], pantothenate kinases from *Escherichia coli* (*Ec*PanK), and *Pseudomonas aeruginosa* (*Pa*PanK). All three bacterial kinases were inhibited by their reaction product ADP, with the inhibition constants (K_i^{ADP}) similar or smaller than the Michaelis−Menten constant (K_m) values of ATP, thus allowing the enzymes to quickly respond to changes of both ADP and ATP level *in vivo*. Interestingly, for the dimeric enzyme *Ec*PanK, ADP enhanced enzyme activity at low ADP concentrations and inhibited the enzyme at high ADP concentrations. A quantitative model of this unusual effect in terms of cooperative interactions between the two subunits of the dimeric enzyme was presented.

The transient ITC assay measured enzyme activity under native conditions, without any modifications of the substrate. Thus, this assay can be generalized as a universal assay to detect kinase/ADP interactions. For instance, many multi-subunit molecular machines are driven by ATP hydrolysis. The transient ITC assay can be used to study protein interactions with ADP, providing detailed information on enzyme mechanisms and regulation. Moreover, kinase activity is regulation by the ratio of ATP/ADP. A substantial decrease of the ATP/ADP ratio has been suggested as a hallmark of cancer cells. The modulation of enzyme activity thus depends on the values of both K_m^{ATP} and K_i^{ADP}, and these can be evaluated by this universal ITC-based assay also.

5.1.2 Allosteric interactions in a kinase active site modulate background ATP hydrolysis

In Chapter 3, we developed a single turn-over ITC assay and an activation ITC assay to characterize ATP hydrolysis by the antibiotic resistance enzyme aminoglycoside-3'-phosphotransferase-IIIa (APH(3')-IIIa). We have measured steady-state and single-turnover enzyme kinetics of ATP background hydrolysis by APH(3')-IIIa, both in the presence and absence of unreactive substrate analogs. We found that binding of non-substrate aminoglycosides (nsAmgs) to the enzyme accelerates the chemical rate of ATP hydrolysis by at least 10 to 20 fold, suggesting a direct allosteric communication between the aminoglycoside- and ATP- binding pockets. Furthermore, detailed kinetic data on association and dissociation rates of nsAmgs and ADP were extracted from the activation ITC assay. These results help to explain the biophysical processes of an ordered bi-bi mechanism.

This study provides kinetic details of how APH(3')-IIIa avoids background ATP hydrolysis while maintaining phosphoryl transfer activity towards its substrates. The methods introduced in this section can be applied to validate potential drugs which could trigger efficient ATP hydrolysis and generate selective pressure against antibiotic resistance enzyme. In addition, this research demonstrated the versatility of ITC-based

enzyme assays, which are capable of measuring both steady state and single-turnover enzyme kinetic parameters, as well as the affinities and binding rates of allosteric effectors. The single-turnover ITC assay, activation ITC assay, combined with the steady-state ITC assay can be applied to study other allosterically modulated systems.

5.1.3 Rapid characterization of Bi-substrate enzymes by 2D-ITC

In a biological process, Bi-substrate enzymatic reactions with two products (Bi-Bi mechanism) are the most common type, and account for over 60% of all known enzymatic reactions.[1] Thus, understanding of their kinetic properties is important. The 2D-ITC method provides direct and rapid characterization of Bi-substrate enzymes and is a potentially powerful assay for enzymologists. In Chapter 4, we developed a 2D-ITC assay which can completely kinetically characterize Bi-substrate enzymes in a single, (2 hour) experiment. The 2D-ITC assay measures the reaction velocity as a function of the concentrations of both substrates to generate full two dimensional maps of ν as a function of both substrate concentrations, thus enabling the identification of the type of Bi-Bi mechanism (sequential or ping-pong) and yielding the values kinetic parameters. In addition, the same ITC experiment also allows discrimination of ordered versus random

sequential mechanisms, based on their different behaviors with respect to product inhibition. For proof-of-concept, comprehensive kinetic analysis of a rabbit muscle pyruvate kinase (rMPK)-catalyzed phosphorylation reaction was studied. The 2D-ITC assay correctly identified the random-BiBi mechanism for rMPK in a single experiment. The kinetic parameters (k_m^{ADP},K_m^{PEP} and V_m) and product inhibition constant (K_i^{ATP}) can be extracted from the same ITC experiment. We obtained hyperbolic (MM/BH) kinetics in the absence of an allosteric effector, phenylalanine, and sigmoidal (non-MM/BH) kinetics in the presence of phenylalanine. The complete kinetic profiles both in the presence and absence of allosteric effector can be directly visualized and compared in the 2D reaction landscapes. This 2D-ITC is ideal for resolving the kinetic properties of Bi-substrate enzymes and is a potentially powerful assay for enzymologists.

5.2 Future Direction

The advantages of ITC-based kinetic assays have been widely recognized. Publications using ITC-based kinetic assays to characterize enzyme biological function and activity have rapidly expanded in the recent years. ITC assays can be applied to the study the thermodynamic or kinetic properties of an enzyme reaction. Our group is more

focused on the development and application of ITC assays in kinetic studies.[2-6] Quantitative information on inhibitor binding is critical for developing drugs and understanding how enzymes function in living systems. ITC kinetics experiments are suitable for all modes of inhibition and can be performed in such a way that the mode and associated parameters are clearly evident. A quantitative analysis of enzyme inhibition typically involves determination of the mode (competitive, uncompetitive, or mixed) and the inhibitor dissociation constant. Characterization of enzyme inhibition can largely be accomplished with the assays described in this thesis. Due to the pandemic of Covid-19, discovery of new treatments for Covid-19 is crucial for scientist in every area. Our group collaborates with the Moitessier lab to identify and validate promising drug candidates for the treatment of Covid-19 by ITC. Drugs to potentially block two enzymes, PL-protease and 3CL-protease have been synthesized. As it has been showed in this thesis, the effects of inhibitor on enzyme activity can be easily measured by ITC assay. This will provide useful guidance for tunning the structures of drug candidates.

Dysregulation of kinase function is essential for the survival and/or proliferation of cancer cells.[7] Small-molecule kinase inhibitors are widely applied in anticancer therapy.[8] The vast majority of kinase inhibitors discovered to date are ATP-competitive inhibitors.[8, 9] These synthetic molecules mimic ATP as non-covalent inhibitors, binding to the active

conformation of kinase. For the purpose of drug screening, enzyme activity assays, such as radiometric based or fluorescence-based assays, haven been widely used.[10, 11] ITC has been proven to be a more efficient and economical assay. Especially, ITC assays developed in this thesis are specifically applied in the study of ADP/ATP inhibition, thus can be effectively applied to kinase ATP inhibitor cancer drug screening. In particular, the transient ITC assay (developed in Chapter 2) could efficiently measure drug inhibition constants (K_i) in less than one hour; the activation assay (in Chapter 3) could resolve binding dynamics of an inhibitor. In addition, complete enzyme activity landscapes can be examined over a wide range of substrate concentrations (i.e. mimicking the physiological concentration) in the absence or presence of drug using the 2D-ITC method (developed in Chapter 4). This could provide important kinetic details of drug inhibition properties.

The ability of ITC to extract kinetic data from complicated heterogeneous systems, such as biopolymer suspensions [12, 13], insoluble substrate and complex biomass[14-18], or even living cells [19-22] holds great promise for understanding enzyme behavior *in situ* and *in vivo*. One could imagine expanding this approach to a multitude of other complex and heterogeneous media, such as purified cellular components, homogenized tissue or soil samples, and nanostructured materials, to name a few. It is our belief that between

advancements in experimental design and analysis and sample selection and preparation, the full potential of ITC to study enzyme kinetics will become evident in the coming years.

5.3 Reference

1. Cornish-Bowden, A., Chapter 6 - Two-substrate reactions. In *Fundamentals of Enzyme Kinetics*, Cornish-Bowden, A., Ed. Butterworth-Heinemann: 1979; pp 99-129.
2. Wang, Y.; Guan, J.; Di Trani, J. M.; Auclair, K.; Mittermaier, A. K., Inhibition and Activation of Kinases by Reaction Products: A Reporter-Free Assay. *Analytical Chemistry* **2019,** *91* (18), 11803-11811.
3. Di Trani, J. M.; Moitessier, N.; Mittermaier, A. K., Complete Kinetic Characterization of Enzyme Inhibition in a Single Isothermal Titration Calorimetric Experiment. *Anal. Chem. (Washington, DC, U. S.)* **2018,** *90* (14), 8430-8435.
4. Di Trani, J. M.; De Cesco, S.; O'Leary, R.; Plescia, J.; do Nascimento, C. J.; Moitessier, N.; Mittermaier, A. K., Rapid measurement of inhibitor binding kinetics by isothermal titration calorimetry. *Nat Commun* **2018,** *9* (1), 893.
5. Di Trani, J. M.; Moitessier, N.; Mittermaier, A. K., Measuring Rapid Time-Scale Reaction Kinetics Using Isothermal Titration Calorimetry. *Analytical Chemistry* **2017,** *89* (13), 7022-7030.
6. Wang, Y.; Mittermaier, A. K., Allosteric interactions in a kinase active site modulate background ATP hydrolysis. *in preparation* **2021**.
7. Weinstein, I. B.; Joe, A. K., Mechanisms of disease: oncogene addiction—a rationale for molecular targeting in cancer therapy. *Nature clinical practice Oncology* **2006,** *3* (8), 448-457.
8. Zhang, J.; Yang, P. L.; Gray, N. S., Targeting cancer with small molecule kinase inhibitors. *Nature reviews cancer* **2009,** *9* (1), 28-39.
9. Pottier, C.; Fresnais, M.; Gilon, M.; Jérusalem, G.; Longuespée, R.; Sounni, N. E., Tyrosine kinase inhibitors in cancer: breakthrough and challenges of targeted therapy. *Cancers* **2020,** *12* (3), 731.
10. Anastassiadis, T.; Deacon, S. W.; Devarajan, K.; Ma, H.; Peterson, J. R., Comprehensive assay of kinase catalytic activity reveals features of kinase inhibitor selectivity. *Nature Biotechnology* **2011,** *29* (11), 1039-1045.
11. Ma, H.; Deacon, S.; Horiuchi, K., The challenge of selecting protein kinase assays for lead discovery optimization. *Expert opinion on drug discovery* **2008,** *3* (6), 607-621.
12. Ali, G.; Dulong, V.; Gasmi, S. N.; Rihouey, C.; Picton, L.; Le Cerf, D., Covalent immobilization of pullulanase on alginate and study of its hydrolysis of pullulan. *Biotechnology Progress* **2015,** *31* (4), 883-889.

13. Henzler, K.; Haupt, B.; Ballauff, M., Enzymatic activity of immobilized enzyme determined by isothermal titration calorimetry. *Analytical Biochemistry* **2008,** *378* (2), 184-189.

14. Lonhienne, T.; Baise, E.; Feller, G.; Bouriotis, V.; Gerday, C., Enzyme activity determination on macromolecular substrates by isothermal titration calorimetry: application to mesophilic and psychrophilic chitinases. *Biochimica et Biophysica Acta (BBA) - Protein Structure and Molecular Enzymology* **2001,** *1545* (1), 349-356.

15. Murphy, L.; Bohlin, C.; Baumann, M. J.; Olsen, S. N.; Sørensen, T. H.; Anderson, L.; Borch, K.; Westh, P., Product inhibition of five Hypocrea jecorina cellulases. *Enzyme and Microbial Technology* **2013,** *52* (3), 163-169.

16. Murphy, L.; Borch, K.; McFarland, K. C.; Bohlin, C.; Westh, P., A calorimetric assay for enzymatic saccharification of biomass. *Enzyme and Microbial Technology* **2010,** *46* (2), 141-146.

17. Murphy, L.; Baumann, M. J.; Borch, K.; Sweeney, M.; Westh, P., An enzymatic signal amplification system for calorimetric studies of cellobiohydrolases. *Analytical Biochemistry* **2010,** *404* (2), 140-148.

18. Murphy, L.; Cruys-Bagger, N.; Damgaard, H. D.; Baumann, M. J.; Olsen, S. N.; Borch, K.; Lassen, S. F.; Sweeney, M.; Tatsumi, H.; Westh, P., Origin of initial burst in activity for Trichoderma reesei endo-glucanases hydrolyzing insoluble cellulose. *J. Biol. Chem.* **2012,** *287* (2), 1252-1260.

19. Lv, M.; Zhang, Y.-J.; Zhou, F.; Ge, Y.; Zhao, M.-H.; Liu, Y.; Yang, K.-W., Real-time monitoring of D-Ala-D-Ala dipeptidase activity of VanX in living bacteria by isothermal titration calorimetry. *Analytical Biochemistry* **2019,** *578*, 29-35.

20. Wang, Q.; He, Y.; Lu, R.; Wang, W.-M.; Yang, K.-W.; Fan, Hai M.; Jin, Y.; Blackburn, G. M., Thermokinetic profile of NDM-1 and its inhibition by small carboxylic acids. *Bioscience Reports* **2018,** *38* (2).

21. Zhang, Y.-J.; Wang, W.-M.; Oelschlaeger, P.; Chen, C.; Lei, J.-E.; Lv, M.; Yang, K.-W., Real-Time Monitoring of NDM-1 Activity in Live Bacterial Cells by Isothermal Titration Calorimetry: A New Approach To Measure Inhibition of Antibiotic-Resistant Bacteria. *ACS Infectious Diseases* **2018,** *4* (12), 1671-1678.

22. Wang, W.-J.; Wang, Q.; Zhang, Y.; Lu, R.; Zhang, Y.-L.; Yang, K.-W.; Lei, J.-E.; He, Y., Characterization of β-lactamase activity using isothermal titration calorimetry. *Biochimica et Biophysica Acta (BBA) - General Subjects* **2017,** *1861* (8), 2031-2038.